Performance of Gold Catalysts for Low Temperature Water Gas Shift

by Stephen Roberts

Submitted in partial fulfilment of the requirements for the degree of
Master of Science in Engineering

October 2001

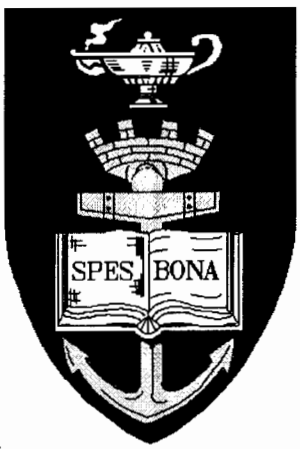

Catalysis Research Unit
Department of Chemical Engineering
University of Cape Town

SYNOPSIS

The ultimate objective of the study was to investigate the performance of suitably prepared gold catalysts for low temperature water gas shift (LTS) — and more specifically to investigate the performance of these catalysts at temperatures below those traditionally utilised. As opposed to the research undertaken to-date on gold catalysed water gas shift, the reaction was performed, as far as possible, under conditions resembling those found industrially, viz. conditions of temperature, pressure, WHSV and dry feed gas composition typical of those applicable to industrial LTS units.

Important to this study was therefore the generation of a comprehensive performance benchmark for the commercially available LTS catalyst, a copper-based material, against which to compare the performance of the gold deposited catalysts.

The gold catalysts were prepared by deposition-precipitation, a preparation procedure found to yield nano-sized gold particles, suggested in literature as being crucial for activity, on the metal oxide support. Using this procedure, gold promoted low (copper) and high (iron oxide) temperature shift catalysts and commercial zinc oxide supports were prepared and tested. A wide spectrum of Au particle sizes were prepared on the supports, ranging from approximately 3 – 500 nm.

The gold promoted LTS catalyst was found to exhibit slightly higher activity than the commercially available catalyst at temperatures below the conventional LTS range. It would appear as if gold promotion is advantageous to the industrial catalyst and could impact greatly on LTS catalyst life.

Even though substantially less active than the commercial copper catalyst was found, the gold promoted commercial zinc oxide catalyst exhibited significantly higher activity than that previously quoted in literature and better performance than the iron oxide supported catalysts of this study. Consequently, the Au/ZnO system exhibits good potential for further developments in terms of water gas shift conversion.

ACKNOWLEDGEMENTS

Firstly, I would like to thank MINTEK for their financial support of the project. Thanks also to MINTEK for their intellectual contributions to the work — for gold catalyst preparation and characterisation. I would also like to acknowledge Süd-Chemie AG and Süd-Chemie Catalysts Japan Inc. for supplying the standard commercial catalyst and other supports on which gold was prepared.

Thanks must also be extended to my supervisor, A/Prof Jack Fletcher, for his extremely important guidance, support and encouragement throughout the project. He gave valuable insight into the experimental work and interpretation of results. Thanks also to Prof Eric van Steen for his helpful input.

A special word of thanks goes to Thomas Tobler for his invaluable technical assistance during the rig setup stages, and who continued to offer practical advice and help thereafter. I really appreciate the devices you 'tinkered' with for me. In this regard, I would also like to thank Joachim Macke and Peter Dobias for the vessels they were able to engineer.

Many thanks must also be extended to Heiko Manstein and Dr Michael Claeys who offered practical and useful advice on various aspects of the research. I would also like to extend general thanks to all the members of the *Catalysis Research Unit* for the friendly and helpful work environment — it made my stay at UCT very enjoyable.

TABLE OF CONTENTS

LIST OF FIGURES

LIST OF TABLES

LIST OF SYMBOLS

Symbol	Description	Units
C_i	Concentration (molar percentage) of component *i*	—
C_p	Molar heat capacity	J/mol.K
$F_{i,j}$	Molar flowrate of component *i* in stream *j*	mol/s
ΔH^f_i	Heat of formation of component *i*	J/mol
ΔH_{rxn}	Heat of reaction	J/mol
ΔG^f_i	Gibbs free energy of formation of component *i*	J/mol
ΔG_{rxn}	Gibbs free energy of reaction	J/mol
K_p	Reaction equilibrium constant	—
P	Pressure	bar
p_i	Partial pressure of component *i*	bar
S_i	Entropy of component *i*	J/mol.K
T	Temperature	°C
X_{CO}	Percentage conversion of CO	—
x_i	Mole fraction of component *i*	—
Y	Relative steam quantity	—
ν	Stoichiometric coefficient	—
R	Universal gas constant	8.314 J/mol.K

GLOSSARY

COP	Coprecipitation
DP	Deposition-precipitation
SEM	Scanning electron microscopy
S / DG	Steam : dry gas ratio
SGHSV	Standard gas hourly space velocity
STP	Standard temperature and pressure (273 K and 1 atm)
MINTEK	Government / private laboratories for minerals technology
TEM	Transmission electron microscopy
WHSV	Weight hourly space velocity
XRD	X-ray diffraction

1. INTRODUCTION

Until recent times, gold was considered to have poor catalytic activity when compared with the other noble metals and, therefore, has found limited application in heterogeneous catalysis. The presumed low catalytic activity of gold was particularly emphasised in earlier review articles on the subject (Bond, 1972; Schwank 1985).

Despite this, the authors did recognise the potential chemical activity of the precious metal. Bond (1972) stated that although the catalytic properties of gold are surpassed by those of the Group VIII metals, especially palladium and platinum, the possible application of gold in catalysis should not be discounted. Schwank (1985) also suggested that, in spite of its low intrinsic activity, gold could influence the activity and selectivity of Group VIII metals.

By the early 1980's, gold catalysts had been shown to be active as oxidation catalysts, however, these did not exhibit any catalytic advantage over other catalyst systems. Many of these studies, though, were performed by applying gold to a more active metal, including the active platinum group metals, in order to promote selectivity at the expense of activity.

The groundbreaking work in this field may be attributed to Haruta and co-workers in the late 1980's (Haruta *et al*, 1987; 1989), when it was shown that gold catalysts could be effective for carbon monoxide oxidation at ambient temperature. It was suggested that the failure to appreciate the necessity of both small gold particles and an appropriate support were major reasons why gold's catalytic activity had for so long not been recognised.

Because gold for so long was considered to be inactive for catalysis, relatively limited work has been done in this field. Over the last 10 years, the potential of gold catalysts has been recognised and investigations have found the metal to be effective for a number of chemical reactions including, selective (Eskendirov *et al*, 1995; Haruta, 1997b; Blick *et al*, 1998) and non-selective (Waters *et al*, 1995;

Thompson, 1999) oxidation of hydrocarbons, methanol synthesis by hydrogenation of carbon oxides (Sakurai *et al*, 1993; Sakurai and Haruta, 1995; 1996), water gas shift conversion (Andreeva *et al*, 1996a; 1996b; 1998a; 1998c; 2001), the hydrogenation of unsaturated hydrocarbons (Haruta, 1997b; Okumura *et al*, 1999), reactions of halogenated compounds (Aida *et al*, 1990; Chen *et al*, 1996) and the reduction of nitric oxide by hydrogen, propene or carbon monoxide (Ueda *et al*, 1997; Thompson, 1998; Ueda and Haruta, 1998; 1999). Gold has already been found to be the catalyst of choice in the hydrochlorination of acetylene (Hutchings, 1996).

Highly dispersed gold catalysts have already found commercial application in odour removal systems and gas sensors (Kobayashi *et al*, 1988; Funazaki *et al*, 1993; Ando *et al*, 1994). Other applications that are technologically ready for application include the utilisation of the catalyst in unheated CO_2 lasers (Minicò *et al*, 1997), CO safety gas masks (Haruta, 1997b), and the selective removal of CO from high purity N_2, O_2 and H_2 streams (Minicò *et al*, 1997). Both chemical processing and environmental protection are foreseen as significant future uses of supported gold catalyst systems (Haruta, 1992; 1997b).

This investigation specifically focuses on the use of gold catalysts for the water gas shift conversion, specifically for shift in the so-called low temperature range. There has been renewed interest in this reaction due to the potential for fuel cell powered vehicles and the fact that carbon monoxide poisons the performance of fuel cells. There is hence a need for very low CO content in the fuel cell H_2 feed, which eventually leads to two research and development drivers:

i. noble metal low temperature catalysts which can deliver very low CO slip (at low temperatures) and which are resistant to deactivation by oxygen which may be present in vehicle fuel processors; and

ii. a general improvement in the life of conventional Cu-LTS catalysts which may be brought about by lower hydrothermal deactivation (sintering), which in turn suggests a lower operation temperature.

Two major objectives were the goal of this work, viz.:

1. to investigate whether gold promoted LTS catalysts could deliver increased activity at temperatures below those traditionally used in low temperature shift, motivated by the expectation that reduced operating temperature and, hence, reduced hydrothermal sintering, would result in extended catalyst life; and

2. to compare the performance of gold and gold promoted catalysts on a selection of metal oxide supports with the performance of commercial shift catalyst under industrially applicable conditions.

2. LITERATURE REVIEW

2.1 Summary of Heterogeneous Gold Catalysed Reactions

Supported gold catalysts have been found to be catalytically active for a number of different reactions. The predominant work to-date has focussed on carbon monoxide oxidation; however, in the last several years a shift towards other industrially applicable reactions has taken place.

Comprehensive reviews of the activity of gold catalysts for a multitude of chemical conversions have recently been published (Thompson, 1998; 1999; Bond and Thompson, 1999). What follows here is a brief summary of the range of reactions for which gold has demonstrated catalytic activity.

2.1.1 Oxidation of carbon monoxide

Haruta and co-workers (1987; 1989) were the first to demonstrate an ability of gold to effectively catalyse the oxidation of carbon monoxide at ambient temperature. These initial studies advanced an understanding of the dependency of catalytic activity on the preparation procedure, or more specifically, on the size of the supported metal particle, as well as the nature of the support (Haruta, 1997b).

A range of metal oxide supports have been investigated for the oxidation of carbon monoxide with early investigations revealing α-Fe_2O_3 to be suitable (Haruta *et al*, 1989). The catalyst was found to be active at sub-ambient temperatures, prompting research into the activity of gold catalysts for other chemical reactions at low temperatures.

Work on this reaction is of particular relevance to the selective oxidation of carbon monoxide in hydrogen streams used as feed for fuel cells. A variety of gold supported manganese oxides have been tested for this application, and results have shown

numerous advantages over Pt-based catalysts — high conversion, readily exceeding 95 %, and relatively high selectivity towards CO conversion (Torres Sanchez *et al*, 1997).

2.1.2 Hydrochlorination of acetylene

Gold supported on activated carbon has been found to yield the highest activity for the hydrochlorination of acetylene to vinyl chloride (Thompson, 1998). Additional advantages of the gold catalyst systems for this reaction are the lower rate of deactivation and the absence of toxicity versus that of the typically practised catalytic systems, notably those based on mercury. In the case of gold catalyst systems, deactivation has been attributed to the reduction of Au(III) to metallic gold.

2.1.3 Oxidation of hydrocarbons

Literature has reported gold catalysts active for the selective oxidation of methane (Eskendirov *et al*, 1995; Blick *et al*, 1998), alkenes (Haruta, 1997b; Hayashi *et al*, 1998) and methanol (Haruta *et al*, 1996; Bond and Thompson, 1999). However, generally the selectivity or activity is lower than that of the current industrially applied catalysts. As an example, Haruta's (1997b) work on propene oxidation demonstrated high selectivity (i.e. greater than 99 %) towards the formation of propene oxide, but at low conversion (approximately 1 %).

The non-selective catalytic combustion of methane, propane, propene and trimethylamine have also been investigated — Au/Co_3O_4 catalysts are claimed to be more active than Pt/Al_2O_3 and equivalent to the commercial Pd/Al_2O_3 for the oxidation of methane and propane (Thompson, 1999). Waters *et al* (1995) have investigated a number of co-precipitated gold catalysts utilising various metal oxide supports for the catalytic combustion of methane and found, similarly to the work of Haruta, that gold supported on Co_3O_4 was most active for this reaction. Nonetheless, for the catalytic combustion of alkenes, gold was found to be less active than platinum and palladium. Andreeva and co-workers (1998b) have also

studied the complete catalytic combustion of benzene over various gold promoted vanadium oxide catalysts, and found that 98 % conversion occurs at approximately 150°C lower than the equivalent palladium or silver promoted vanadium oxide catalysts.

2.1.4 Hydrogenation of carbon oxides

The hydrogenation of carbon monoxide and carbon dioxide over gold deposited on TiO_2, Fe_2O_3, ZnO and $ZnFe_2O_3$ between 150 and 400°C has been studied by Sakurai and Haruta (1995; 1996) and found to yield methanol, as opposed to the formation of methane by other noble metals. In particular, Au/ZnO and Au/$ZnFe_2O_3$ showed high methanol selectivities from carbon dioxide, comparable to those obtained from copper catalysts.

2.1.5 Reduction of nitric oxide

The reduction of nitric oxide with carbon monoxide (in the absence of oxygen) was found to take place below 100°C over gold supported on α-Fe_2O_3 and $NiFe_2O_4$, yielding nitrogen as the main product, while, over unsupported gold, mainly nitrous oxide was produced (Haruta, 1997a). Ueda and co-workers (1997; 1998) also investigated the reduction of nitric oxide to nitrogen using propene over various gold promoted catalysts between 200 and 500°C. Gold supported on alumina was found to yield the highest conversion of nitric oxide. The conversion has also been reported to be enhanced by the addition of Mn_2O_3 to the Au/Al_2O_3, producing catalytic performances comparable with those displayed by the best nitric oxide reduction catalysts developed to date (Ueda and Haruta, 1999).

2.2 Factors Affecting the Activity of Gold Catalysts

It has gradually emerged over the past decade that three main factors influence the activity of gold as a catalyst; namely (1) the gold particle size on the support, (2) the precipitation procedure and (3) the particular support material used. As early as 1985, Schwank concluded that the nature of the support and preparative conditions play a decisive role in determining the microstructural characteristics of the active metal surface (Schwank, 1985).

2.2.1 Gold particle size and morphology

The catalytic activity of gold appears to be highly sensitive to the particle size (Haruta *et al*, 1993; Haruta, 1997b; Bond and Thompson, 1999). Haruta, in his review of the size dependency of gold catalysts (1997b), postulates that catalysts exhibit surprisingly high activity and/or selectivity for a range of reactions only when gold is deposited on selected metal oxides as hemispherical ultra-fine particles with diameters smaller than 5 nm. Similarly, Bond and Thompson (1999) suggest that significant chemisorption, and hence catalysis, occurs only when a sufficient number of low coordination surface atoms are present (i.e. on Au particles small enough such that full metallic character is not exhibited).

Catalytic activity, achieved only when the gold is highly dispersed, has led researchers to propose that the gold/metal-oxide perimeter interface acts as at least one of the active moieties mediating the chemical reaction, with the support making a vital contribution (Bond and Thompson, 1999). Consequently, the importance of careful preparation of the supported gold catalyst has recently been emphasised by two of the leaders in the field of heterogeneous gold catalysis, Haruta (1997b) and Hutchings (1996).

Early attempts to produce supported gold catalysts used the simplest classical method, impregnation — since most noble metal catalysts are prepared by this procedure. Except for a few cases where low metal loadings are employed, impregnation

techniques have shown limited success in achieving highly dispersed gold within the size range required for high activity. Ion-exchange procedures (in particular gold / zeolite catalyst preparations), also common for catalyst preparation, have found limited application with gold perhaps due to the limited number of cationic gold complexes available (Bond and Thompson, 1999).

Generally, therefore, only certain preparation methods have been found to successfully produce a variety of supported metal oxide catalysts with the small gold particle sizes required for good catalytic activity. These are presented below:

2.2.1.1 Coprecipitation

The detailed work by Haruta and co-workers (1989; 1993) has led to an understanding of the superior catalytic activity of coprecipitated materials — the catalysts which have found the widest application in gold catalyst research today. Coprecipitation (COP) involves the simultaneous precipitation of two hydroxides (and in some cases also hydrated oxides) by the addition of chloroauric acid ($HAuCl_4$) and a metal nitrate to a solution of sodium carbonate (Haruta, 1997b). The precipitate is then washed, dried and calcined in air at a variety of temperatures ranging between 200 and 800°C (Bond and Thompson, 1999). The dried precipitate is most often established as an hydroxide, but sometimes it forms an amorphous or poorly defined structure which first has to be dehydrated in order to establish the desired hydroxide. Haruta (1997b) reports that this procedure may lead to significant concentrations of sodium or chlorine (depending on the metal precursor), being contained in the catalyst, both of which are considered detrimental to catalyst performance.

2.2.1.2 Deposition-precipitation

In the case of the deposition-precipitation (DP) technique, the precursor of the active gold species is slowly precipitated (in the form of an hydroxide) from the solution in the presence of the metal oxide support by raising the pH to between 6 and 10. The metal oxide, which can be added to the solution in any desired form, for example powder or formed pellet, acts as a nucleating agent for precipitation. Similar to the aforementioned preparation method, the catalyst is washed, dried and calcined.

The resulting gold particle size is strongly influenced by the pH at which precipitation takes place, and careful control allows the desired particle size to be formed. Deposition-precipitation has the advantage over coprecipitation in that most of the active component remains on the surface of the support and is not taken up within the bulk catalyst (Bond and Thompson, 1999). This procedure allows gold to be deposited on a wide range of supports. Moreover, Haruta *et al* (1993) report that it is often preferred over coprecipitation in that it gives a narrower particle size distribution.

2.2.1.3 Chemical vapour deposition or grafting

These methods are similar, differing only in whether a solvent is present or not. Chemical vapour deposition involves the attachment of an active gold precursor to the surface of a metal oxide support by means of a chemical reaction between the two. The volatile organic gold component is transported to the high area support either by an inert gas or under vacuum, where it is decomposed into small metal particles. In the grafting technique, a gold complex in solution reacts with the surface, where it is later converted to the catalytically active gold metal form. These two methods, however, have not frequently been reported in literature for the preparation of active gold catalysts.

2.2.2 The support material

It is clear that gold dispersed on a transition metal oxide exhibits an intimate interaction with the support and gold alone is far less active as a catalyst than its supported counterpart. It is still unclear, however, how the interaction with different materials promotes an increase in activity.

Coprecipitation is the most frequently applied preparation procedure for heterogeneous gold catalysts, allowing both the formation of the active ultra-fine particles and the formation of the support which may participate in the reaction and/or stabilise the gold species. Coprecipitation, as mentioned previously, involves the formation of an

hydroxide or hydrated oxide of the support metal. This limits the type of support metal cations to those of the elements from predominately the first row of the transition series of metals (i.e. from scandium to zinc), with a few pre- and post-transition elements (e.g. Mg, Al, Si, Sn) — because only these elements are able to form hydroxides or hydrated oxides under the alkaline conditions required for fine particle deposition. Gold supported on mixed metal oxides, namely $NiFe_2O_4$ and $ZnFe_2O_4$ (Haruta, 1992), as well as gold supported on zeolites, namely zeolite Y (Salama *et al*, 1995; Kang and Wan, 1997) and MCM-41 (Haruta, 1997a), have also been prepared.

The importance of a high surface area support has been highlighted (Haruta *et al*, 1993), which can be achieved by lower calcination temperatures in the catalyst preparation step, or by omitting calcinations altogether as has been done by some authors. Evidence also suggests that the nature of the support does not greatly affect the size or size distribution of the gold particles obtained from the various preparation techniques (except for grafting) (Bond and Thompson, 1999).

2.3 The Supported Gold Particles

As mentioned previously, the activity of supported gold catalysts is reported to be strongly affected by the particle size deposited on the metal oxide support. The influence of the metal particle size on activity is not well understood, at least partly because the study of this phenomenon is hampered by two main factors, viz.:

i. monodispersed metallic particles (i.e. where the particles all have the same size) is virtually impossible to achieve and, therefore, it is difficult to recognise catalytic effects as a consequence of size — especially for the very narrow size range said to yield active gold catalysts, and

ii. the small metal particles are unstable with respect to the bulk metal, with the driving force directed towards sintering. Consequently, the metal particles need to be supported on a high surface area solid; however, the interaction between the solid and the metal may affect the properties and/or behaviour of the particles.

The dependence of high activity on the gold particle size has led some researchers (Bamwenda *et al*, 1997) to believe that the interface between the gold and the support, and the interaction between the gold and the support are of particular importance. The hemispherical ultra-fine particles are strongly attached to the metal oxide support at their flat planes and, are thereby rendered more thermally stable than spherical particles (Haruta, 1997b). This strong interaction can be attributed to the affinity the hydroxylic, oxidic or organic precursors have for the metal oxide.

Until recently, most of the literature available on heterogeneous gold catalysis reported the metallic gold as the active species. However, Thompson (1999) has highlighted the possibility of a monolayer of gold oxide present at the surface perimeter interface during oxidation reactions.

Much attention has been given in the literature to the lattice structure of the small Au particles. The question arises whether the particles remain in their 'normal' (i.e. bulk metal) face-centered-cubic form, or whether as some calculations seem to suggest, the icosahedral form becomes more stable as the size is decreased. Bond and Thompson (1999) suggest that there is little to choose between the two in terms of stability; indeed, using transmission electron microscopy (TEM), rapid fluctuations between different structures are observed. 'Unsupported' gold particles (that is those particles that are prepared by vacuum evaporation or as colloids and deposited on a solid to allow for analysis, but which are unsuitable as catalysts) examined using transmission electron microscopy and x-ray diffraction (XRD) have also been found to exhibit the fcc structure. For certain oxides of Au, however, other forms such as octahedral, cubo-octahedral and multiply twinned particles have also been observed (Cunningham *et al*, 1997).

2.4 The Water Gas Shift Reaction

2.4.1 Background of the water gas shift reaction

The water gas shift reaction, first reported in 1888 (Rhodes *et al*, 1995) and of particular interest to the ammonia synthesis industry, involves the 'shifting' of carbon monoxide gas via steam to carbon dioxide and hydrogen;

$$CO + H_2O \leftrightarrows CO_2 + H_2 \qquad \Delta H = -41.1 \text{ kJ/mol}$$

The water gas shift reaction is applied industrially for the production of hydrogen in its pure form, as a mixture with nitrogen for the synthesis of ammonia, or as a mixture with CO for methanol or hydrocarbon synthesis, the latter via the Fischer-Tropsch process.

The conversion of the carbon monoxide occurs in what are called shift reactors and, under the process conditions applied, no significant side reactions occur. Depending on the purity of the product stream required, this reaction is implemented in either a one or two step process. In the case of pure hydrogen and ammonia synthesis gas production, a two-stage adiabatic reactor configuration is used. The first reactor, or high temperature shift (HTS) converter, operates in the temperature range of 350 – 450°C, and converts the majority of the CO to CO_2. This is followed by a second reactor, the low temperature shift (LTS) converter, operating in the range 200 - 240°C, converting the remaining CO to CO_2 (Kirk-Othmer, 1995). The industrial processes operate in a range of pressures between 25 and 35 bar (Rhodes *et al*, 1995).

The HTS catalyst, promoted iron-oxide/chromia, exploits the more rapid kinetics available at the higher temperature, while the LTS catalyst, copper-oxide/zinc-oxide/alumina, exploits the more favourable equilibrium conversion available at lower temperatures. The iron oxide catalyst is the more 'robust' of the two catalysts and can withstand higher temperatures and feed impurities, while the copper catalyst more readily undergoes hydrothermal sintering. At the typical operating conditions of the HTS converter, CO slip is in the range of 2 - 4 %, whereas for LTS converter, CO slip in the range of 0.1 - 0.3 % is attainable (Twigg, 1989).

2.4.2 Thermodynamics of the water gas shift reaction

2.4.2.1 Temperature

The choice of reaction temperature is dependent on the maximum operating temperature of the catalyst, the endo/exo-thermic nature of the reaction and the position of the reaction equilibrium.

In the case of the water gas shift reaction, these factors work against one another. The water gas shift reaction is moderately exothermic ($\Delta H_{rxn,\ 25°C}$ = -41.1 kJ/mol) — thus the equilibrium constant, $K_p = (p_{H_2} \cdot p_{CO_2})/(p_{H_2O} \cdot p_{CO})$, decreases with increasing temperature. For reversible exothermic reactions, Le Chatelier's principle prescribes a low operating temperature in order to increase the conversion of the reactants (i.e. carbon monoxide and water). A trade-off, however, between reaction rate and conversion is required, since at the lower temperatures the rate is significantly depressed.

The high and, to a lesser extent, low temperature shift reactions are thermodynamically limited. Under the adiabatic operating conditions of the reactors, the heat of reaction results in an increase in temperature through the catalyst bed. Since the water gas shift reaction is exothermic, the increase in temperature reduces the maximum attainable conversion of the reactants (at a particular rate of reaction). The temperature increase over the HTS reactor is generally quite substantial (50 – 90°C) owing to the extensive conversion of the reactants in this converter. A smaller temperature rise, typically 10 – 20°C, occurs in the LTS converter.

2.4.2.2 Pressure

By Le Chatelier's principle, when pressure is applied to a system at equilibrium, the system will adjust to minimise the increase. For the water gas shift reaction, an equimolar gas phase reaction, the total number of moles of reactant and product at a particular time in the gas phase is not dependant on the relative position of the forward and reverse reaction, and thus the equilibrium constant is essentially independent of pressure. Literature reports that the rate of reaction increases with pressure up to

approximately 5 bar, after which further increase in pressure has little effect on the rate (Twigg, 1989).

2.4.2.3 Steam : carbon ratio

The equilibrium conversion of CO is increased as the ratio of steam to carbon monoxide is increased. In industry, the HTS stage is operated at a steam to carbon monoxide ratio of between 2.5 and 5 to enhance equilibrium conversion, as well as to limit carbon deposition on the catalyst (Twigg, 1989).

2.4.3 Proposed mechanism of the water gas shift reaction

Although the reaction appears not to be complex, a totally satisfactory and universally accepted mechanistic description of the water gas shift reaction has not been verified for either of the catalytic materials generally employed, namely chromium promoted magnetite and zinc oxide supported metallic copper. The catalysts have been found to be susceptible to small changes in the operating conditions, thus complicating the study. Two contrasting mechanistic pathways have been proposed based on either: (a) an associative mechanism or (b) a regenerative mechanism (Rhodes *et al*, 1995). Armstrong and Hilditch (1920) first proposed the associative mechanism using data obtained from a copper chromite catalyst. It involves the adsorption of carbon monoxide and water onto the catalyst surface to form an intermediate species of unspecified structure that then decomposes into the products.

$$CO + H_2O \rightarrow (\text{intermediate}) \rightarrow CO_2 + H_2 \qquad \textbf{eqn 2-1}$$

The regenerative mechanism, also originally proposed by Armstrong and Hilditch (1920), proposes a cyclic change in the oxidation state of the active catalytic material, brought about by the reactants (i.e. successive oxidation and reduction of the surface). In its simplest form, the regenerative mechanism can be seen as the lysis of water on the catalyst to produce hydrogen gas and an absorbed oxygen

species on the catalyst surface. The catalyst surface is then reduced by carbon monoxide, yielding carbon dioxide, while subsequently returning the catalyst surface to its original state.

$$H_2O + Red \rightarrow H_2 + Ox \qquad \textbf{eqn 2-2}$$

$$CO + Ox \rightarrow CO_2 + Red \qquad \textbf{eqn 2-3}$$

For the copper/zinc-oxide/alumina catalyst used industrially for low temperature shift conversion, the metallic copper appears as small islands on the support. Evidence suggests that the zinc-oxide/alumina plays little to no role in the reaction (Rhodes *et al*, 1995), although researchers do allude to a possible synergism between the copper and zinc. Despite the LTS catalyst's extensive characterisation, uncertainty still exists over the precise nature of the active site — the presence of both Cu(0) and Cu(I) species on the surface have caused this to be a subject of much debate and it is likely that both species are required.

The metallic copper islands can accommodate the dissociative adsorption of water required for the redox mechanism and the reactions needed to produce and decompose intermediate formate species. There is strong evidence supporting both the associative and regenerative mechanistic pathways and, as yet, it is still unknown which pathway is followed under reaction conditions.

There is considerably less uncertainty regarding the pathway followed over the high temperature shift catalyst. The redox couple (i.e. Fe^{2+} / Fe^{3+}) has been found to be highly labile and able to readily dissociate water under reaction conditions (Rhodes *et al*, 1995). A redox type mechanism like that described by the regenerative mechanistic pathway is therefore generally believed to occur. Magnetite, which is characterised as an inverse spinel structure, has been found to possess unique properties that are particularly well suited to the operation of a redox water gas shift catalyst when compared to other spinel-type materials.

2.4.4 Low temperature water gas shift reaction over Au/α-Fe_2O_3

Since gold catalysis is a relatively new field, limited studies on the use of gold promoted metal oxides for the water gas shift reaction have been undertaken. Andreeva *et al* (1996a) first investigated the use of gold for the catalysis of this reaction — in particular, three different samples, namely Au/α-Fe_2O_3, Au/Al_2O_3 and α-Fe_2O_3 prepared by coprecipitation techniques (with Au:Fe and Au:Al ratios of 1:22). The Au/α-Fe_2O_3 catalyst exhibited high catalytic activity in the low temperature shift range. This activity (defined as the amount of CO converted per m^2 of catalyst surface area per hour) was claimed to be higher than that of the most effective industrially applied water gas shift catalyst, copper-oxide/zinc-oxide/alumina, measured under identical conditions. The gold-free α-Fe_2O_3 sample was found to exhibit high catalytic activity only in the higher temperature range — corresponding to the well-documented high temperature shift activity of iron oxide in its magnetite form. A comparison of the activity of the four catalyst materials is illustrated in Figure 2-1.

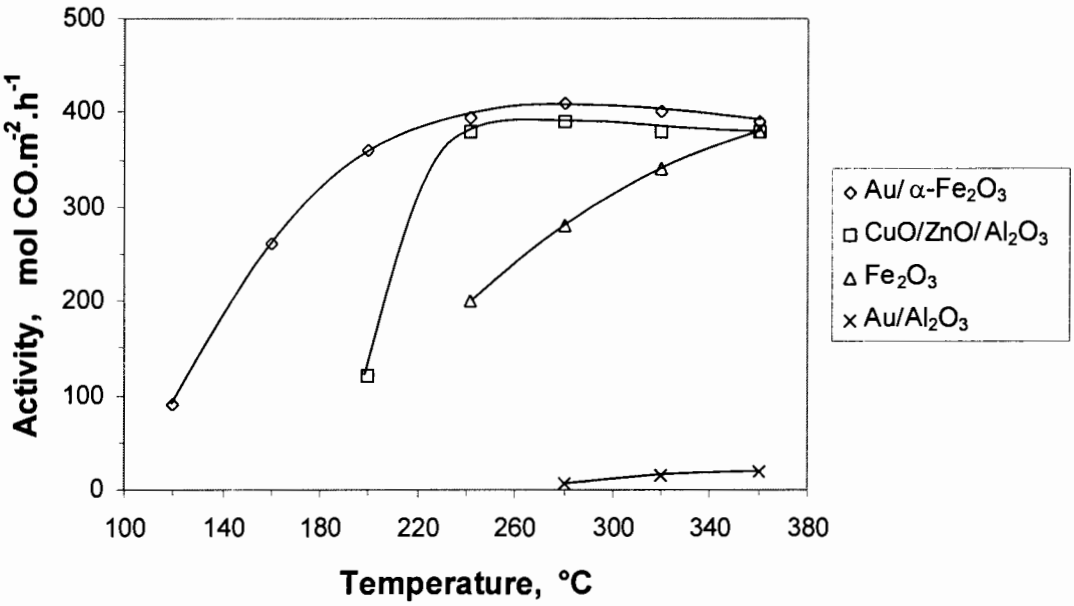

Figure 2-1 : Comparison of the activities of four catalysts for the WGSR

(Adapted from D. Andreeva *et al*, Journal of Catalysis, 1996a)

The catalytic activity of the Au/α-Fe_2O_3 was considerably higher than that of the catalyst containing only α-Fe_2O_3 in the low to medium temperature range, while Au/Al_2O_3 displayed very low activity for the water gas shift reaction. Electron microscopy indicated that the gold particles occurred as finely dispersed metallic particles (with similar average particle sizes) for both the α-Fe_2O_3 and the Al_2O_3 supports. It may thus be concluded that a specific interaction between the gold particles and the ferric oxide support is responsible for this increased activity. Andreeva *et al* (1996b) studied two identically loaded Au/α-Fe_2O_3 catalysts prepared by co-precipitation using slightly different precipitation techniques. The two catalysts prepared were found to have significantly different gold particle sizes — the one with the smaller particles displaying the higher catalytic activity for the water gas shift reaction.

Haruta *et al* (1993) have shown, however, that catalysts prepared by coprecipitation for CO oxidation display cluster formation. They report that samples having small gold clusters in addition to metallic gold were not catalytically more active than samples without gold clusters. On the basis of this result, the authors concluded that metallic gold is responsible for CO oxidation. Also, this technique leads to an incorporation of the gold into the bulk iron oxide support — thus being unavailable for surface catalysis.

Work by Andreeva *et al* (1998a) demonstrated that Au/α-Fe_2O_3 prepared via a modified deposition-precipitation (DP) procedure displayed higher conversion than the equivalent catalyst prepared via coprecipitation (COP), shown in Figure 2-2.

The deposition-precipitated catalyst also exhibited higher stability under the same conditions. Moreover, Andreeva *et al* (1998a) showed that gold catalysts prepared via modified deposition-precipitation results in smaller gold particles with a greater resistance to hydrothermal sintering. In addition, the majority of the gold metal remains on the support surface, thus being accessible to catalysis. Accordingly, the authors suggested that the modified deposition-precipitation technique results in a weaker interaction between the gold particles and the support, which they considered advantageous for catalysis.

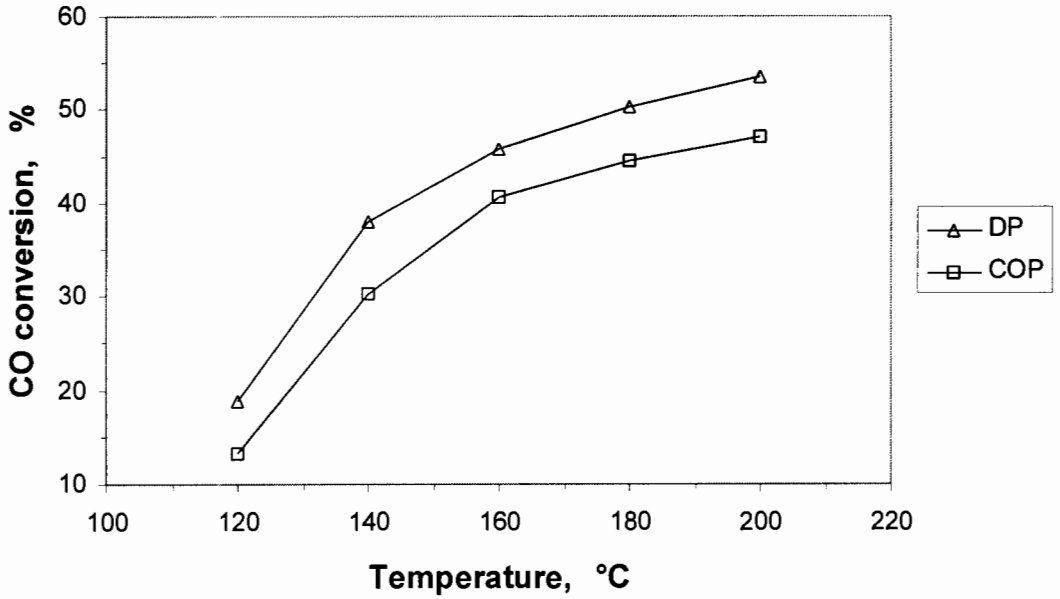

Figure 2-2 : Catalytic activity of Au/α-Fe_2O_3 prepared by deposition-precipitation and coprecipitation

(Adapted from D. Andreeva *et al*, Applied Catalysis A: General, 1998a)

2.4.5 Water gas shift reaction mechanism on Au/α-Fe_2O_3

Investigations by Andreeva *et al* (1996a) into the catalytic activity of Au/α-Fe_2O_3 for the water gas shift reaction have apparently shown a considerably higher activity than the most active catalyst commercially manufactured, namely the copper-oxide/zinc-oxide/alumina low temperature shift catalyst. Higher activity was also achieved with the Au/α-Fe_2O_3 catalyst in comparison to that excluding gold, while low activity was achieved with Au/Al_2O_3. Consequently, it can be concluded that the high activity of the Au/α-Fe_2O_3 is due to a specific interaction between the gold particle and the iron oxide support. This phenomenon of increased catalytic activity has also been reported by Haruta *et al* (1993), who stated that a gold-metal oxide combination is indispensable for the genesis of high activity.

Andreeva *et al* (1996b) have proposed an associative type of mechanism for the low temperature activity of the Au/α-Fe_2O_3 catalyst, involving the formation of intermediate formate and carbonate species, while incorporating the $Fe^{2+} \leftrightarrow Fe^{3+}$ redox cyclic transition, generally accepted for iron-based HTS catalysts. An important step in this associative mechanism is the formation of an intermediate surface compound through the interaction between CO and an hydroxyl group. With respect to the investigations by Andreeva *et al* on the effect of the size of the gold particles, IR spectra performed by Ilieva *et al* (1997) indicated a significant increase in the quantity of hydroxyl groups and non-dissociatively bonded water molecules on the surface of the catalyst with the smaller particles. This significant increase in adsorbed hydroxyl species was confirmed by temperature programmed desorption studies. A prerequisite for the high activity of the water gas shift reaction seems to be the presence of a sufficiently high concentration of surface active hydroxyl groups on the catalyst. In this regard, coordinatively unsatured surface metal atoms have been found to be unusually reactive. For highly dispersed gold in the Au/α-Fe_2O_3 catalyst, high levels of these high energy metal atoms are present on the surface; consequently generating elevated concentrations of hydroxyl surface species.

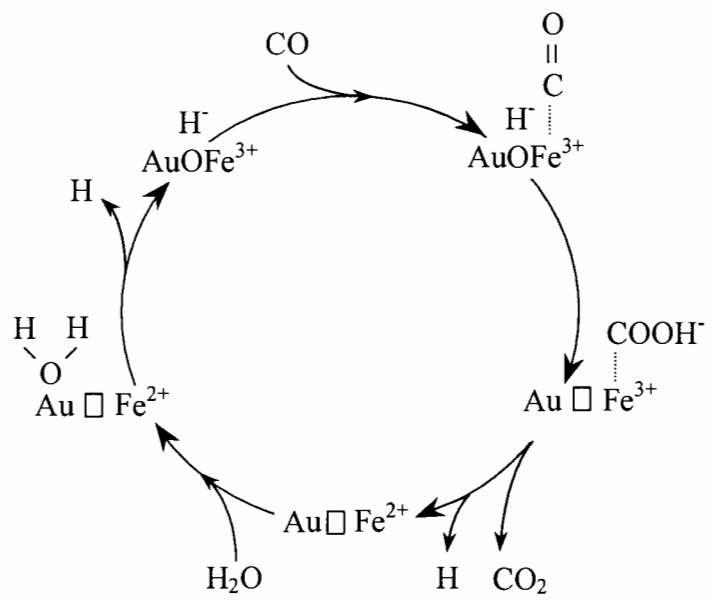

Figure 2-3 : Possible pathway of the WGSR mechanism on Au/α-Fe_2O_3

(D. Andreeva *et al*, Applied Catalysis A: General, 1996b)

The scheme illustrated in Figure 2-3 proposes a possible pathway of the water gas shift reaction on Au/α-Fe_2O_3 via the associative mechanism proposed by Andreeva *et al* (1996b). The important steps in this mechanism are the dissociative adsorption of water on the small gold particles, followed by the spill-over of active hydroxyl groups onto the adjacent sites of the ferric oxide. The formation and decomposition of the carbonate species to yield the carbon dioxide product is associated with the redox alteration $Fe^{3+} \rightarrow Fe^{2+}$ in magnetite (Fe_3O_4) and the dissociation of an adsorbed water molecule with the opposite redox transfer, $Fe^{2+} \rightarrow Fe^{3+}$.

Ilieva *et al* (1997) have reported that, according to this reaction mechanism, magnetite can be envisaged as the "working catalytic system". Temperature programmed reduction studies (Ilieva *et al*, 1997) performed on the α-Fe_2O_3 and Au/α-Fe_2O_3 have shown that the hematite (Fe_2O_3) to magnetite (Fe_3O_4) transition occurs at a considerably lower temperature (approximately 140°C lower) on the latter. Thus, in the presence of gold, the 'working state' of the catalyst is attained at a significantly lower temperature — which accounts for the low temperature water gas shift activity of the iron oxide catalyst containing gold. Furthermore, it has been found that the hematite-magnetite transition is shifted to higher temperatures when the hydroxyl groups are removed from the finely divided gold containing catalyst surface (yet still being lower than the temperatures for the transition without gold present). Thus, the activated hydroxyl groups also participate in the reduction of the α-Fe_2O_3.

2.4.6 Low temperature water gas shift reaction over Au/TiO_2 and Au/Co_3O_4

According to the reaction mechanism proposed by Andreeva *et al* (1996b), both an activated hydroxyl group and a redox pair $M^{n+} \leftrightarrow M^{(n+1)+}$ should be present in an active catalyst for the water gas shift reaction. For this reason it has subsequently been suggested that a readily reducible metal oxide (e.g. Co_3O_4) promoted with gold would also be active for the water gas shift reaction; while a metal oxide that is not readily reducible (e.g. TiO_2) promoted with gold would not be active (Andreeva *et al*, 1998c).

Andreeva *et al* (1998c) investigated the activity of supported gold catalysts based on three different supports, namely Fe_2O_3, Co_3O_4 and TiO_2, all prepared by deposition-

precipitation, which had previously been shown to produce the highest catalytic activity (Andreeva *et al*, 1998a; see Figure 2-2). Three Au/TiO_2 samples were also prepared by the deposition-precipitation method; the first catalyst on freshly prepared titanium hydroxide, the second on commercially available TiO_2 and the third on anatase. Two samples on Co_3O_4 were also prepared, one by deposition-precipitation (DP) on freshly prepared cobalt hydroxide and the other by coprecipitation (COP). The catalytic performance of these materials is presented in Figure 2-4.

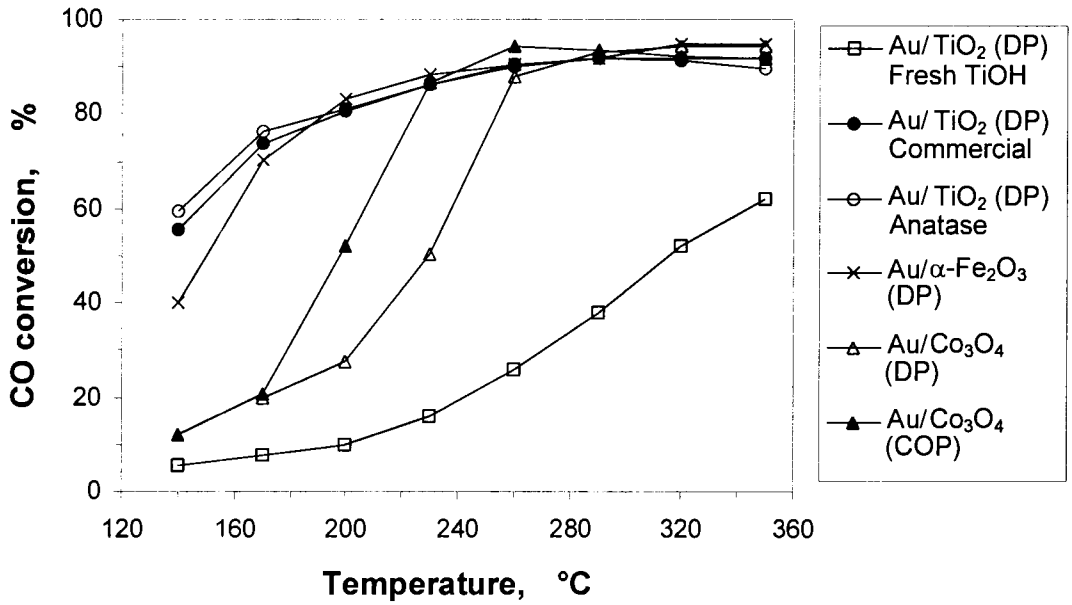

Figure 2-4 : Catalytic activity of Au/TiO_2, $Au/\alpha\text{-}Fe_2O_3$ and Au/Co_3O_4 prepared by various techniques

(Adapted from D. Andreeva *et al*, Bulgarian Chemical Communications, 1998c)

The gold/TiO_2 catalysts prepared on anatase and commercial TiO_2 were found to have the highest catalytic activity at low temperatures, with that on promoted iron oxide similar except below 180°C where performance of the former catalysts were superior. The TiO_2 catalyst prepared by deposition-precipitation on freshly prepared titanium hydroxide showed the lowest activity.

In the case of Co_3O_4, the catalyst prepared by coprecipitation was found to yield higher activity than that prepared by deposition-precipitation, contrary to the results

obtained on Fe_2O_3 (Andreeva *et al*, 1998a). The study also found that non-promoted TiO_2 is inactive for the water gas shift reaction, while non-promoted Co_3O_4 exhibits significant activity between 200 – 360°C.

The Au/Co_3O_4 catalysts were also found to deactivate extremely rapidly. Temperature programmed reduction studies indicated that in the presence of gold, the reduction of Co_3O_4 to elemental cobalt is achieved at approximately 200°C lower than non-gold-promoted Co_3O_4. In the temperature range of the low temperature water gas shift reaction, elemental cobalt, which is inactive for the said reaction, is formed.

In the study by Andreeva *et al* (1998a), the Au/α-Fe_2O_3 catalyst prepared by deposition-precipitation from freshly prepared iron hydroxide yielded an active catalyst, while Au/TiO_2 prepared by the same procedure from the hydroxide equivalent did not. It can be concluded, therefore, that the activity is dependent on the nature of the support.

Similarly, Sakurai *et al* (1997) investigated the influence of preparation procedure on catalyst activity. Au/TiO_2 catalysts were prepared with varying gold loadings and similar gold particle sizes of between 3 and 5 nm by both deposition-precipitation and coprecipitation. In agreement with the work of Andreeva *et al* (1998c), Sakurai and co-workers found that Au/TiO_2 catalyst prepared by coprecipitation was less active than catalyst prepared by deposition-precipitation, despite higher metal loading and smaller particle sizes. Moreover, for the deposition-precipitated Au/TiO_2 catalysts, the activity was found to increase with increasing gold loading in the range 3 – 10 metal wt %.

2.4.7 Water gas shift reaction mechanism on Au/TiO_2

Infrared spectroscopic analysis performed on highly active Au/TiO_2 (anatase) and non Au-promoted TiO_2 catalysts, revealed lower surface concentrations of both hydroxyl and co-ordinated water species on the Au-promoted catalyst surface (Andreeva *et al*, 1998c). The non-promoted material was, however, found to be inactive for the water gas shift reaction. Ilieva *et al* (1997) reported the opposite dependence for iron oxide. Taking into account the associative mechanism previously proposed for the low temperature water gas shift reaction on Au/α-Fe_2O_3 and Au/Co_3O_4, the high

catalytic activity exhibited by the Au/TiO_2 catalyst seems out of place. For this reason, an alternative mechanism has been proposed.

It has been shown that the presence of water enhances the adsorption of CO on the surface of gold particles (Boccuzzi *et al*, 1996). CO is also known to adsorb significantly on TiO_2 (Iizuka *et al*, 1997). It has further been reported that water is dissociatively adsorbed on titanium dioxide. The high dispersion of the gold particles also justifies the assumption of sufficient energy-rich gold atoms at the surface to accommodate both CO and water. Andreeva *et al* (1998c) therefore propose that the water gas shift mechanism on TiO_2, indicated in Figure 2-5, involves the adsorption of CO on the finely divided gold particles and the dissociative adsorption of water onto titanium dioxide, followed by the formation of a formate species and the subsequent product decomposition.

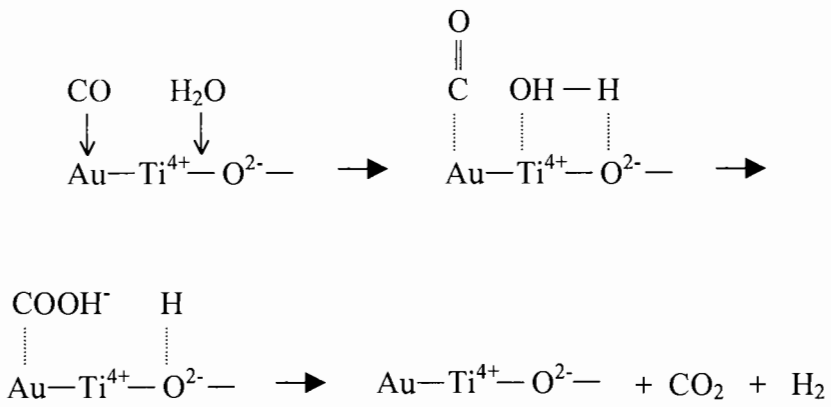

Figure 2-5 : Possible scheme of the WGSR mechanism on Au/TiO_2 catalyst

(Adapted from D. Andreeva *et al*, Bulgarian Chemical Communications, 1998c)

3. OBJECTIVES OF THIS STUDY

Water gas shift is and will remain a crucial industrial reaction for both hydrogen production and chemical synthesis and, with the ever-increasingly stringent allowable pollution levels, for CO emission control as well. Since the discovery of nano-particle gold as a possible catalyst, a number of chemical reactions have been evaluated for the potential of applying gold catalysis. Water gas shift, which is currently catalysed by copper-based catalysts, shows substantial opportunity in this regard. Gold, which occurs in the same group as copper on the periodic table, in theory should exhibit similar chemical properties as that metal, and for this reason it is proposed that gold will exhibit significant water gas shift activity.

Based on the preceding literature review, water gas shift activity is found to occur on gold supported on a range of metal oxides. Previous work on gold catalysed water gas shift has, however, been performed at atmospheric pressure, and neither feed gas compositions nor space velocities resembling those industrially applicable have been used (Andreeva *et al*, 1996a; 1996b; 1998a).

The objectives of this study are to investigate the performance of gold catalysts under industrially applicable conditions, relative to a commercial reference catalyst. Important to this study is, therefore, the accumulation of comprehensive benchmark data.

Moreover, this study on the water gas shift performance of gold-based catalysts seeks answers to the following key questions :

- Can the high activity of gold catalysts for the water gas shift conversion quoted in literature (e.g. Andreeva *et al*, 1996) be reproduced ?
- Can the activity of the commercial LTS catalyst be promoted by gold so as to be active at lower temperatures ?
- Is zinc oxide a suitable carrier for supported gold water gas shift catalysts ?
- How does the metal loading of the gold catalysts affect their activity for water gas shift ?

4. EXPERIMENTAL

4.1 Catalyst Preparation and Characterisation

4.1.1 Catalyst preparation

4.1.1.1 Non-gold loaded catalyst preparation

The industrial high temperature (Fe_2O_3/Cr_2O_3 – Süd-Chemie G-3 C) and low temperature ($CuO/ZnO/Al_2O_3$ – Süd-Chemie C 18-7) shift catalysts were supplied in pellet form, and zinc oxide (ZnO/Al_2O_3 – Süd-Chemie G-72 D) was supplied in extrudate form. For practical purposes, the pellets / extrudates are manually crushed in a mortar and pestle in order to obtain a catalyst particle size range between 300 and 500 μm.

4.1.1.2 Gold loaded catalyst preparation

MINTEK (government / private research laboratories for minerals technology, Randburg, South Africa) performed the preparation of the Au-loaded catalysts. Gold was precipitated onto the various substrates according to the deposition-precipitation method of Haruta (1993), as summarised below.

Commercial catalyst pellets and extrudates are crushed and sieved to obtain a particle size range of between 50 and 425 μm. The crushed metal oxide particles are added to distilled water in a stirred vessel so as to form a dilute slurry, the temperature of which is increased to 70°C and the pH adjusted to 8. Chloroauric acid, dissolved in distilled water to a desired concentration, and 0.1 M Na_2CO_3 is added simultaneously dropwise to the metal oxide slurry maintaining the pH of the slurry at 8, after which the mixture is stirred at 70°C for 1 hour. In certain cases, this procedure is followed by an aging step at room temperature for a further hour. The solid-liquid mixture is filtered and the precipitate washed several times with warm distilled water until no ions are detected in solution as determined by a conductivity meter. The precipitate is dried

overnight under vacuum at 90°C, after which it is calcined in air for 4 hours at either 300°C or 400°C, depending on the support.

The experimental conditions used during the preparation of the Au based catalysts are summarised in Table 4-1. The aim of the preparation programme was to prepare in each series of metal oxides, catalysts with three different Au loadings.

Table 4-1 : Preparation parameters of the various Au loaded catalysts

Sample *	[Substrate] (g/l)	[Au] (g/100g substrate)	[$HAuCl_4.4H_2O$] (M)	Calcination temperature (°C)	Ageing time (hr)
Au/LTS-04	20	1.625	0.066	300	1
Au/LTS-38	10	13	0.066	300	0
Au/LTS-84	20	13	0.066	300	1
Au/HTS-18	20	2	0.0102	400	1
Au/HTS-42	10	13	0.066	400	0
Au/HTS-66	20	13	0.066	400	1
Au/ZnO-06	10	13	0.066	300	0
Au/ZnO-27	20	6.5	0.066	300	1
Au/ZnO-71	20	13	0.066	300	1

* LTS (C 18-7), HTS (G-3 C) and ZnO (G-72 D) denote the substrate on which gold was deposited, while the number following the substrate denotes the gold loading in wt % (i.e. Au/LTS-38 denotes a 3.8 wt % Au loading on commercial C 18-7 low temperature shift catalyst — see also Table 4-2).

4.1.1.3 Commercial Au/Fe_2O_3 toilet deodorisation catalyst preparation

A commercially available catalyst for toilet deodorisation, AUS ($Au/Fe_2O_3/Al_2O_3$), supplied by Süd-Chemie Catalysts Japan Inc. has also been tested for water gas shift activity. This catalyst consists of iron impregnated spherical alumina particles in the size range 2.2 to 4.0 mm, onto which 0.3 wt % Au is loaded by means of a deposition-precipitation method similar to that mentioned previously. This procedure leads to the deposition of gold on the external geometric surface of the catalyst spheres (i.e. egg-shell type loading). Consequently, it is not practicable to obtain a granulate of uniform composition by crushing the commercial pellets. Instead, the commercial sample was sieved to obtain the smallest size fraction possible, viz. 2.2 – 2.8 mm spheres, and was tested as whole spheres.

4.1.2 Catalyst characterisation

4.1.2.1 Catalyst composition

A chemical analysis was performed by MINTEK (Physical Metallurgy Division, Randburg, South Africa) on the prepared catalysts to ascertain the gold loading and other metal contents. The results are shown in Table 4-2, along with the calculated compositions of the non-gold loaded commercial catalysts as determined from the manufacturers' specifications for the various materials.

It can be noted that the metal weight ratio of Cu/Zn in the commercial LTS catalyst is 0.89, and for the gold loaded equivalents this weight ratio ranges between 0.81 and 0.94. The Fe/Cr weight ratio in the commercial HTS catalyst is 11, with the gold loaded HTS catalysts ranging between 14 and 16. These differences, by and large, may be attributed to analytical experimental error and do not necessarily represent real differences in support composition. In contrast, the Zn/Al weight ratio in the commercial ZnO catalyst is calculated to be 14, while those determined for the Au/ZnO catalysts are between 36 and 45. A certain amount of Al leaching in the alkali medium appears to have taken place during the deposition of gold on this support. This difference, however, is not thought to significantly affect the performance of these catalysts.

Table 4-2 : Composition (metal content) of the catalysts

Sample	Specific Metal Content, wt %					
	Au	Cu	Fe	Zn	Cr	Al
LTS (C 18-7) *	—	33.6	—	37.8	—	5.3
HTS (G-3 C) *	—	1.6	62.3	—	5.5	—
ZnO (G-72 D) *	—	—	—	72.3	—	5.3
AUS *	0.3	—	unknown	—	—	unknown
Au/LTS-04	0.4	30.1	—	35.8	—	4.5
Au/LTS-38	3.8	27.9	—	29.6	—	4.6
Au/LTS-84	8.4	25.4	—	31.4	—	3.9
Au/HTS-18	1.8	—	50.8	—	3.7	—
Au/HTS-42	4.2	—	56.9	—	3.6	—
Au/HTS-66	6.6	—	50.4	—	3.4	—
Au/ZnO-06	0.6	—	—	68.3	—	1.9
Au/ZnO-27	2.7	—	—	62.9	—	1.4
Au/ZnO-71	7.1	—	—	56.4	—	1.3

* Metal content of these catalysts was not determined by analysis, but rather by calculation from manufacturers' specifications, calculated to a 100 % balance on an oxide basis.

4.1.2.2 Catalyst particle size

Insufficient gold loaded catalyst was available in the desired particle size range of 300 – 500 microns. As a consequence, the particle size range for all catalysts tested is not the same, and Table 4-3 lists the actual catalyst particle size ranges tested.

Table 4-3 : Catalyst particle size range tested

Sample	Catalyst Particle Size (μm)
LTS (C 18-7)	300 – 500
HTS (G-3 C)	300 – 500
ZnO (G-72 D)	300 – 500
AUS	2200 – 2800
Au/LTS-38	100 – 250
Au/HTS-42	250 – 425
Au/ZnO-06	150 – 425
Au/ZnO-27	150 – 425
Au/ZnO-71	150 – 425

4.1.2.3 Gold particle size

MINTEK performed secondary and back-scattered images for one gold loading of each of the various metal oxide supports, namely Au/LTS-04, Au/HTS-18 and Au/ZnO-27. Although relatively unclear, gold particles between 300 and 500 nm in size (and larger) are discernible in the back-scattered image of Au/HTS-18 (Figure 4-1), however, the magnification on the images does not allow for smaller particles to be seen.

A series of transmission electron microscopy (TEM) micrographs, shown in Figures 4-2 to 4-5 were taken of the non-gold loaded and gold loaded ZnO materials (i.e. ZnO, Au/ZnO-06, Au/ZnO-27 and Au/ZnO-71 respectively). Although not particularly clear in the scanned images of Figures 4-2 to 4-5, the original micrographs distinctly show the nanometer sized Au particles.

On the Au deposited zinc oxide, small gold particles in the 3 – 6 nm size range generally considered necessary for catalytic activity (Haruta, 1997b) are visible — increasing in number as the wt % Au loading increases. The same is true for the Au/LTS and Au/HTS catalysts.

Therefore, both large (100 nm +) and small (3 – 6 nm) Au particles are known to be present on the metal oxide supports. Furthermore, the limited number of micrographs taken does not allow for a quantitative statement on the relative dispersion of Au metal.

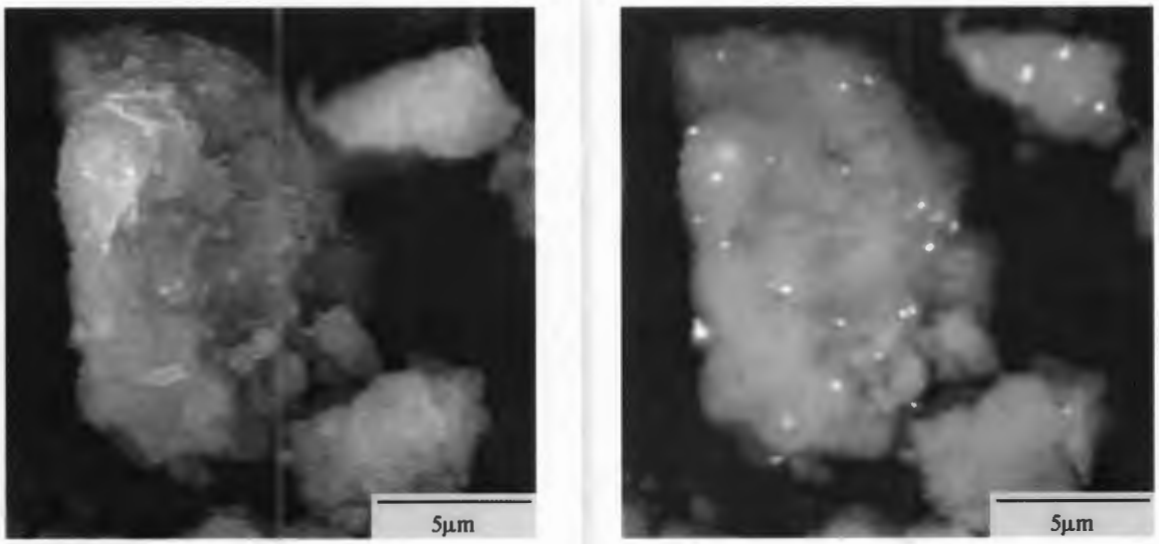

Figure 4-1 : Secondary and back-scattered images of Au/HTS-18

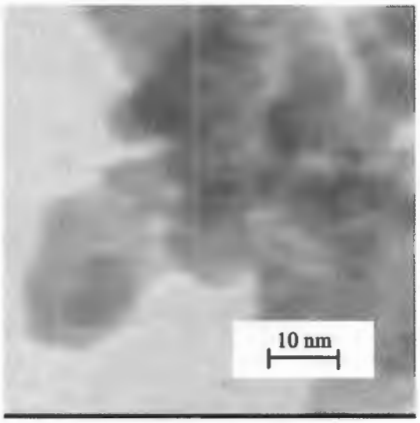

Figure 4-2 : TEM of ZnO

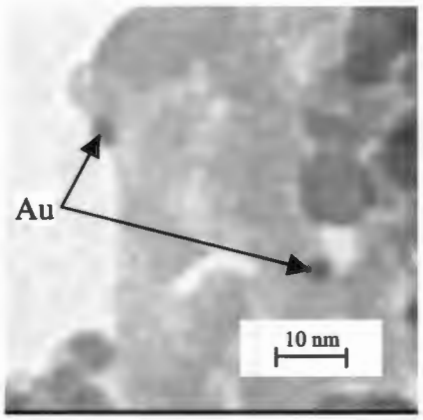

Figure 4-3 : TEM of Au/ZnO-06

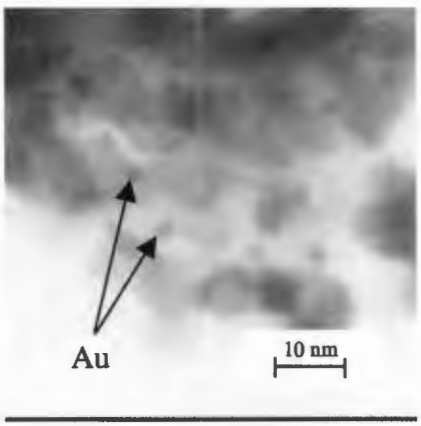

Figure 4-4 : TEM of Au/ZnO-27

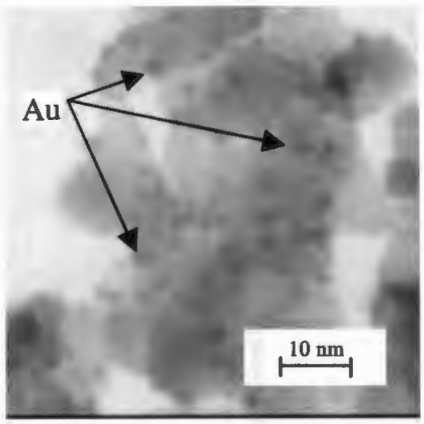

Figure 4-5 : TEM of Au/ZnO-71

4.2 Experimental Apparatus

A diagrammatic flowsheet of the steady state, continuous flow experimental apparatus constructed and used is shown in Figure 4-6. It consists of a down-flow packed bed reactor (PBR) preceded by a feed delivery system including a water evaporator for steam delivery and followed by a steam condenser to remove water prior to system depressurisation via a back-pressure regulator. A summary for the major components of the system follows, including a description of how these units are integrated.

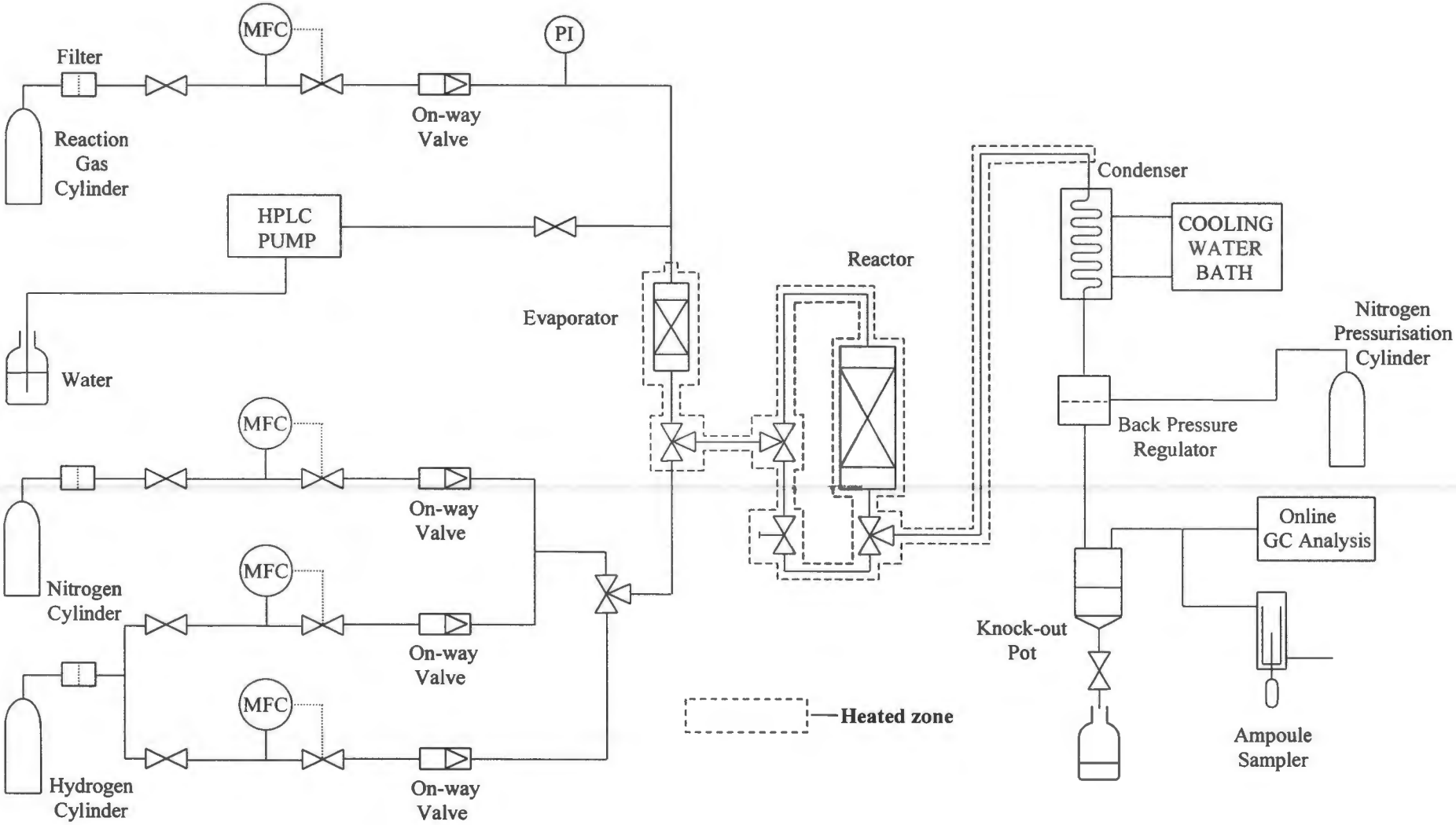

Figure 4-6 : Flowsheet of the experimental apparatus

4.2.1 Evaporator

A premixed reaction dry gas, supplied from a cylinder and the flowrate of which is controlled by a mass flow controller (Brooks Instruments, 5850 TR Series), is mixed with water, delivered by means of an isocratic HPLC pump (Spectrachrom, Series II Isocratic Pump), at the entrance of a packed bed down-flow evaporator. The evaporator is packed with 2 mm diameter glass beads, which have been thoroughly cleaned. A temperature gradient, produced by uneven coiling of heating tape around the vessel, ensures a steady evaporation of the entering water. After exiting the evaporator, a completely mixed steam/dry gas vapour phase feed of the desired composition flows to the reactor.

4.2.2 Reactor

Certain feed / product lines before and after the reactor (shown by the dotted region in Figure 4-6) are heated to prevent water condensation. This is achieved using coiled heating tape controlled by temperature controllers.

The reactor consists of an approximately 32 cm long stainless steel tube with an internal diameter of approximately 15 mm and is operated in down-flow mode. It incorporates a thermowell of outer diameter 3 mm, running down the entire length of the vessel, positioned axially in the reactor. The reactor includes an external aluminium heat sink which fits snugly in a heating furnace — an arrangement to maximise heat transfer and thus to ensure the required isothermal conditions. The reactor temperature is controlled close to the outside of a ceramic jacket surrounding the aluminium jacket. The reactor has been found to be isothermal down the entire length of the bed. [Refer to *Appendix IV* for a diagrammatic representation of the reactor.]

The reactor and thermowell dimensions yield an effective bed volume of approximately 1.9 cm^3 per cm of bed length. 0.75 g of the catalyst is diluted in 4.5 cm^3 of an inert silicon carbide packing (yielding a 7:1 dilution on a volume basis), taking up an effective length of approximately 2.5 cm in the reactor. The diluted catalyst zone and the silicon carbide packing zones are compacted by gently tapping the vessel. A 35 cm^3 inert packing volume (serving as a pre-heating zone) and a

20 cm^3 inert packing volume are filled above and below the catalyst bed, respectively. The reaction zone and upper and lower heating zones are separated from one another by a thin packing of silane treated glass wool. Both the upper and lower ends of the reactor are also closed off with silane treated glass wool to keep the packing in place. Figure 4-7 shows the packing of the various materials within the reactor.

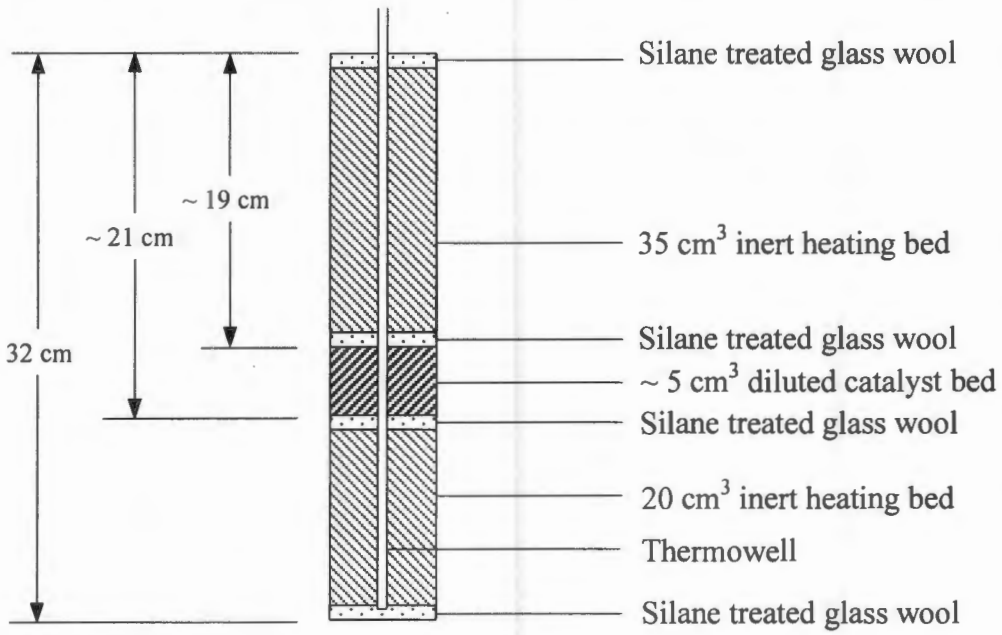

Figure 4-7 : Diagrammatic representation of the reactor packing

Due to the moderate exothermic nature of the water gas shift reaction, the actual catalyst bed is also diluted with the inert packing — in such a way as to limit a temperature gradient within the catalyst bed as far as possible. Silicon carbide granulate (size fraction of 200 – 400 μm), with a tapped bulk density of approximately 1.7 g/cm^3, has been used as the inert material.

4.2.3 Condenser

The excess / unconverted steam is condensed after the reactor yielding a dry gas product for analysis. The condenser consists of a jacketed 3 m long × 1/8 inch (OD) coil, with an approximate volume of 15 cm^3, operating in down-flow mode through which the reactor product is passed, cooled by a water-ethylene glycol solution circulating at 1°C outside. The water is expelled from the condenser to the back-pressure regulator under gravity and flow. The condenser is designed to have a residence time of between 1 and 2 minutes (depending on the space velocity applied).

4.2.4 Back-pressure regulator

The system is held at pressure by means of a back-pressure regulator (Grove Valve & Regulator Co.) positioned after the condenser. It is operated in two phase down-flow mode (since it can not be heated) — the water is slowly discharged past the diaphragm along with the gas. A cylinder of nitrogen is used to provide the back-pressure to the diaphragm.

A sealed glass vessel, which also contains a cooling coil through which the coolant at 1°C is circulated, acts as a water knock-out pot. It is positioned after the back-pressure regulator and collects the liquid dripping from that device, while allowing the gas to escape. This pot is emptied on a daily basis. Calculations have been performed to ensure that the loss of gas (in particular CO_2) by dissolution into the water in the knock-out pot does not significantly alter the gas composition analysis (see *Appendix V*).

4.2.5 Adaptations for sampling

Two 3-way switching valves, one positioned before and the other positioned after the reactor, are used to allow bypass (unconverted) samples to be taken. High temperature valves, able to withstand temperatures of above 200°C, are needed for this application — because of the heated lines preventing condensation. The

composition of the product dry gas is determined using on-line gas chromatography equipped with a thermal conductivity detector. (A complete description of the gas chromatography apparatus and sampling technique can be found in section *4.5.1 Gas chromatography*.)

An ampoule sampling device is also set up on the experimental rig in order to take off-line samples if necessary.

4.2.6 Adaptations for catalyst reduction

Catalyst reduction is performed on-line using a combination of hydrogen and nitrogen gas (see section *4.4.2 Catalyst activation / reduction* for a description of this procedure). The volumetric flowrates of the individual reduction gases, supplied from gas cylinders, are controlled by means of mass flow controllers (Brooks Instruments, 5850 TR Series), two controllers for H_2 and one for N_2 as shown in Figure 4-6. A 3-way valve, positioned between the evaporator and reactor, allows either the steam / gas mixture or the reduction gases to be passed to the reactor.

4.3 Experimental Operating Conditions

4.3.1 Standard conditions

Preliminary experiments indicated a decay in the initial activity of the fresh commercial LTS catalyst. After a 'bedding-in' period, the catalyst performance attains a pseudo-steady state, after which time negligible activity loss is observed with further time on stream. (This observation is discussed in detail in section *5.1.2 Initial deactivation of fresh catalysts*.) Consequently, prior to the commencement of all catalyst performance tests, the catalyst is run at a constant set of "standard" conditions until the apparent pseudo-steady state is reached. These standard conditions are presented in Table 4-4. The standard conditions are returned to

at intermediate periods throughout the temperature-conversion data accumulation to confirm that no further catalyst deactivation has occurred.

Table 4-4 : Standard conditions

$SGHSV_{dry}$ *	10000 hr^{-1}
$WHSV_{dry}$ **	4.0 hr^{-1}
Steam / Dry Gas Ratio	1
Pressure	20 barg
Temperature	192°C

* $SGHSV_{dry}$ denotes the gas hourly space velocity for the dry reaction gas under standard temperature of 273 K and pressure of 1 atmosphere for the commercial LTS catalyst only.

** $WHSV_{dry}$ denotes the corresponding weight hourly space velocity of the dry reaction gas for the catalysts at STP.

The various catalyst deactivation experiments are carried out at the same dry gas WHSV, which corresponds to a $SGHSV_{dry}$ of 10000 hr^{-1} for the commercial LTS catalyst. Because the catalyst bed is diluted with inert silicon carbide, the catalyst volume for the space velocity calculations is not taken as total volume of the catalyst packing zone, but rather as the volume occupied by the actual catalyst as determined from the packed bulk density measurements. The packed bulk density of the commercial LTS catalyst, crushed to the desired size range listed in Table 4-3, is found to be approximately 1.15 g/cm^3. Table 4-5 lists the correlation between the $SGHSV_{dry}$ for the commercial LTS catalyst and the corresponding $WHSV_{dry}$ for the both the commercial and gold loaded catalysts.

Table 4-5 : Relation between gas hourly and weight hourly space velocities

$SGHSV_{dry}$	(ml dry gas / ml LTS catalyst . hour)	5000 hr^{-1}
$WHSV_{dry}$	(gram dry gas / gram catalyst . hour)	2.0 hr^{-1}
$SGHSV_{dry}$	(ml dry gas / ml LTS catalyst . hour)	10000 hr^{-1}
$WHSV_{dry}$	(gram dry gas / gram catalyst . hour)	4.0 hr^{-1}

4.3.2 Reaction conditions for performance evaluation

After the initial deactivation period, the WGS performance of the various catalysts is investigated across a range of operating conditions — most notably, temperature and space velocity.

4.3.2.1 Temperature

The catalyst performance evaluation is conducted in the temperature range between 188°C and 204°C (with measurements taken in increments of 4°C), or sometimes higher if no / low CO conversion is observed in this range.

At the experimentally applied steam : dry gas ratio of 1 and pressure of 20 barg, water condenses at 180°C. Consequently, 188°C is considered the lowest practical operating temperature for testing, as care has to be taken to avoid condensation — a major cause of LTS catalyst deactivation (Twigg, 1989).

4.3.2.2 Pressure

In general, the experiments are carried out at 20 barg. Other experiments performed to investigate the effect of pressure on the water gas shift activity of gold catalysts utilise pressures of between 10 and 25 barg.

4.3.2.3 Space velocity

Water gas shift is performed at a standard gas hourly space velocity of approximately 4000 hr^{-1} on a dry basis industrially (Kirk-Othmer, 1995). Consequently, it was decided to test the commercial LTS catalyst at dry gas (i.e. gas without water vapour) gas hourly space velocities between 5000 hr^{-1} and 15000 hr^{-1} measured at STP. This is to ensure that, as far as possible, the conversion is not equilibrium limited. For comparison purposes, experiments are performed on a basis of catalyst weight — i.e. catalysts are compared on the basis of constant $WHSV_{dry}$.

For the LTS catalyst, temperature-conversion data has been collected at three $WHSV_{dry}$, viz. at 2.0 hr^{-1}, 4.0 hr^{-1} and 6.0 hr^{-1}, corresponding to $SGHSV_{dry}$ of 5000, 10000 and 15000 hr^{-1} respectively. $WHSV_{dry}$ of 2.0 hr^{-1} and 4.0 hr^{-1}, only, have been applied for the gold loaded catalysts. Due to different catalyst bulk densities, these $WHSV_{dry}$ correspond, only nominally, to $SGHSV_{dry}$ of 5000 and 10000 hr^{-1}.

4.3.2.4 Steam : dry gas ratio

On recommendation of the industrial catalyst supplier, three steam : dry gas ratios of 0.5, 1 and 1.5 (mol/mol) have been tested for the commercial LTS catalyst. It was, however, decided that two dry gas weight hourly space velocities for the gold containing catalysts only need be tested at a constant steam : dry gas ratio of 1.

Preliminary experiments at the higher and lower steam : dry gas ratios indicate an apparent catalyst deactivation thought to be associated, respectively, with H_2O condensation and carbon deposition (see Figure 5-2 in section *5.1.3 Effect of steam : dry gas ratio on catalyst stability*). This has resulted in the standard ratio of 1 being applied for all experiments.

4.4 Experimental Operating Procedures

4.4.1 Catalyst loading procedure

The catalyst loading procedure is performed identically for all the different catalysts, so that flow patterns and temperature zones within the reactor are not altered. The reactor loading is carried out from top-to-bottom with respect to its functioning down-flow orientation (see *Appendix IV* for a diagrammatic representation of the reactor). This involves mounting the reactor in an inverted (upside-down) orientation in a bench vice, and sequential loading of the various packed layers with the top, preheat zone, loaded first.

Silane treated glass wool, which acts as a separation between the catalyst and packing layers as well as a barrier on the two extremities, is filled into the reactor with a metal tube until a firm layer is formed. The first inert packing of 35 cm^3 (measured in a measuring cylinder by tapping until compact) is filled into the reactor by means of a funnel. After each granular layer is added to the reactor, the external reactor wall is gently tapped for approximately 1 minute to ensure that that layer is completely compact. This is followed by a separating layer of silane treated glass wool. The catalyst and diluting silicon carbide (1 : 7 on a volume basis) are accurately measured, mechanically mixed with a spatula and then funneled into the reactor. Thereafter, another layer of inert material (20 cm^3) is added, following the same procedure explained above. The layout of packing in the reactor can be seen in Figure 4-7.

4.4.2 Catalyst activation / reduction

The catalyst-loaded reactor is inserted into the heating furnace and then connected to the entering and exiting gas lines. A leak test is performed at approximately 10 barg using N_2 gas, which also serves to purge the reactor and connecting gas lines of air. The leak test is usually performed approximately 2 hours prior to commencement of a run; thereafter, the system is depressurised back to atmospheric pressure. Pressurisation of the system occurs at approximately 2 bar per minute. Inlet and outlet connecting lines

are traced separately with heating tapes. The reduction procedure utilises both hydrogen (99.999 % purity, < 2 ppm H_2O and < 3 ppm O_2) and nitrogen (99.995 % purity).

The catalyst reduction procedure is performed consistently for all catalysts as follows:

- A dilute reduction gas mixture, 2 vol % H_2 in inert N_2, is fed to the reactor at atmospheric pressure and a high flowrate of 120 standard cubic centimetres per minute (SCCM), equivalent to a $SGHSV_{dry}$ of approximately 11000 hr^{-1}.
- The temperature of the reactor is ramped at a heating rate of 1°C per minute from ambient temperature to 204°C, and held at this temperature for 16 hours.
- Finally, the reactor feed is changed to pure H_2 at 80 SCCM for 1 hour, to complete the reduction procedure.

4.4.3 Reaction / reactor operation

4.4.3.1 Dry gas composition

Two cylinders containing the reaction gas mixture (dry gas) of hydrogen, nitrogen, carbon monoxide and carbon dioxide, supplied by Messer Fedgas, have been used during the experimental programme. The gas mixtures are made up to approximate the actual gas composition of the feed to the low temperature shift stage in industry. Nitrogen (approximately 2 vol %) is included as an internal standard in the mixture, since argon is used as the carrier gas for gas chromatographic analysis of feed and product streams. Table 4-6 shows the Messer Fedgas analysis of the two reaction gas mixtures.

Table 4-6 : Dry gas composition

Component	Mixture 1 (vol %)	Mixture 2 (vol %)
Hydrogen	78.3	77.9
Nitrogen	1.7	1.9
Carbon Monoxide	2.9	2.9
Carbon Dioxide	17.1	17.3

4.4.3.2 Start-up procedure

- The reduction procedure as detailed in section *4.4.2 Catalyst activation / reduction* is followed for all catalysts.
- At the completion of the 1 hour pure H_2 reduction step, reduction gas is switched off.
- The 3-way valves before and after the reactor are set to the bypass mode, followed by the commencement of flow of the reaction gas (excluding H_2O).
- Directly thereafter, the heating of the evaporator is initialised. A controller setting of approximately 210°C at the bottom generates the desired temperature profile — a temperature below 180°C (the condensation temperature of water at 20 barg, S/DG = 1) at the top/entrance of the evaporator, and above that temperature at the bottom/exit of the evaporator. Typical inlet and exit temperatures are 150°C and 210°C respectively.
- All heated lines indicated in Figure 4-6 are maintained well above the condensation temperature, typically in the range 210 – 220°C.
- Cooling of the reactor to the desired run starting temperature of 192°C is begun (i.e. conditions mentioned in section *4.3.1 Standard conditions*).
- After purging the lines of N_2 and after the evaporator has reached the desired temperature (i.e. after approximately 5 minutes), the system is slowly pressurised to 20 barg. This operation takes approximately 20 minutes. The water pump is then started and the water line valve opened.
- The system is kept on bypass until the deionised water (18 MΩ/cm) has sufficiently penetrated the system. In this way, conditions of minimal H_2O in the reactor are prevented — a condition which is found to cause deactivation of the catalyst.

- After approximately 10 minutes, the two 3-way valves are switched to pass the steam/feed gas mixture to the reactor and careful adjustment of the pressurisation line to the back-pressure regulator is made to obtain a pressure of 20 barg within the system.

4.4.3.3 On-line procedures

The procedures mentioned below are followed when changing from one condition to another. After changing a condition, a time interval of at least 2 hours is allowed to elapse before a sample is taken — this is to allow the system to re-stabilise.

Temperature

- When changing the temperature in the reactor from a lower to a higher level, the temperature is ramped at 1°C per minute.
- When reducing the temperature, the lower desired set-point is set and the reactor allowed to cool naturally.

Pressure

- When pressurising the system (done when taking the system to 25 bar during the pressure effect test), the back-pressure regulator is pressurised from the N_2 cylinder. Care has to be taken during this operation, since at the increased pressure the condensation temperature of water increases to approximately 189°C.
- When decreasing the pressure in the reactor, the N_2 line pressurising the diaphragm in the back-pressure regulator is slowly vented to the atmosphere until the desired pressure is reached.

Space velocity

- When changing the space velocity, both the gas and water feed rates have to be adjusted accordingly such that a steam : dry gas ratio of 1 is maintained.
- Upon increasing and decreasing space velocity, the dry gas and water flowrates, respectively, are adjusted first to avoid any possibility of condensation in the system or on the catalyst.

4.4.3.4 Shut-down procedure

- After completion of the experimental run, the water pump is switched off and the necessary valves to the system closed, and slow depressurising of the system is initiated while keeping the reactor at temperature.
- Sufficient time, typically 1 hour, is allowed to elapse before suspending the dry feed gas flowrate in order to ensure the complete removal of H_2O from the system.
- Finally, the heating to the reactor and gas lines are switched off; about 5 hours is needed to cool the reactor to a manageable temperature before the catalyst can be unloaded.

4.5 Feed and Product Gas Analysis

4.5.1 Gas chromatography

4.5.1.1 Sampling procedure

The sampling is achieved by means of an on-line 6-way gas sampling valve. During general operation of the experimental apparatus, the water-free product gas is passed to the gas chromatograph, where it enters the 6-way valve and is directly vented, while the argon carrier gas passes through the sample loop. When sampling, the 6-way valve is switched in such a way as to allow the product gas to pass through the sample loop. After waiting for approximately 30 seconds to allow the product gas to completely flush the sample loop, the valve is switched back to the starting position, where the argon carrier gas transports the sample to the column.

After adjusting any of the reactor operating conditions, an approximately 2 hour wait is required to allow the system to re-stabilise prior to product stream analysis.

The above procedure is repeated approximately 5 times at each sampling condition in order to obtain an average analysis suitably free from sampling errors.

4.5.1.2 Chromatographic conditions

The gas composition is determined using a Varian 3300 Gas Chromatograph (GC) fitted with a thermal conductivity detector (TCD), in conjunction with a Varian 4400 Integrator. The GC is fitted with a Carbosieve S-II column (supplied by Supelco), specifically set up for CO/CO_2 analysis. Table 4-7 lists the column characteristics and GC settings. Under the conditions listed in Table 4-7, all the various components of the gas sample elute within 10 minutes. Argon (Messer Fedgas, 99.999% purity) is used as the inert carrier gas. Gas samples are introduced into the GC by means of an on-line gas sampling valve fitted with an 875 µl sample loop.

Table 4-7 : Gas chromatograph conditions

Column length	10 feet
Column diameter (OD)	⅛ inch
Column material	Stainless steel
Column packing	Carbosieve S-II
Injector port temperature	150 °C
Column temperature	150 °C
Detector temperature	250 °C
Argon flowrate	30 ml(STP)/min

4.5.1.3 Chromatographic analysis and calibration

Figure 4-8 shows a typical chromatogram of the inorganic gas analysis, while Table 4-8 lists the residence times of the individual gaseous components. The species responsible for each peak has been indicated on the diagram for convenience. As shown in Figure 4-8, a depression of the baseline occurs upon sample introduction as a result of the sample loop being at lower pressure (atmospheric) than the argon carrier (66 psig). Baselines used for interpretation are also shown in the figure.

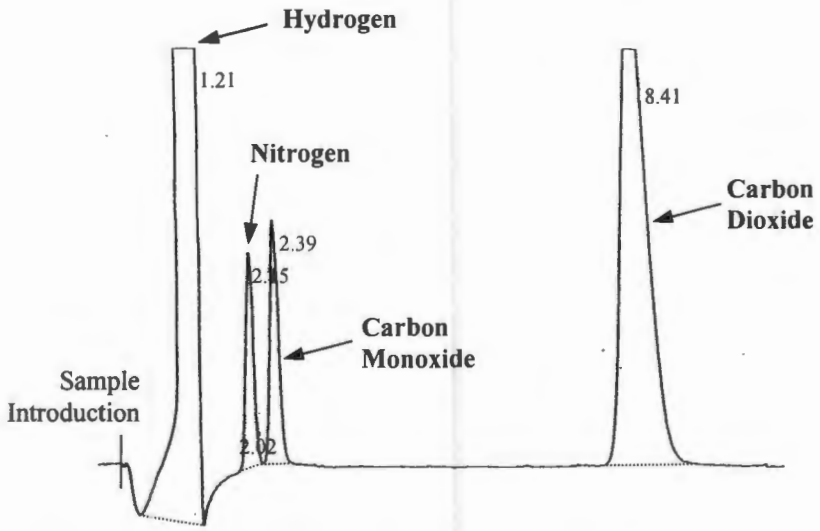

Figure 4-8 : A typical chromatogram of the dry gas analysis

Table 4-8 : Component retention times

Component	Retention Time (minutes)
Hydrogen	1.21
Nitrogen	2.15
Carbon Monoxide	2.39
Carbon Dioxide	8.41

* Baseline re-correction occurs at approximately 2.02 minutes

The GC-TCD analytical approach is favoured over infrared detection since it allows for detection of hydrogen, nitrogen and methane in addition to the carbon oxides.

4.5.2 Data work-up

Although water gas shift is a balanced equimolar reaction (i.e. for every molecule of reactant consumed, a molecule of product is formed), conversion of CO cannot be determined directly from CO concentration in the analysed samples. The flowrate of the product stream after the condenser is dependent on conversion, since at high conversion, more water (which is removed) is converted to unremoved hydrogen. Thus, as conversion increases, the total dry gas flowrate after the condenser increases, with the direct consequence that the 'relative concentration' of CO in the sample decreases. The directly calculated conversion (shown as equation 4-1) is therefore higher than that actually obtained. Since the feed dry gas contains only 2.9 % CO, this adjustment typically changes the uncorrected conversion calculated only by between 0 and 0.6 percentage points, however, for correctness, it has been included.

For the procedures below, all composition data is determined on a dry gas basis.

$$X_{CO} = \frac{F_{CO,feed} - F_{CO,product}}{F_{CO,feed}} \times 100\ \% \qquad \textbf{eqn 4-1}$$

$$X_{CO} = \frac{x_{CO,feed} \cdot F_{DRY,feed} - x_{CO,product} \cdot F_{DRY,product}}{x_{CO,feed} \cdot F_{DRY,feed}} \times 100\ \% \qquad \textbf{eqn 4-2}$$

For a normalised initial total dry gas flowrate ($F_{DRY,feed}$) of 100 mol/s in the feed and a known composition (e.g. 2.9 % CO in dry gas mixture 1, or $x_{CO,feed} = 0.029$, listed in Table 4-6), equation 4-2 simplifies to equation 4-3.

$$X_{CO} = \frac{2.9 - x_{CO,product} \cdot F_{DRY,product}}{2.9} \times 100\ \% \qquad \textbf{eqn 4-3}$$

Taking into account the change in $F_{DRY,product}$ as a function of conversion, CO conversion is determined according to equation 4-4.

$$X_{CO} = \frac{2.9 - x_{CO,product} \cdot \left(100 + 2.9 \times \left(\frac{X_{CO}}{100}\right)\right)}{2.9} \times 100\ \% \qquad \textbf{eqn 4-4}$$

A calibration curve was developed for CO, CO_2 and H_2, relating the integrated peak area count obtained from the gas chromatogram to the mole fraction of the respective component in the sample loop.

At high CO conversions (i.e. when the dry gas consisted of less than 0.7 mol % CO or greater than 76 % CO conversion occurred), the calibration curve became non-linear, due mainly to a relatively large integration error associated with the small CO peak relative to the noise signal. Consequently, under these conditions, the CO conversion was determined by back-calculation from the increase in CO_2 and assuming a 100 % carbon balance using an equivalent calculation to equation 4-4, shown in equation 4-8.

$$F_{CO_2,product} = F_{CO_2,feed} + F_{CO,feed} \cdot \frac{X_{CO}}{100} \qquad \textbf{eqn 4-5}$$

$$X_{CO} = \frac{F_{CO_2,product} - F_{CO_2,feed}}{F_{CO,feed}} \times 100\,\% \qquad \textbf{eqn 4-6}$$

$$X_{CO} = \frac{x_{CO_2,product} \cdot F_{DRY,product} - 17.1}{2.9} \times 100\,\% \qquad \textbf{eqn 4-7}$$

$$X_{CO} = \frac{x_{CO_2,product} \cdot \left(100 + 2.9 \times \left(\frac{X_{CO}}{100}\right)\right) - 17.1}{2.9} \times 100\,\% \qquad \textbf{eqn 4-8}$$

A carbon balance, based on the calculated molar flowrates for CO and CO_2, has been performed, where possible, on the dry gas product and is provided for all analyses in *Appendix II* from which it can be seen that carbon balances were generally in the range 98 – 102 %. Consequently, the assumption of 100 % carbon balance for X_{CO} determination by back-calculation from CO_2 analyses is justified at high CO conversion.

The linearity of the detector calibrations for the other components were found not to change over the experimental range. This was aided by the fact that the carbon dioxide and hydrogen concentrations in the feed were high, and therefore did not change significantly (even after high CO conversion).

5. RESULTS

For convenience, *Appendix I* takes the form of a fold-out reference table containing both catalyst and experimental run data for the complete experimental programme. It is suggested that this appendix be used simultaneously with Chapters 5 and 6 to provide the reader with a simple reference to experimental conditions associated with the results presented in these chapters. Furthermore, the complete tabulated experimental and worked-up data is presented in *Appendix II*.

Table 5-1 below lists the experimental runs performed on the various catalysts and the various experimental conditions. All experiments were first carried out at standard conditions, namely temperature of 192°C, $WHSV_{dry}$ of 4.0 hr^{-1} and steam : dry gas ratio of 1 (see Table 4-5), unless otherwise specified.

Table 5-1 : Summary of experimental runs

Experiment Number	Catalyst Tested	Experimental Conditions			
		S / DG	$WHSV_{dry}$ (hr^{-1})	Pressure (barg)	Temperature (°C)
1	LTS	0.5	4.0	20	192
2	LTS	1.5	4.0	20	192
3	LTS	1.0	4.0	20	192
4	LTS	1.0	2.0, 4.0, 6.0	20	188 - 204
5	Au/LTS-38	1.0	2.0, 4.0	20	188 - 200
6	Au/HTS-42	1.0	2.0, 4.0	20	192 - 240
7	Au/ZnO-27	1.0	2.0, 4.0	20	188 - 204
8	Au/ZnO-71	1.0	2.0, 4.0	20	188 - 200
9	Au/ZnO-06	1.0	2.0, 4.0	20	188 - 200
10	ZnO	1.0	4.0	20	192 - 220
11	AUS	1.0	2.0, 4.0	20	192 - 320
12	LTS	1.0	4.0	10, 15, 20, 25	204
13	Au/ZnO-27	1.0	2.0	10, 15, 20, 25	204

Due to the nature and length of the individual experiments, it was decided to investigate the influence of gold deposited on the various metal oxides at the intermediate loading of between 2.5 and 4 wt % Au (depending on the availability of the catalyst). Only for the most promising of the gold catalysts, viz. Au/ZnO, has the effect of loading been studied. Three gold loadings were investigated, viz. 0.6, 2.7 and 7.1 wt % Au. The copper-zinc and the iron oxide catalysts tested have loadings of 3.8 and 4.2 wt % Au respectively.

5.1 Preliminary Findings

5.1.1 Carbon balance

The carbon balance was found to be accurate within 100 ± 2 % throughout the conversion range (see *Appendix II* for data). This justifies the use of a 100 % carbon balance in determining the degree of CO conversion via back-calculation from CO_2 data above 76 % CO conversion (see section *4.5.2 Data work-up* for full details on conversion calculations).

5.1.2 Initial deactivation of fresh catalysts

Early experiments with the commercial LTS catalyst displayed an initial period of approximately 2 – 3 days during which the fresh catalyst activity declines relatively strongly. After this "bedding-in" period, the catalyst performance reaches a pseudo-steady state during which time activity declines negligibly with further time-on-stream. Similarly, this initial activity decline is found to occur for the other gold and non-gold loaded catalysts — usually between 30 and 60 % loss in initial CO conversion, measured under standard conditions.

Consequently, all catalysts were kept at constant "standard" conditions (i.e. $WHSV_{dry}$ of 4.0 hr^{-1}; steam : dry gas ratio of 1, pressure of 20 barg and temperature of 192°C)

for between 24 and 72 hours to achieve pseudo-steady state behaviour after which experimental conditions are varied and performance data collected. In order to confirm pseudo-steady state behaviour during data collection, all experiments include intermediate periods at standard conditions to evaluate the steady state performance.

Figure 5-1 shows an example of conversion as a function of time-on-stream for the commercial LTS catalyst, highlighting the initial deactivation at standard conditions, activity measurements at various temperatures, and intermediate evaluations at standard conditions to confirm pseudo-steady state activity.

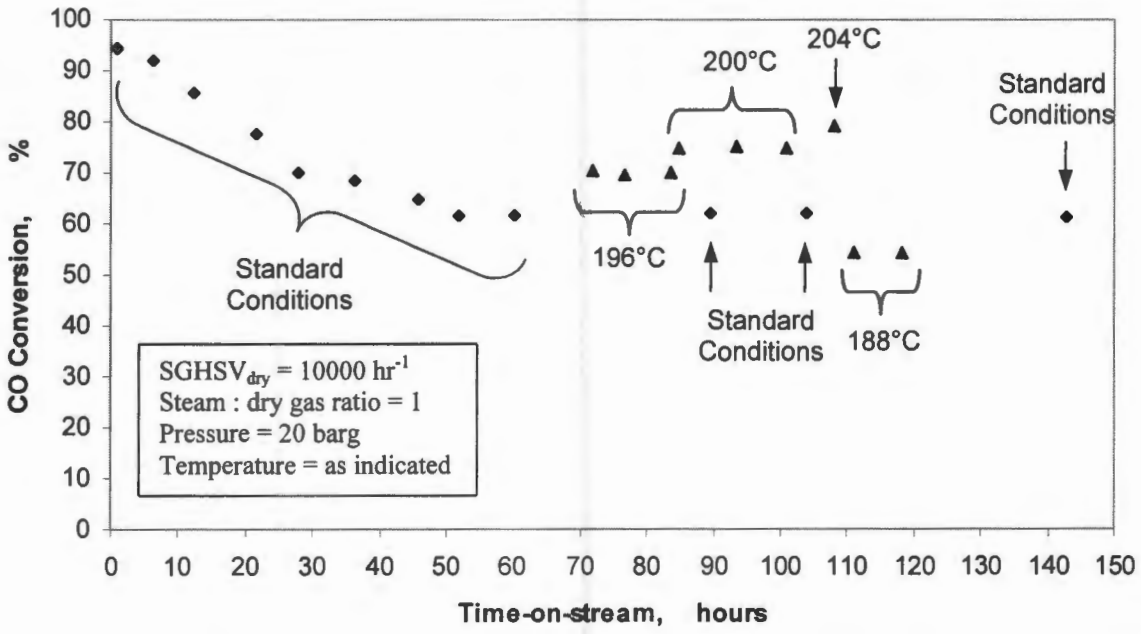

Figure 5-1 : Time-on-stream performance of commercial LTS catalyst under both standard and experimental conditions (experiment 4)

5.1.3 Effect of steam : dry gas ratio on catalyst stability

The ratio of steam to dry gas is known to influence both the equilibrium and the kinetics of water gas shift. Three ratios have initially been investigated, namely 0.5, 1 and 1.5 (experiments 1, 3 and 2 respectively). Figure 5-2 shows the performance of the commercial LTS catalyst as a function of steam : dry gas ratio. These investigations have been performed prior to instituting the 'standard' conditions for the attainment of pseudo-steady state, and therefore the ratio of 0.5 and 1.5 have been performed at a space velocity of 5000 hr^{-1}, whereas the ratio of 1 was conducted at 10000 hr^{-1}.

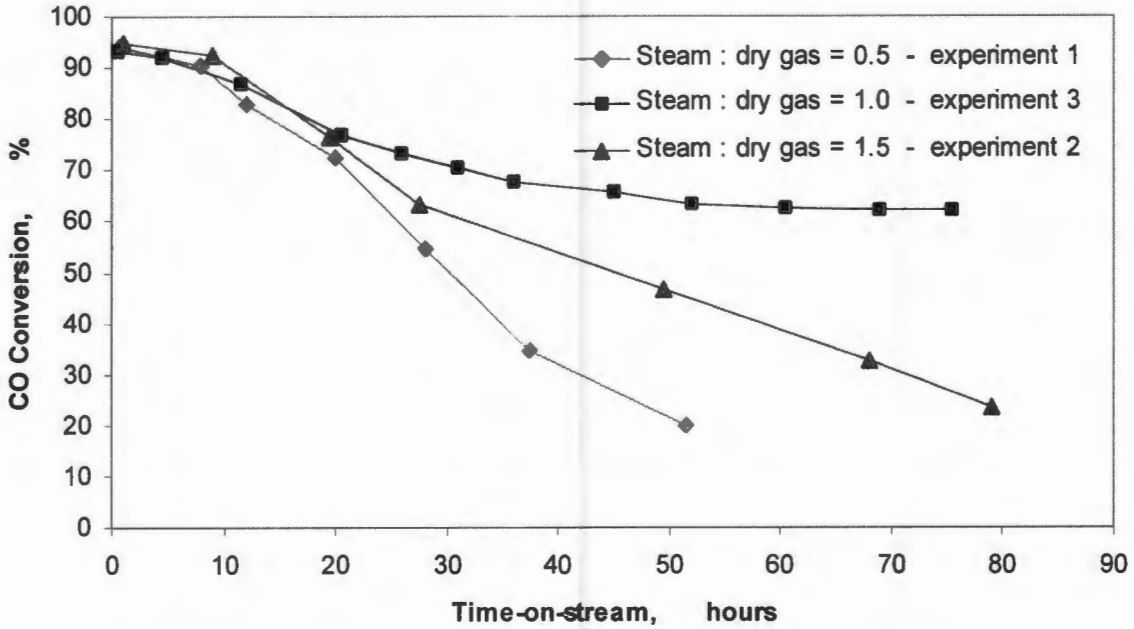

Figure 5-2 : Initial performance of the commercial LTS catalyst at various steam : dry gas ratios

At all three of the tested ratios, the initial activity directly following reduction is found to be approximately the same (all within 3 or 5 % of equilibrium conversion — see *Appendix III*). At a steam : dry gas ratio of 0.5, an error in the experimental operation of the water pump led to exceptionally low water levels over the catalyst bed, consequently exhibiting continued decline in the catalyst performance with time-on-stream, and therefore the experiment was abandoned. A possible explanation for the

continued deactivation of the catalyst may be due to the presence of carbon laydown on the catalyst. This possibility was visually supported by the blackened exterior of the glass bead packing in the reactor.

At a steam : dry gas ratio of 1, catalyst performance decreases steadily over approximately 48 hours and levels off at a pseudo-steady state activity.

At a steam : dry gas ratio of 1.5, the condensation temperature of water is 189°C; the experiment was performed at a temperature of 192°C. A subsequent steady decrease in activity is observed. Condensation of steam in the reactor is therefore suspected, confirmed by rapid temperature fluctuations detected by the interior reactor thermocouple. Literature confirms that water condensation on the commercial copper-zinc catalyst does indeed lead to deactivation (Twigg, 1989).

As a consequence of the above early findings, a standard condition for steam : dry gas ratio equal to unity was applied throughout the remaining catalyst evaluation programme.

However, subsequent experimental runs (data not presented here) at the low steam : dry gas ratio of 0.5 do not yield the continued loss in activity shown in Figure 5-2. It is proposed that an operating error in experimental procedure led to this initial finding, and that it is indeed possible to operate the system at a steam : dry gas ratio of 0.5 (an industrially applicable ratio).

5.1.4 Reproducibility of results

Figure 5-3 shows the time-on-stream behaviour under standard conditions of two different samples (experiments 3 and 4) of the industrial reference catalyst during the bedding-in phase. Good reproducibility is observed — both runs starting with an initial activity of close to equilibrium conversion (i.e. 98 % CO conversion), deactivating at the same rate and stabilising at a CO conversion of approximately 62 % after 50 hours.

At high CO conversions (i.e. above approximately 75 %), the relatively small chromatographic CO response makes using the CO peak area as a measure of conversion difficult. For this reason, the significantly larger CO_2 signal is used to back-calculate the CO conversion. A far greater degree of experimental scatter is found to occur when using CO_2 analysis as compared to CO, as illustrated by the larger error bars at high conversion in Figure 5-3. (A measure of analytical accuracy can be obtained from the experimental run data presented in *Appendix II*.)

As a further measure of the reproducibility of the gas chromatographic results on a day-to-day basis, the consistency of the CO and CO_2 peak area counts of the by-pass (i.e. feed gas) samples were compared over the duration of the experimental programme. The average bypass area counts for the respective dry gas feed mixtures, along with their corresponding standard deviations, are tabulated in Table 5-2. The scatter in CO peak area integration (taken as the standard deviation in the dry feed gas analysis) represents an 'uncertainty' of less than 0.6 % CO conversion.

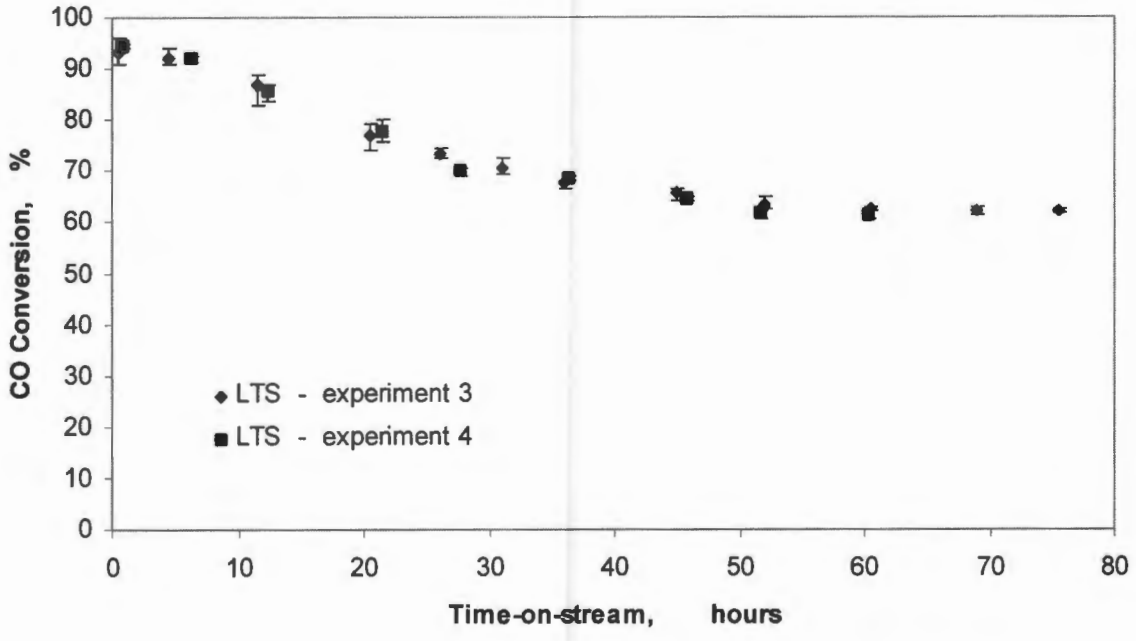

Figure 5-3 : Reproducibility of the time-on-stream behaviour for the commercial LTS catalyst under standard conditions

Table 5-2 : Standard deviations in peak area for the dry feed gas analysis

Feed Mixture	Avg. CO Peak	Std Deviation	Avg. CO_2 Peak	Std Deviation
1	84191	572	444671	3437
2	84471	332	451143	3027

5.2 Industrial Reference Catalyst — $CuO/ZnO/Al_2O_3$ (C 18-7)

5.2.1 Experimental runs

Five separate experimental runs have been performed using the commercial LTS catalyst. Experiments 1 to 3 have been carried out to investigate the effect of steam : dry gas ratio on the performance of the catalyst — in two of these cases (see section *5.1.3 Effect of steam : dry gas ratio on catalyst stability*) this leads to continuous decline in activity of the fresh catalyst. Experiment 4 at a steam : dry gas ratio of 1 has been used to generate the temperature-conversion data for the reference catalyst. This catalyst is also used in experiment 12 to investigate the effect of pressure on CO conversion.

Figure 5-4 shows the time-on-stream conversion data for experiment 4, highlighting the temperature-conversion data collection at the three $SGHSV_{dry}$.

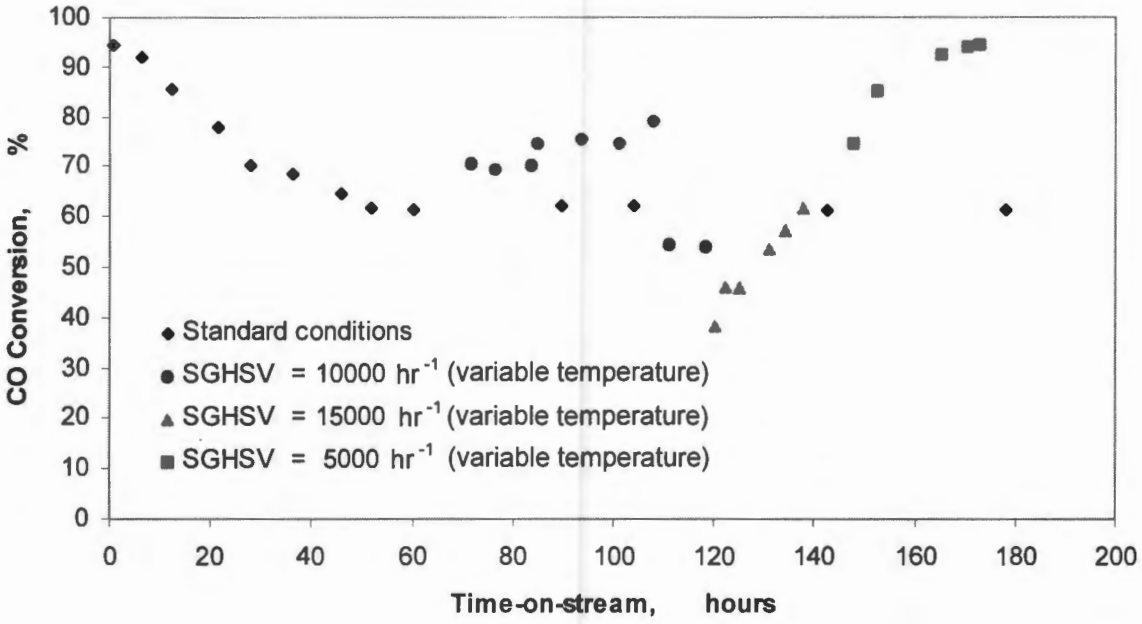

Figure 5-4 : Performance of the commercial LTS catalyst at variable temperatures throughout the entire test period (experiment 4)

5.2.2 Effect of temperature

The rate of reaction and, therefore, the degree of CO conversion increases as the temperature increases (Figure 5-5). At the lowest space velocity tested ($SGHSV_{dry}$ = 5000 hr^{-1}), conversion reaches the maximum attainable equilibrium conversion at approximately 200°C. At higher space velocities, equilibrium conversion would be achieved at temperatures higher than those tested (i.e. above 204°C).

5.2.3 Effect of space velocity

Detailed temperature-conversion data has been generated for the commercial LTS catalyst in the 'usual' LTS range of 195°C to 204°C as well as lower temperatures (limited by the condensation point of water at 180°C), in order to have a good basis for comparison of the various gold-metal oxide catalysts.

Three different dry gas standard gas hourly space velocities ($SGHSV_{dry}$) were tested, namely 5000 hr^{-1}, 10000 hr^{-1} and 15000 hr^{-1} (corresponding to dry gas weight hourly space velocities of 2.0 hr^{-1}, 4.0 hr^{-1} and 6.0 hr^{-1} respectively), at a steam : dry gas ratio of 1. Figure 5-5 shows the results of the activity tests performed on the commercial LTS catalyst, relative to the maximum conversion attainable at equilibrium. At a $SGHSV_{dry}$ of 5000 hr^{-1} the steady state activity achieved is approximately 75 % CO conversion at 188°C, which begins to approach the equilibrium conversion at the higher temperature of 204°C. A similar trend is found for the other two $SGHSV_{dry}$ but, as expected, at lower conversion levels.

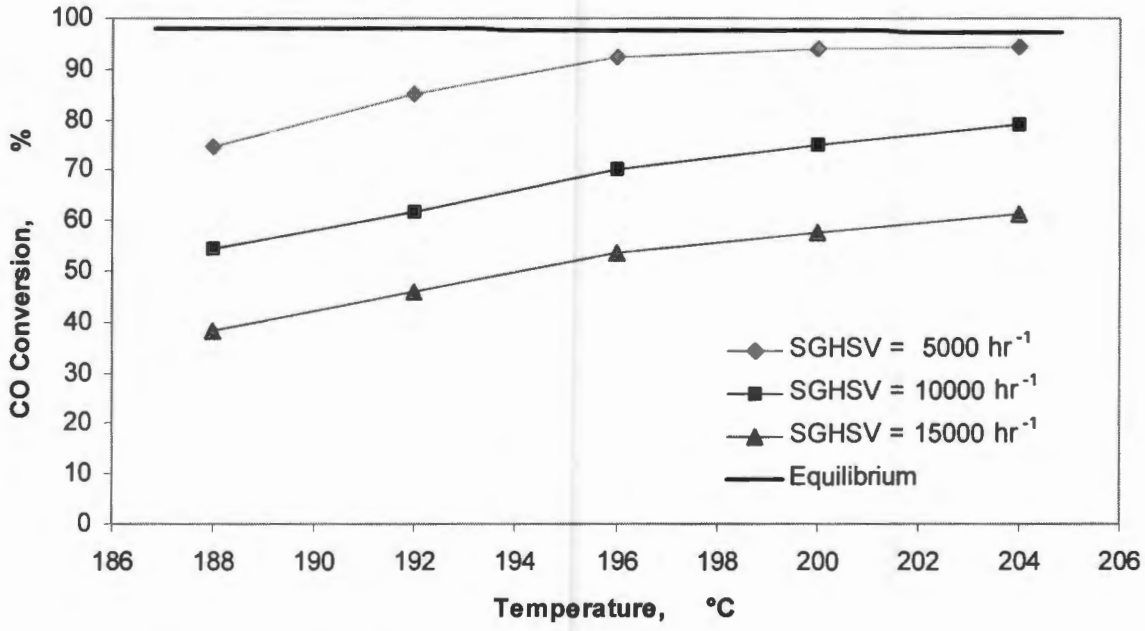

Figure 5-5 : LTS catalyst performance as a function of space velocity (experiment 4)

5.2.4 Effect of pressure

Previous work on gold catalysed water gas shift (Andreeva *et al*, 1996a; 1996b; 1998a) has been performed at atmospheric pressure, and therefore the effect of pressure on the adsorption of reactants and, consequently, the rate of reaction has not been investigated. For purposes of comparison, the effect of pressure on commercial LTS was also determined. In order to be sufficiently far away from equilibrium, this investigation was performed at a temperature of 204°C and a space velocity of 10000 hr^{-1} (at which approximately 79 % conversion is obtained; see Figure 5-5) with pressures varying between 10 and 25 barg. It is important to note that this conversion has been calculated from the CO data obtained (as opposed to back calculation from CO_2 data usually applied for conversions over 76 %), since the relatively large experimental scatter (i.e. ± 2 %) would not allow for comparison. The actual conversion obtained, however, is close to 76 % and is therefore not thought to influence the calculation by a significant margin. LTS catalyst performance is, therefore, essentially independent or only very slightly influenced by pressure in the typical LTS range (see Figure 5-13).

5.3 Au Promoted LTS Catalyst — Au/LTS-38

5.3.1 Experimental run

During experiment 5, feed dry gas mixture 1 (see Table 4-6) ran out and therefore a complete set of temperature-conversion data (i.e. no data collected at 188°C for a $WHSV_{dry}$ of 2.0 hr^{-1}) was not obtained, nor was the catalyst performance after the space velocity measurements at the standard conditions measured. The time-on-stream conversion data for experiment 5 at the standard bedding-in conditions and the two $WHSV_{dry}$ is shown in Figure 5-6.

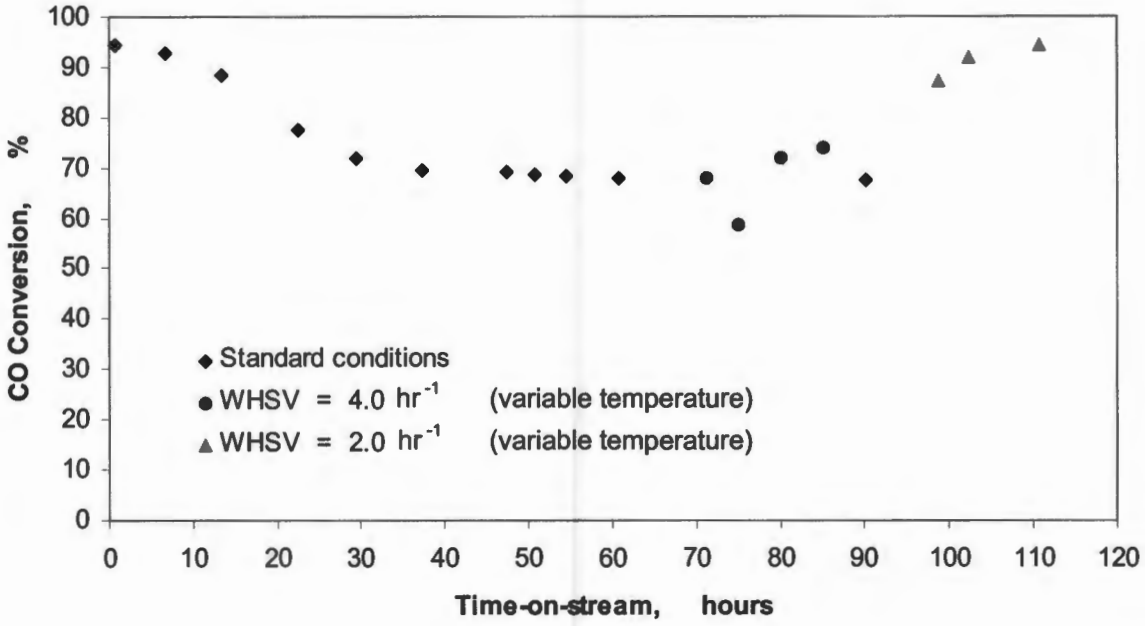

Figure 5-6 : Performance of Au/LTS-38 throughout the entire test period (experiment 5)

5.3.2 Initial deactivation

The initial performance of Au/LTS-38 (experiment 5) is shown in Figure 5-7. As per the case for the commercial reference LTS catalyst, high conversion approaching equilibrium is initially observed, followed by a steady decrease in activity to a steady state conversion of approximately 68 % after 48 hours. Although in all respects the initial performance of the gold promoted and reference LTS catalysts are similar, it appears from Figure 5-7 that the Au/LTS-38 catalyst retains a steady state conversion slightly higher than that of the reference LTS catalyst at steady state.

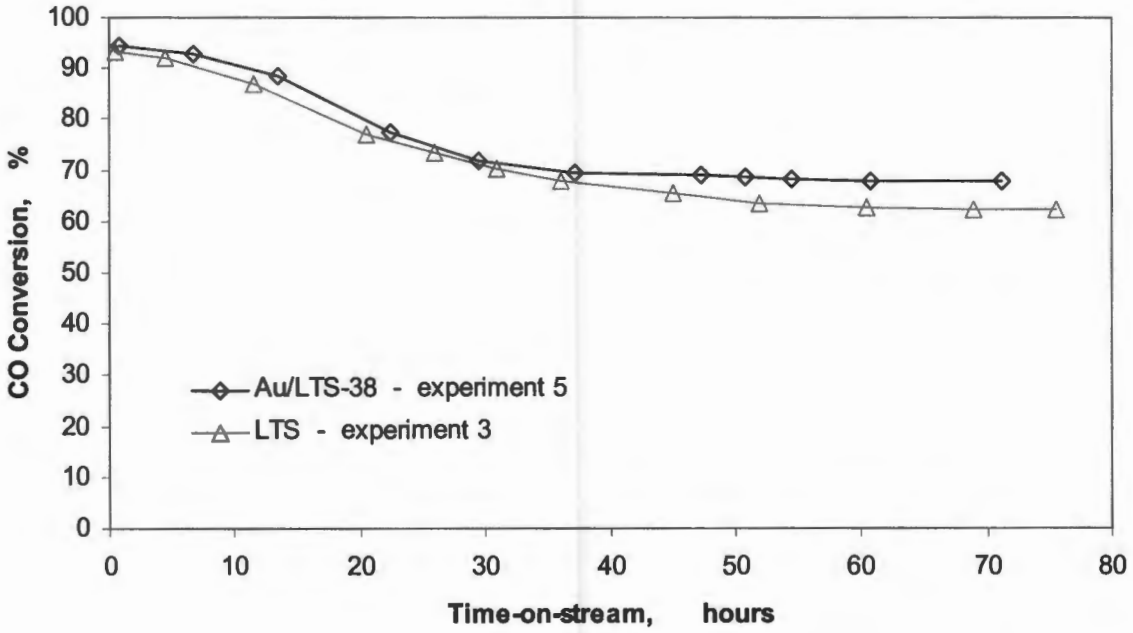

Figure 5-7 : Initial performance of Au/LTS-38 at standard conditions

5.3.3 Catalyst performance

CO conversion as a function of temperature is shown for two space velocities in Figure 5-8 and Figure 5-9. While CO conversion approaches equilibrium above 196°C at the lower space velocity, CO conversion at the higher space velocity is well below the equilibrium conversion throughout the LTS temperature range.

The data of Figures 5-7, 5-8 and 5-9 suggest that the gold promoted catalyst (Au/LTS-38) exhibits slightly higher activity than the commercial LTS catalyst. This is particularly noticeable at higher space velocity and lower temperatures where catalyst performance is most removed from any possible equilibrium control (Figure 5-9). The lack of performance differentiation at low space velocity (Figure 5-8), especially at the higher temperatures, may be due to both the influence of equilibrium and the reduced accuracy of CO conversion data at the very high conversion levels

associated with these conditions (where CO conversion must be calculated from CO_2 data).

Even so, at a temperature of 192°C and $WHSV_{dry}$ of 2.0 hr^{-1} the CO conversion on Au/LTS-38 is 87 %, as opposed to 82 % on the commercial LTS catalyst, whereas at the higher space velocity comparative CO conversions are 68 % for Au/LTS-38 versus 62 % for LTS. If these differences are to be believed, it would appear as if Au promotion of the commercial catalyst enhances performance to the extent that the gold promoted catalyst exhibits an approximately 2 – 3°C activity advantage at the higher space velocity and temperatures below 196°C.

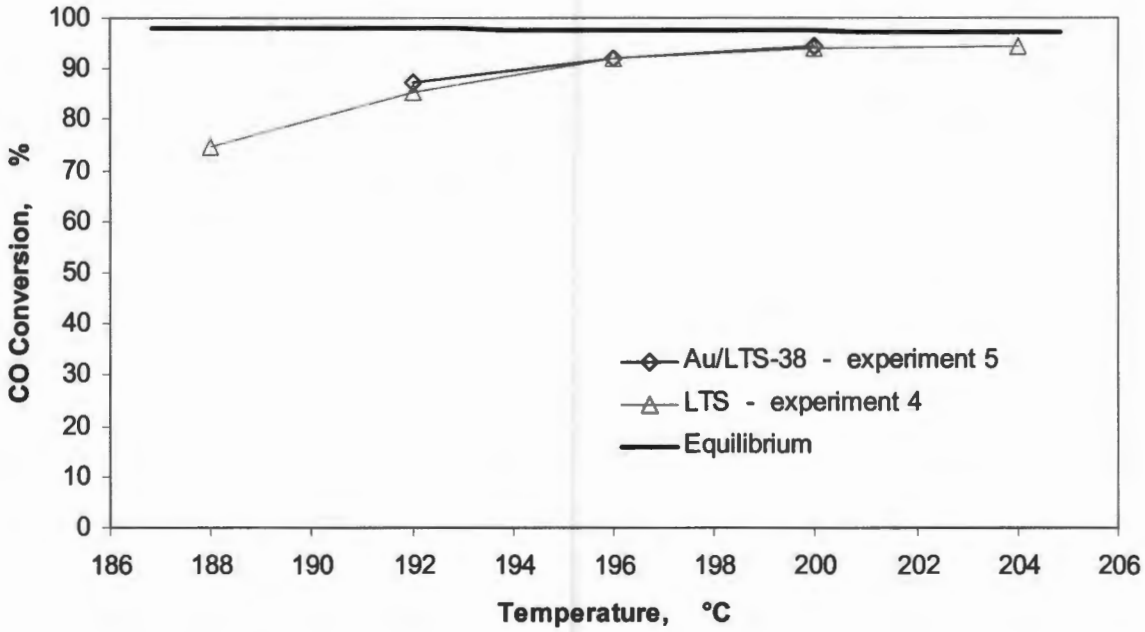

Figure 5-8 : Performance of Au/LTS-38 and commercial LTS catalyst at a $WHSV_{dry}$ of 2.0 hr^{-1}

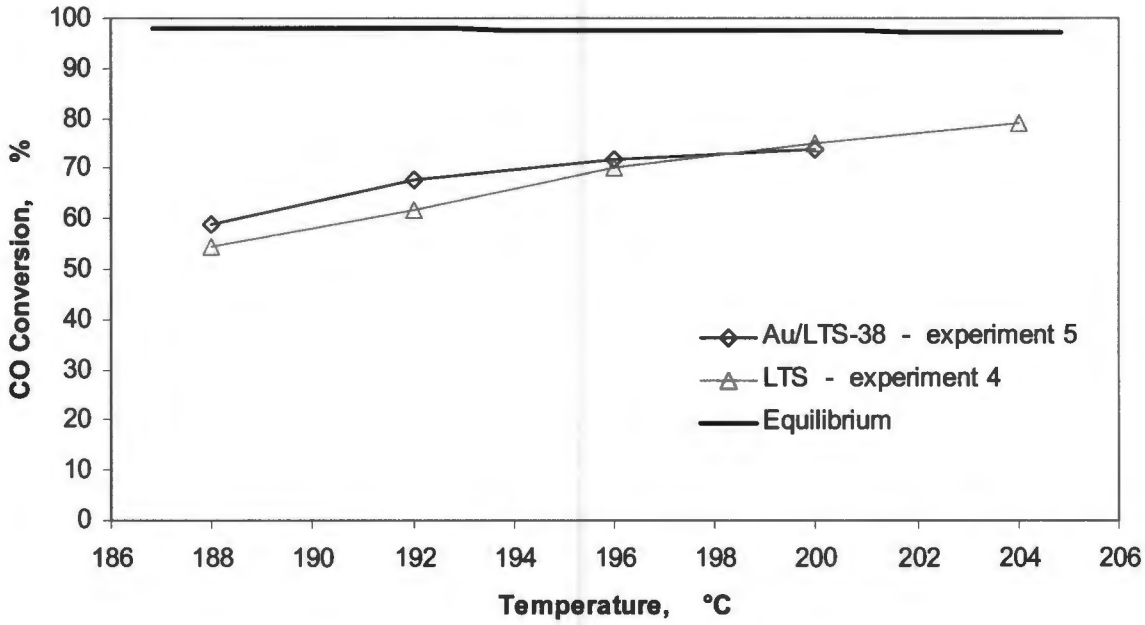

Figure 5-9 : Performance of Au/LTS-38 and commercial LTS catalyst at a $WHSV_{dry}$ of 4.0 hr^{-1}

5.4 Commercial ZnO (G-72 D)

Commercial ZnO (G-72 D) exhibited no initial activity and, therefore, the usual catalyst "bedding-in" procedure at standard conditions was not followed. The temperature was increased stepwise up from 192°C to 220°C in order to determine whether water gas shift activity could be observed at higher temperatures. No CO conversion is observed throughout this temperature range and consequently the ZnO support alone may be considered totally inert in respect of low temperature shift conversion.

5.5 Au Promoted ZnO — Au/ZnO-06, -27 and -71

5.5.1 Initial deactivation

Given that these materials proved moderately active and, hence, clearly demonstrate the LTS activity of gold on this support, three different metal loadings were tested, namely 0.6 wt %, 2.7 wt % and 7.1 wt % Au (experiments 9, 7 and 8 respectively). The catalyst with the intermediate loading (i.e. Au/ZnO-27) is found to exhibit the highest initial activity of the three — approximately 25 % CO conversion. This activity decreases over a 70 hour period, levelling off at a conversion of approximately 8 % (data, not shown in Figure 5-10, show the conversion to remain constant at 8 % to 110 hours and later times). Consequently, all further temperature-conversion data was obtained under non-deactivating conditions.

Au/ZnO-71 exhibits an initial CO conversion of 15 % and Au/ZnO-06 of 7 %. The latter catalyst is found to deactivate for only about 30 hours, stabilising at a conversion of 2 %. Au/ZnO-71 was thought to have stabilised after 54 hours, after which time the activity measurements at the various temperatures and space velocities were recorded. Although this assumption of lined-out activity was largely correct, after the temperature and space velocity experiments conversion at standard conditions was observed to have declined slightly from 3 % before the tests to approximately 2 % after the tests. Nonetheless, this difference is relatively small and, consequently, it may be accepted that the effects of temperature and space velocity are accurately represented by the data obtained.

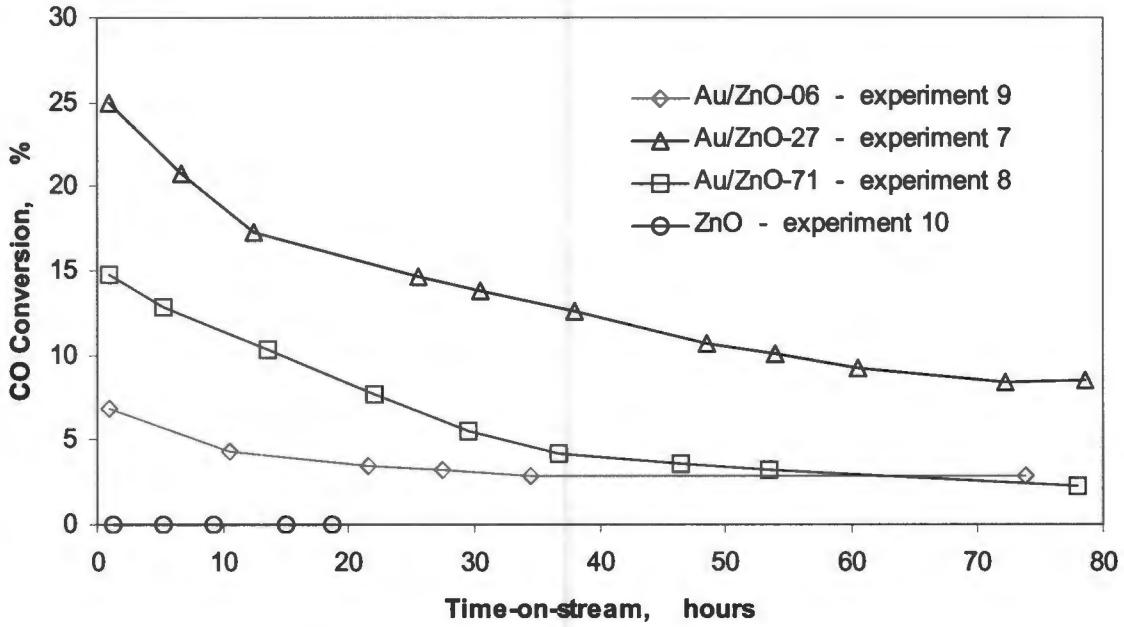

Figure 5-10 : Initial performance of Au/ZnO-06, Au/ZnO-27, Au/ZnO-71 and commercial ZnO catalyst at standard conditions

5.5.2 Effect of Au loading and space velocity on catalyst performance

At a $WHSV_{dry}$ of 2.0 hr^{-1}, shown in Figure 5-11, both the high (Au/ZnO-71) and low (Au/ZnO-06) gold loaded catalysts exhibit similar low activities between 5 % and 9 % CO conversion over the temperature range 188°C – 200°C. Au/ZnO-27 exhibits a significantly better performance at the same conditions. Conversion increased steadily from 15 % to 34 % over the temperature range 188°C – 204°C.

At the higher space velocity of 4.0 hr^{-1}, shown in Figure 5-12, similar activities of Au/ZnO-06 and Au/ZnO-71 were still observed. As in the case of the lower space velocity, the performance Au/ZnO-27 is substantially better than that of Au/ZnO-06 and Au/ZnO-71.

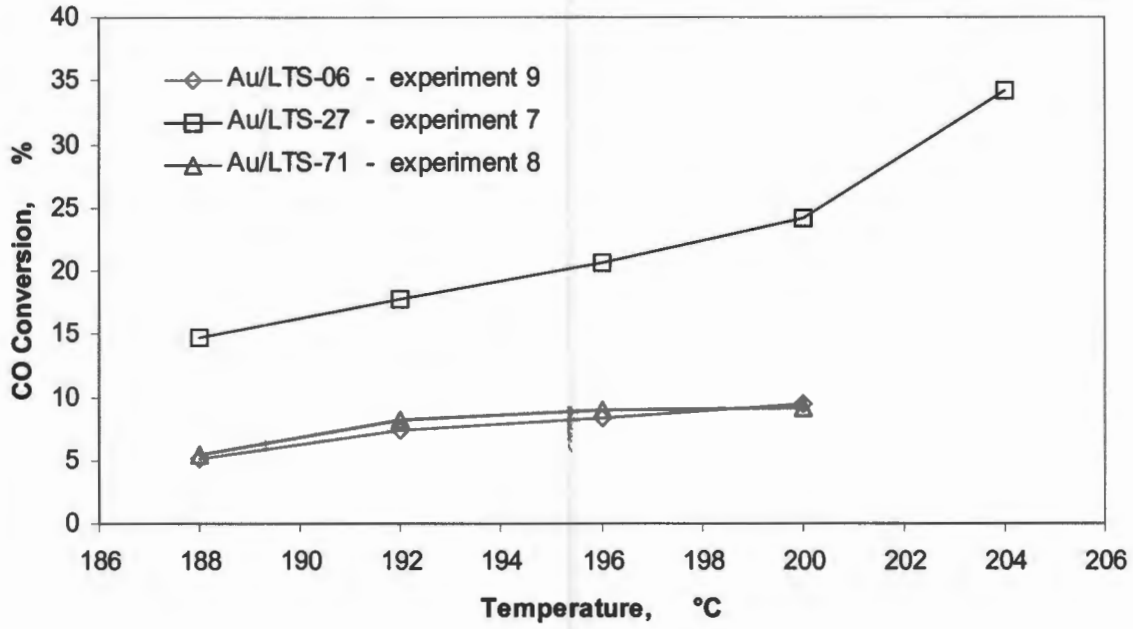

Figure 5-11 : Performance of Au/ZnO-06, Au/ZnO-27, Au/ZnO-71 at a $WHSV_{dry}$ of 2.0 hr^{-1}

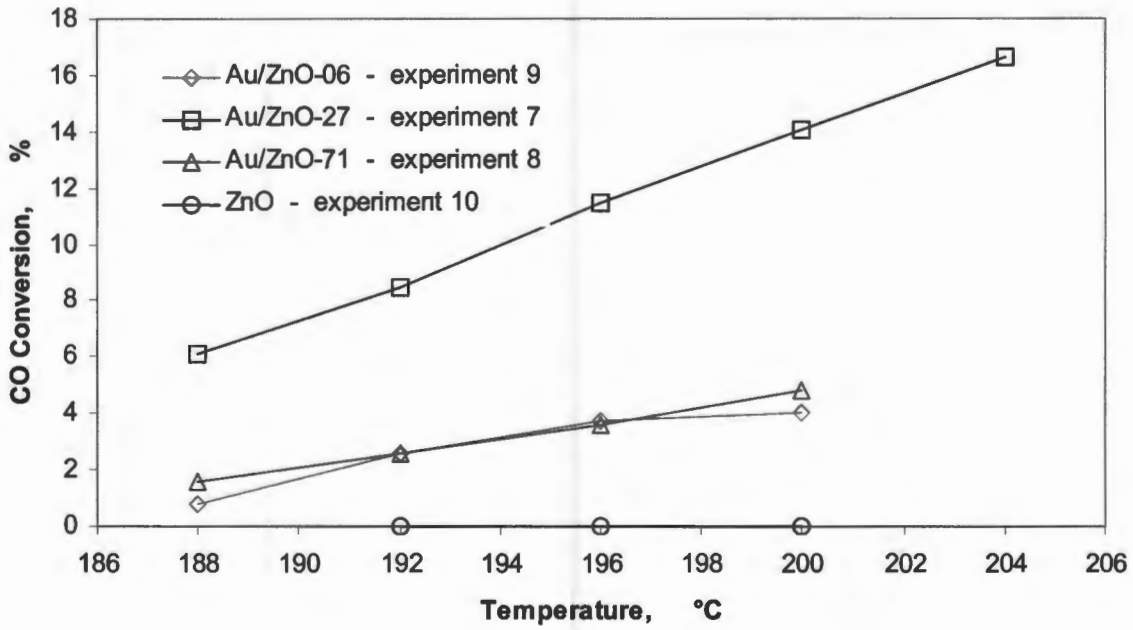

Figure 5-12 : Performance of Au/ZnO-06, Au/ZnO-27, Au/ZnO-71 and commercial ZnO catalyst at a $WHSV_{dry}$ of 4.0 hr^{-1}

5.5.3 Effect of pressure on Au/ZnO-27 performance

Similarly to the test performed on commercial LTS catalyst (experiment 12), the effect of pressure on performance has been studied at a fixed temperature of 204°C and pressures between 10 and 25 barg for Au/ZnO-27 (experiment 13). A $WHSV_{dry}$ of 2.0 hr^{-1} (as opposed to the higher WHSV used for the LTS catalyst test) and steam : dry gas value of 1 was used. Conversion is found to increase with increasing reactor pressure. At 10 barg, 30 % CO conversion is observed, increasing to 36 % conversion at 25 barg. Figure 5-13 shows the CO conversion as a function of pressure for both the commercial LTS and Au/ZnO-27 catalyst. Note, however, that significantly different overall conversions were obtained for the two catalysts.

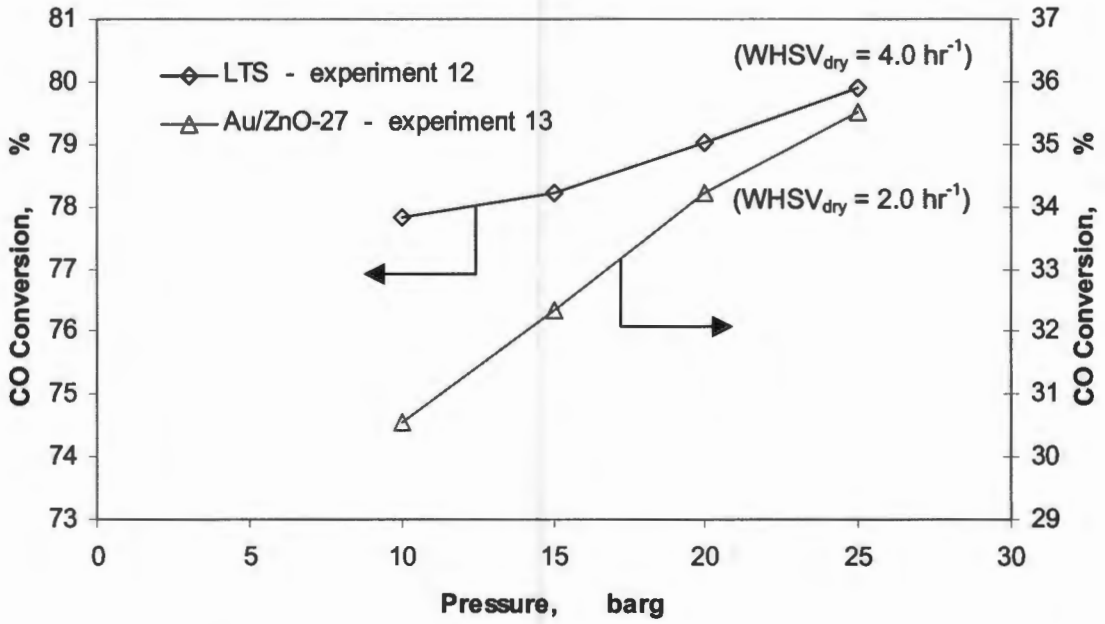

Figure 5-13 : Pressure effect on catalyst performance for commercial LTS catalyst and Au/ZnO-27

The data seems to suggest that a change in pressure (between 10 and 25 barg) more strongly affects the performance of Au/ZnO-27 than commercial LTS catalyst.

5.6 Au Promoted HTS Catalyst — Au/HTS-42

5.6.1 Initial deactivation

For the Au/HTS-42 catalyst (experiment 6), an initial CO conversion of 34 % declines rapidly to below 8 % after 38 hours.

5.6.2 Catalyst performance

Figure 5-16 shows the performance of Au/HTS-42 as a function of temperature, after "bedding in" at standard conditions for approximately 40 hours. Although conversion appears to increase only slightly with increasing temperature, the fact that conversion is always lower than that at the lower "bedding-in" temperature of 192°C, suggests that the catalyst activity had not yet stabilised (see Figure 5-14) prior to the temperature test series. Consequently, it must be noted that the Au/HTS-42 data at both low and high space velocities (Figures 5-15 and 5-16 respectively) are compromised by likely significant deactivation occurring progressively with increasing temperature and concomitant time-on-stream.

As a further consequence of the observed low activity of the catalyst, it was decided to increase the temperature outside the conventional LTS range to investigate whether activity increases meaningfully at higher temperatures, viz. 210°C and 220°C.

At the lower $WHSV_{dry}$ of 2.0 hr^{-1}, and taking into account the observed low activity of the catalyst (Figure 5-16), it was decided to test the performance at still higher temperatures, viz. 220°C and 240°C. Again, only poor activity is observed as shown in Figure 5-15.

5.7 Commercial AUS — $Au/Fe_2O_3/Al_2O_3$

5.7.1 Initial deactivation

Unlike all the other catalysts, AUS is found not to deactivate with initial time-on-stream. Conversion remains constant at approximately 4 % at standard conditions over a 30 hour period (Figure 5-14).

5.7.2 Catalyst performance

The commercial AUS catalyst exhibits approximately 4 % CO conversion at 192°C and 200°C at a $WHSV_{dry}$ of 4.0 hr^{-1} (Figure 5-16). It was therefore decided to investigate the lower $WHSV_{dry}$ in more detail to ascertain whether higher activity would be achieved at higher temperatures (220°C – 320°C) outside the LTS range (Figure 5-15). Surprisingly, no distinguishable increase or decrease in conversion was evident — the conversion of CO was between 5 and 5.5 % throughout the temperature range. Since iron oxide is the catalyst of choice for high temperature shift, one may have expected the activity of this Fe_2O_3 based gold catalyst to exhibit a significant increase in activity over the temperature range tested, especially at 320°C. These findings in respect to CO conversion with temperature possibly suggest that the combination of low space velocity and large (2.2 – 2.8 mm in diameter) pellets result in a severely external mass-transfer limited system.

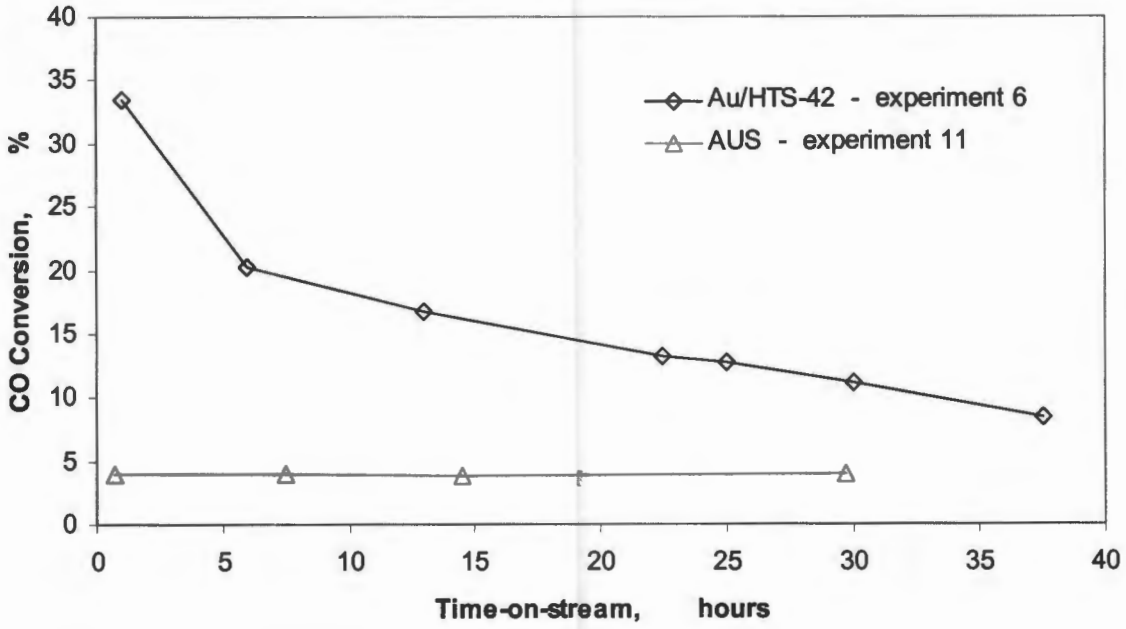

Figure 5-14 : Initial performance of Au/HTS-42 and AUS at standard conditions

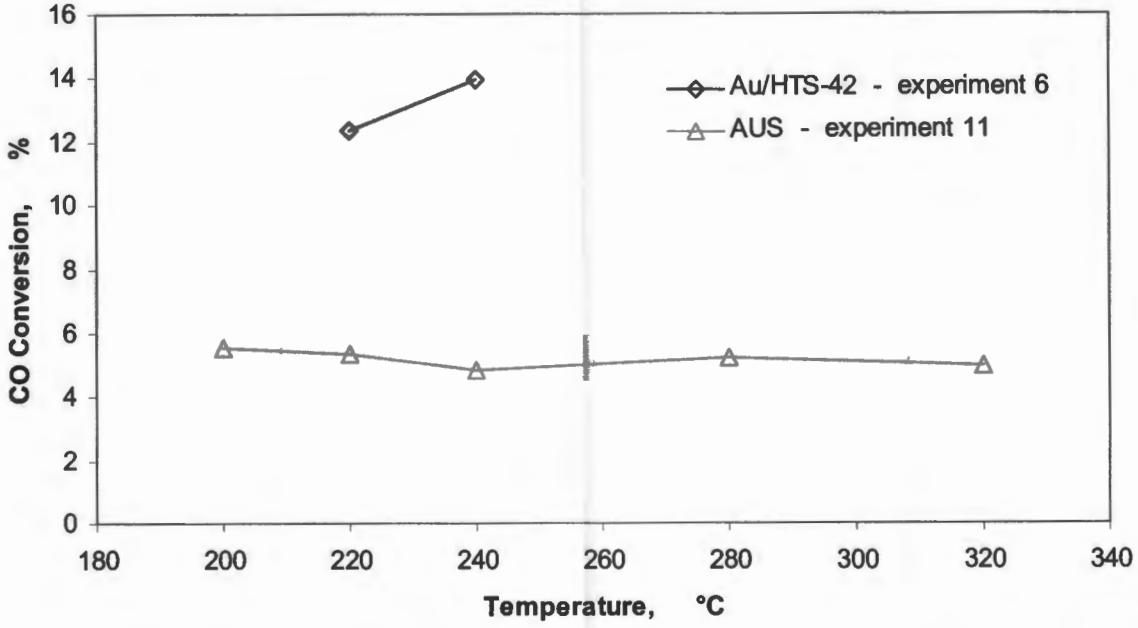

Figure 5-15 : Performance of Au/HTS-42 and AUS at a $WHSV_{dry}$ of 2.0 hr^{-1}

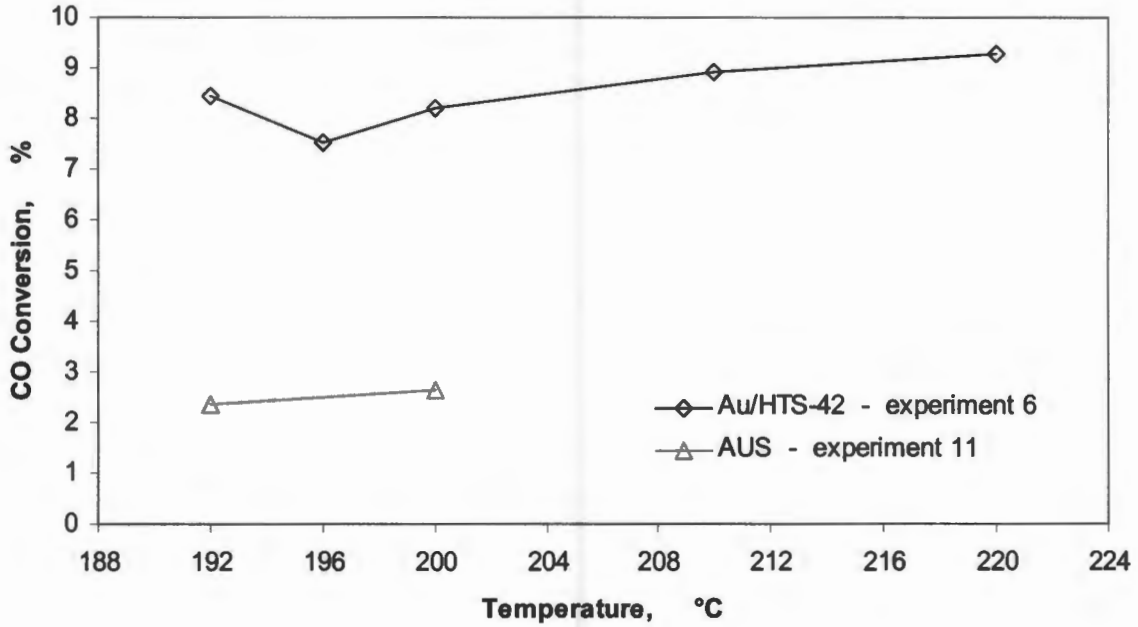

Figure 5-16 : Performance of Au/HTS-42 and AUS at a $WHSV_{dry}$ of 4.0 hr^{-1}

6. DISCUSSION

6.1 Influence of Reaction Variables

One of the major aims of this work has been to generate detailed performance data for the commercially applied copper-zinc LTS catalyst under industrially applicable conditions. The research into gold catalysed water gas shift has typically not been performed under these conditions, but rather at atmospheric pressure, low space velocities and feed gas streams not resembling those undergoing low temperature shift industrially (Andreeva *et al*, 1996a; 1998a).

For the commercial LTS catalyst, CO conversion increases steadily with increasing temperature in the range tested, reaching equilibrium conversion at approximately 200°C for the lowest $SGHSV_{dry}$ applied in this study. This finding is consistent with literature where, at $GHSV_{dry}$ of 4000 hr^{-1}, a CO slip of approximately 0.2 % (corresponding to approximately 93 % CO conversion in the low temperature shift stage) is obtained (Twigg, 1989).

As expected, CO conversion over the commercial LTS catalyst is found to decrease with increasing space velocity, since at the higher space velocities the 'contact time' of the reactant gas with the catalyst is decreased. However, the higher $SGHSV_{dry}$ of 10000 and 15000 hr^{-1} are useful conditions under which to compare low shift performance, since all catalysts exhibit performance free of equilibrium control at these conditions.

Difficulty in operating the system at steam : dry gas ratios other than 1 has not allowed this influence to be more thoroughly investigated. It should be noted, however, that subsequent studies have shown that, at least for the lower steam : dry gas ratio of 0.5, stable catalyst operation can be achieved (data not included in this study).

Even though the reference catalyst exhibits a progressive increase in CO conversion with increasing pressure, this effect is small. LTS catalyst performance is found, therefore, to be essentially independent or only very slightly influenced by pressure in the typical industrial LTS operating range.

Similarly, regarding the influence of temperature and space velocity on conversion, the above mentioned trends are also observed for the gold loaded catalysts. Pressure is found not to significantly influence the degree of CO conversion, however, the data seems to suggest that pressure more strongly influences the gold catalyst performance than that of the commercial LTS catalyst.

6.2 Au Promotion of Commercial $CuO/ZnO/Al_2O_3$ LTS Catalyst

Initially, the gold promoted commercial low temperature catalyst, similar to the unpromoted LTS catalyst, exhibits close to equilibrium conversion at the standard conditions of 192°C, $WHSV_{dry}$ of 4.0 hr^{-1} and steam : dry gas ratio of 1, decreasing with time-on-stream until a pseudo-steady state is reached. The pseudo-steady state activity achieved is approximately 68 %, as opposed to 62 % obtained for the commercial LTS catalyst under standard conditions.

Similarly, under pseudo-steady state activity conditions, the performance of the gold-promoted catalyst (Au/LTS-38) appears enhanced over that of the unpromoted catalyst. A fairly significant difference in performance is observed at the lower temperatures (188 and 192°C) and higher WHSV tested. Hence, from the limited results obtained, gold promoted LTS catalyst does appear to exhibit slightly higher activity than the unpromoted commercial equivalent. If these results are to be trusted, it would appear as if gold promotion is advantageous to the industrial catalyst, exhibiting an approximately 2 – 3°C activity advantage at high space velocity and temperatures below 196°C. No distinguishable performance improvement is evident at the lower space velocity.

After pseudo-steady state activity is achieved at standard conditions (i.e. approximately 40 hours), no further measurable activity loss was found to occur over the duration of the catalyst performance testing period of 86 hours, suggesting that the performance of the gold-promoted LTS catalyst is stable under typical LTS conditions.

6.3 Au / ZnO Catalysts

The overall performance of the gold deposited on industrial zinc oxide catalysts is significantly lower than that of the industrial reference catalyst. In the case of the intermediately gold-loaded ZnO it is higher than that for the 4.2 % Au loaded HTS catalyst. Au/ZnO-27, even though yielding 9 percentage points less initial activity at standard conditions than Au/HTS-42, attains a higher pseudo-steady state activity of no less than 2 percentage points. Gold deposited on commercial zinc oxide, however, yields the highest overall increase in CO conversion with regards to the activity of the non gold-loaded support material (which at the experimental conditions yields no apparent conversion).

Even though these catalysts do not exhibit high activity in the range of the commercial LTS catalyst, it is interesting to see the effect of gold deposition on this material. To our knowledge, a gold promoted zinc oxide catalyst for water gas shift conversion is only cited once in literature (Sakurai *et al*, 1997) — a 5 atom% Au catalyst (expressed as a percentage of gold in the starting solution) prepared by coprecipitation techniques, as opposed to the deposition-precipitation preparation procedure employed in this investigation. Sakurai *et al* (1997) quote a 14 times slower rate of reaction for the gold catalyst versus a commercial $CuO/ZnO/Al_2O_3$ catalyst, though, at 100°C, these data must be under conditions of very low conversion. Calculating the rate of reaction at 200°C for the industrial LTS catalyst and for Au/ZnO-27, it can be seen that the Au loaded zinc catalyst displays only 4.5 times lower reaction rate — a marked improvement on the coprecipitated catalyst performance.

An interesting observation relates to the effect of gold loading on performance. Of the three metal loadings tested, viz. 0.6 wt %, 2.7 wt % and 7.1 wt % Au, the performance of the 2.7 wt % Au/ZnO catalyst is markedly better than that of the ZnO catalyst of lower and higher metal loading. This effect has previously been noted in literature. Haruta and co-workers (Haruta, 1989) tested a variety of gold catalysts with varying Au loadings between 0 and 100 % for H_2 and CO oxidation — the findings yield a parabolic change in catalytic activity with gold loading. It was found that maximum activities were obtained at an optimal loading of 5 atom% Au (expressed as a percentage of Au in the starting solution) for Au/α-Fe_2O_3 and Au/Co_3O_4 materials, and an optimal loading of 10 atom% Au for the Au/NiO catalyst. Haruta proposed that this

observed trend was due to the coagulation of Au particles at higher loadings. Similarly, the effect of gold loading was also reported for methane oxidation using Au/MgO catalysts (Blick, 1998). The production of CO reached a maximum at an intermediate gold loading of approximately 3 wt % (however, this reaction yields a complex product spectrum, and therefore these results are less conclusive).

Literature strongly emphasises the necessity of gold particles in the nanometer size range for high catalytic activity. Haruta (1997) proposed that only when gold is deposited as hemispherical ultra-fine particles with diameters smaller than 5 nm does it generate high catalytic activity. It was proposed that the gold – metal oxide perimeter interface acts as a site for activating at least one of the reactants; therefore the surface area to volume ratio of the Au particle plays a significant role in the observed activity. Regardless of the accuracy of Haruta's perimeter site theory mechanism, the need for small Au particles, smaller than 5 nm, is generally accepted (Bond and Thompson, 1999).

In the case of the gold loaded catalysts tested in this study, gold particles were observed to range greatly from approximately 3 nm up to approximately 500 nm — the former in the suggested particle size range, while the latter 2 orders of magnitude larger.

The phenomenon of gold loading on catalyst performance may be due to the fact that as the Au metal content increases, the exposed Au surface area (or perimeter) increases. Further addition of gold to the surface may lead to coagulation / agglomeration of the active metal, thus causing the observed decrease in conversion at higher loadings. It is important to note, however, that although this explanation is plausible, there is no evidence regarding dispersion of the various gold loadings on ZnO and, although empirical data suggests the intermediate loading to be better, highly variable dispersion with preparation is distinctly possible.

6.4 Au / Fe-oxide Catalysts

Both of the gold containing iron oxide catalysts tested, viz. Au/HTS-42 and AUS, do not yield significant activity in the LTS range. This result is contrary to the findings of Andreeva and co-workers (Andreeva *et al*, 1996a; 1998a); 3 wt % Au loaded Fe_2O_3 catalysts prepared by deposition precipitation were reported to yield approximately 83 % CO conversion at 200°C utilising a steam : dry gas ratio of 0.7 and a total flow space velocity of 4000 hr^{-1}. The activity of AUS is found to be surprisingly low, even at higher temperatures approaching the HTS range (i.e. 320°C) where Fe_2O_3 is active for water gas shift. No activity change was observed between 200 and 320°C, suggesting that mass-transfer limitations may have been significant in the case of the AUS tests, which employ spherical catalyst pellets in the 2.2 – 4.0 mm size range.

Although poor performance is exhibited by the gold / iron oxide catalysts compared to the LTS and Au/LTS-38 catalysts, these are early attempts from MINTEK. Large gold particles are known to be present on the surface (from the SEM images and previous work by MINTEK on Au/hopcalite systems), and hence poor dispersion of Au is likely. As a consequence, it is possible that the Fe_2O_3 supported catalysts of this study are not necessarily representative of the best literature performance of iron oxide catalysts.

7. CONCLUDING REMARKS

This work has succeeded in developing a performance benchmark of the commercial catalyst at true industrial conditions, including temperature, pressure, space velocity, steam : dry gas ratio and dry gas feed composition, against which the performance of gold catalysts can be compared.

Although the evidence is not conclusive, gold does appear to promote the commercial LTS catalyst activity at lower temperatures than those traditionally applied for low temperature water gas shift. This effect was particularly evident at temperatures of 188 and 192°C and a high space velocity where a 5 to 6 percentage point increase in CO conversion was observed. If this increase in performance can be confirmed, it could have significant impact on the life of commercial LTS catalysts.

Zinc oxide supported gold catalysts are active for the water gas shift conversion. Even though these catalysts did not exhibit high activity in the range of the commercial LTS catalyst, ZnO shows promise as a support for gold water gas shift catalysts. This study also shows that a large scope exists for improving Au metal dispersion on the ZnO support and, hence, much improved performance may yet be expected of the Au/ZnO system.

It is, however, important to recognise that the Au/ZnO catalysts were prepared on commercially available zinc oxide, which contains approximately 10 wt % aluminium oxide as a binding agent. Since little is known of the dispersion and positioning of Au on these catalysts, the effect of Au/Al_2O_3 on activity cannot be discounted.

It is recommended that the effect of gold promotion on the commercial LTS catalyst performance be confirmed and extended, since the initial indications are particularly positive. In order to investigate the effects of the gold more closely careful decreasing of the steam : dry gas ratio will allow for investigations at lower temperatures where gold showed performance advantages over the industrial reference catalyst.

It is also recommended to benchmark the Au/ZnO performance obtained in this study versus the best performing literature Au / metal oxide catalysts, under the same experimental operating conditions.

8. REFERENCES

Aida, T., Higuchi, R. & Niiyama, H., Decomposition of Freon-12 and Methyl Chloride over Supported Gold Catalysts, *Chemistry Letters* (1990) 2247 - 2250

Ando, M., Kobayashi, T. & Haruta, M., Enhancement in the optical CO sensitivity of NiO film by the deposition of ultrafine gold particles, *Journal of Chem. Soc. Faraday Trans.* **90** (1994) 1011 - 1013

Andreev, A., Halachev, T. & Shopov, D., *Communications Dept. Chem. Bulg. Acad. Sci.* **21** (1988) 307

Andreeva, D., Idakiev, V., Tabakova, T. & Andreev, A., Low-Temperature Water-Gas Shift Reaction over Au/α-Fe_2O_3, *Journal of Catalysis* **158** (1996a) 354 – 355

Andreeva, D., Idakiev, V., Tabakova, T., Andreev, A. & Giovanoli, R., Low-temperature water-gas shift reaction on Au/α-Fe_2O_3, *Applied Catalysis A: General* **134** (1996b) 275 - 283

Andreeva, D., Tabakova, T., Idakiev, V., Christov, P. & Giovanoli, R., Au/α-Fe_2O_3 catalyst for water-gas shift reaction prepared by deposition-precipitation, *Applied Catalysis A: General* **169** (1998a) 9 - 14

Andreeva, D., Tabakova, T., Idakiev, V. & Naydenov, A., Complete Oxidation of Benzene over Au-V_2O_5/TiO_2 and Au-V_2O_5/ZrO_2 Catalysts, *Gold Bulletin* **31** 3 (1998b) 105 - 106

Andreeva, D., Idakiev, V., Tabakova, T. & Giovanoli, R., Low-Temperature Water-Gas Shift Reaction On Au/TiO_2, Au/α-Fe_2O_3, and Au/Co_3O_4 Catalysts, *Bulgarian Chemical Communications*, Vol. 30 Numbers 1- 4 (1998c) 59 - 67

Armstrong, E. & Hilditch, T., *Proc. Royal Society* **A97** (1920) 265

Bamwenda, G., Tsubota, S., Nakamura, T. & Haruta, M., The influence of the preparation methods on the catalytic activity of platinum and gold supported on TiO_2 for CO oxidation, *Catalysis Letters* **44** (1997) 83 - 87

Blick, K., Mitrelias, T., Hargreaves, J., Hutchings, G., Joyner, R., Kiely, C. & Wagner, F., Methane oxidation using Au/MgO catalysts, *Catalysis Letters* **50** (1998) 211 - 218

Boccuzzi, F., Chiorino, A., Manzoli, M., Andreeva, D. & Tabakova, T., FTIR Study of Carbon Monoxide Oxidation and Scrambling at Room Temperature over Gold Supported on ZnO and TiO_2, *Journal of Physical Chemistry* **100** (1996) 3625 - 3631

Bond, G., The Catalytic Properties of Gold (Potential applications in the chemical industry), *Gold Bulletin* **5** (1972) 11 - 13

Bond, G. & Thompson, D., Catalysis by Gold, *Catalyst Reviews — Science and Engineering* **41** 3&4 (1999) 319 - 388

Chen, B., Bai, C., Cook, R., Wright, J. & Wang, C., Gold/cobalt oxide catalyst for oxidative destruction of dichloromethane, *Catalysis Today* **30** (1996) 15 - 20

Cunningham, D., Vogel, W., Kageyama, H., Tsubota, S. & Haruta, M., The Relationship between the Structure and Activity of Nanometer Size Gold When Supported on $Mg(OH)_2$, *Journal of Catalysis* **177** (1998) 1 - 10

Eskendirov, I., Coville, N. & Sokolovskii,V., Methane oxidative coupling on the $Au/La_2O_3/CaO$ catalyst in the presence of hydrogen peroxide, *Catalysis Letters* **35** (1995) 33 - 37

Funazaki, N., Henmi, A., Ito, S., Asano, Y., Yamashita, S., Kobayashi, T. & Haruta, M., Development of carbon monoxide detector using Au fine particles-doped α-Fe_2O_3, *Sensors and Actuators* **B13-14** (1993) 536 - 538

Haruta, M., Kobayashi, T., Sano, H. & Yamada, N., Novel gold catalysts for the oxidation of carbon monoxide at a temperature far below 0°C, *Chemistry Letters* **829** (1987) 405 - 408

Haruta, M., Yamada, N., Kobayashi, T. & Iijima, S., Gold Catalysts Prepared by Coprecipitation for Low-Temperature Oxidation of Hydrogen and of Carbon Monoxide, *Journal of Catalysis* **115** (1989) 301 - 309

Haruta, M., Preparation and environmental applications of supported gold catalysts, *Now & Future* (Japan Ind. Technol. Assoc.) **7** (1992) 13 - 16

Haruta, M., Tsubota, S., Kobayashi, T., Kageyama, H., Genet, M. & Delmon, B., Low-Temperature Oxidation of CO over Gold Supported on TiO_2, α-Fe_2O_3, and Co_3O_4, *Journal of Catalysis* **144** (1993) 175 - 192

Haruta, M., Ueda, A., Tsubota, S. & Torres Sanchez, R., Low-temperature catalytic combustion of methanol and its decomposed derivatives over supported gold catalysts, *Catalysis Today* **29** (1996) 443 - 447

Haruta, M., Novel catalysis of gold deposited on metal oxides, *Catalysis Surveys Japan* **1** (1997a) 61 - 73

Haruta, M., Size- and support-dependency in the catalysis of gold, *Catalysis Today* **36** (1997b) 153 - 166

Hayashi, T., Tanaka, K. & Haruta, M., Selective Vapor-Phase Epoxidation of Propylene over Au/TiO_2 Catalysts in the Presence of Oxygen and Hydrogen, *Journal of Catalysis* **178** (1998) 566 - 575

Hutchings, G., Catalysis: A Golden Future, *Gold Bulletin* **29** 4 (1996) 123 - 130

Iizuka, Y., Fujiki, H., Yamauchi, N., Chijiiwa, T., Arai, S., Tsubota, S. & Haruta, M., Adsorption of CO on gold supported on TiO_2, *Catalysis Today* **36** (1997) 115 - 123

Ilieva, L., Andreeva, D. & Andreev, A., TPR and TPD investigation of Au/α-Fe_2O_3, *Thermochimica Acta* **292** (1997) 169 - 174

Kang, Y. & Wan, B., Gold and iron supported on Y-type zeolite for carbon monoxide oxidation, *Catalysis Today* **35** (1997) 379 - 392

Kirk-Othmer, *Encyclopaedia of Chemical Technology* Vol. 13 (4^{th} Edition), John Wiley & Sons, New York (1995) 852 - 861

Kobayashi, T., *et al*, A selective CO sensor using Ti-doped α-Fe_2O_3 with coprecipitated ultrafine particles of gold, *Sensors and Actuators* **13** (1988) 339 - 349

Minicò, S., Scire, S., Crisafulli, C., Visco, A. & Galvagno, S., FT-IR study of Au/Fe_2O_3 catalysts for CO oxidation at low temperature, *Catalysis Letters* **47** (1997) 273 - 276

Okumura, M., *et al*, The Abilities and Potentials of Gold as a Catalyst: Selective Hydrogenation — Hydrogenation of Butadiene, *Report of the Research Achievements of Interdisciplinary Basic Research Section 1994 – 1999* No.393 (1999) 54 - 55

Rhodes, C., Hutchings, G. & Ward, A., Water-gas shift reaction: finding the mechanistic boundary, *Catalysis Today* **23** (1995) 43 - 58

Sakurai, H., Tsubota, S. & Haruta, M., Hydrogenation of CO_2 over gold supported on metal oxides, *Applied Catalysis A: General* **102** (1993) 125 - 136

Sakurai, H. & Haruta, M., Carbon dioxide and carbon monoxide hydrogenation over gold supported on titanium, iron, and zinc oxides, *Applied Catalysis A: General* **127** (1995) 93 - 105

Sakurai, H. & Haruta, M., Synergism in methanol synthesis from carbon dioxide over gold catalysts supported on metal oxides, *Catalysis Today* **29** (1996) 361 - 365

Sakurai, H., Ueda, A., Kobayashi, T. & Haruta, M., Low-temperature water-gas shift reaction over gold deposited on TiO_2, *Chemical Communications* (1997) 271 - 272

Salama, T., Shido, T., Minagawa, H. & Ichikawa, M., Characterization of Gold(I) in NaY Zeolite and Acidity Generation, Journal of Catalysis 152 (1995) 322 - 330

Sandler, S., *Chemical And Engineering Thermodynamics*, 2nd Edition, John Wiley & Sons (1989) 504 - 506

Schwank, J., Gold in bi-metallic catalysts, *Gold Bulletin* **18** (1985) 2 - 10

Taylor, S., Meyer, R., Klingbiel, I., Glaner, L., Bollmann, A. & van der Lingen, E., The beneficial effect of gold additions on the activity of 'hopcalite' catalyst used for the low temperature oxidation of carbon monoxide, *New Industrial Uses for Gold : Catalytic Gold Abstracts* (2001) 41

Thompson, D., New Advances in Gold Catalysis Part I*, *Gold Bulletin* **31** 4 (1998) 111 - 118

Thompson, D., New Advances in Gold Catalysis Part II*, *Gold Bulletin* **32** 1 (1999) 12 - 19

Torres Sanchez, R., Ueda, A., Tanaka, K. & Haruta, M., Selective Oxidation of CO in Hydrogen over Gold Supported On Manganese Oxides, *Journal of Catalysis* **168** (1997) 125 - 127

Twigg, M., The Water-gas Shift Reaction, *Catalyst Handbook* (2nd Edition), Wolfe Publishing Ltd., 1989, 283 - 339

Ueda, A., Oshima, T. & Haruta, M., Reduction of nitrogen monoxide with propene in the presence of oxygen and moisture over gold supported on metal oxides, *Applied Catalysis B: Environmental* **12** (1997) 81 - 93

Ueda, A. & Haruta, M., Reduction of nitrogen monoxide with propene over Au/Al_2O_3 mixed mechanically with Mn_2O_3, *Applied Catalysis B: Environmental* **18** (1998) 115 - 121

Ueda, A. & Haruta, M., NO reduction with CO, H_2 and hydrocarbons over gold catalysts, *Gold Bulletin* **32** (1999) 3 - 11

Waters, R., Wiemer, J. & Smith, J., An investigation of the activity of coprecipitation gold catalysts for methane oxidation, *Catalysis Letters* **30** (1995) 181 – 188

APPENDICES

APPENDIX I

Tabulated Summary of Catalysts Tested and Experimental Operating Conditions

Table AI-1 : Summary of catalyst composition and particle size tested

Sample	Specific Metal Content (wt %)						Particle Size
	Au	Cu	Fe	Zn	Cr	Al	(μm)
LTS (C 18-7)	—	33.6	—	37.8	—	5.3	300 – 500
HTS (G-3 C)	—	1.6	62.3	—	5.5	—	300 – 500
ZnO (G-72 D)	—	—	—	72.3	—	5.3	300 – 500
AUS	0.3	—	unknown	—	—	unknown	2200 – 2800
Au/LTS-38	3.8	27.9	—	29.6	—	4.6	100 – 250
Au/HTS-42	4.2	—	56.9	—	3.6	—	250 – 425
Au/ZnO-06	0.6	—	—	68.3	—	1.9	150 – 425
Au/ZnO-27	2.7	—	—	62.9	—	1.4	150 – 425
Au/ZnO-71	7.1	—	—	56.4	—	1.3	150 – 425

Table AI-2 : Summary of experimental run conditions

Experiment Number	Catalyst Tested	Experimental Conditions			
		S / DG	$WHSV_{dry}$ (hr^{-1})	Pressure (barg)	Temperature (°C)
1	LTS	0.5	4.0	20	192
2	LTS	1.5	4.0	20	192
3	LTS	1.0	4.0	20	192
4	LTS	1.0	2.0, 4.0, 6.0	20	188 - 204
5	Au/LTS-38	1.0	2.0, 4.0	20	188 - 200
6	Au/HTS-42	1.0	2.0, 4.0	20	192 - 240
7	Au/ZnO-27	1.0	2.0, 4.0	20	188 - 204
8	Au/ZnO-71	1.0	2.0, 4.0	20	188 - 200
9	Au/ZnO-06	1.0	2.0, 4.0	20	188 - 200
10	ZnO	1.0	4.0	20	192 - 220
11	AUS	1.0	2.0, 4.0	20	192 - 320
12	LTS	1.0	4.0	10, 15, 20, 25	204
13	Au/ZnO-27	1.0	2.0	10, 15, 20, 25	204

APPENDIX II

Experimental Data

Experiment 1 — Commercial LTS Catalyst (S/DG = 0.5)

Experiment 2 — Commercial LTS Catalyst (S/DG = 1.5)

Experiment 3 — Commercial LTS Catalyst (S/DG = 1.0)

Experiment 4 — Commercial LTS Catalyst, LTS

Experiment 5 — Au Promoted Commercial LTS Catalyst, Au/LTS-38

Experiment 6 — Au Promoted Commercial HTS Catalyst, Au/HTS-42

Experiment 7 — Au Promoted Commercial ZnO Catalyst, Au/ZnO-27

Experiment 8 — Au Promoted Commercial ZnO Catalyst, Au/ZnO-71

Experiment 9 — Au Promoted Commercial ZnO Catalyst, Au/ZnO-06

Experiment 10 — Commercial ZnO Catalyst, ZnO

Experiment 11 — Commercial AUS Catalyst, AUS

Experiment 12 — Commercial LTS Catalyst (Pressure Effect)

Experiment 13 — Au Promoted Commercial ZnO Catalyst (Pressure Effect)

Explanation of data in tables :

The raw data was worked up according to the equations shown in section *4.5.2 Data work-up*.

1. Experimentally determined mole fractions of CO and CO_2 (x_{CO} and x_{CO2} respectively) in each sample are presented in the data.

2. At low CO conversion, conversion was determined by equation 4-4.

3. At high CO conversion (i.e. greater than 76 %), conversion was determined by back-calculation from the CO_2 data (equation 4-8).

4. In the instances of high CO conversion, conversion was calculated on the basis of a 100 % carbon balance. The carbon balance, determined from the combined normalised flowrate (F'_{CO+CO2}) of CO and CO_2, is also shown in the results. The calculations were done on the basis of a normalised dry feed gas flowrate (F'_{DRY}) of 100 mol/s. For gas mixtures 1 and 2, a 100 % carbon balance represents a total carbon flowrate (F'_{CO+CO2}) of 20.0 and 20.2 mol/s, respectively.

5. The back-calculated normalised CO flowrate (F'_{CO}) is shown in *italics*.

6. The calculated carbon balance data, for CO conversion less than 76 %, ranges between 98 and 102 % — 98 % representing less 'carbon' detected than actually present, 102 % the opposite.

7. Multiple analysis data is reported for each experimental condition (as discussed in section *4.5.1 Gas chromatography*), showing the consistency of results.

EXPERIMENT 1 - Commercial LTS (Initial Performance, $WHSV_{dry}$ = 2.0 hr^{-1})

Time-on-stream (hours)	X_{CO} (%)	C balance (%)	x_{CO} (%)	x_{CO2} (%)	F'_{CO} (mol/s)	F'_{CO2} (mol/s)	F'_{CO+CO2} (mol/s)
0.75	**92.9**	*100.0*		0.193	*0.21*	19.79	*20.0*
	94.8	*100.0*		0.193	*0.15*	19.85	*20.0*
	94.2	*100.0*		0.193	*0.17*	19.83	*20.0*
	91.5	*100.0*		0.192	*0.25*	19.75	*20.0*
	94.9	*100.0*		0.193	*0.15*	19.85	*20.0*
	93.7						
8	**89.4**	*100.0*		0.192	*0.31*	19.69	*20.0*
	92.4	*100.0*		0.193	*0.22*	19.78	*20.0*
	91.7	*100.0*		0.193	*0.24*	19.76	*20.0*
	89.8	*100.0*		0.192	*0.30*	19.70	*20.0*
	90.1	*100.0*		0.192	*0.29*	19.71	*20.0*
	89.6	*100.0*		0.192	*0.30*	19.70	*20.0*
	90.5						
12	**81.4**	*100.0*		0.190	*0.54*	19.46	*20.0*
	83.3	*100.0*		0.191	*0.48*	19.52	*20.0*
	83.4	*100.0*		0.191	*0.48*	19.52	*20.0*
	82.8	*100.0*		0.190	*0.50*	19.50	*20.0*
	82.7						
20	**72.4**	100.3	0.008	0.189	0.80	19.27	20.1
	72.0	98.5	0.008	0.185	0.81	18.90	19.7
	73.1	99.0	0.008	0.186	0.78	19.01	19.8
	73.8	99.2	0.007	0.187	0.76	19.09	19.8
	72.8						
28	**54.1**	98.6	0.013	0.181	1.33	18.39	19.7
	55.1	99.3	0.013	0.183	1.30	18.55	19.9
	55.0	99.5	0.013	0.183	1.31	18.60	19.9
	54.8	99.5	0.013	0.183	1.31	18.59	19.9
	54.3	100.2	0.013	0.184	1.33	18.71	20.0
	54.7						
37.5	**34.7**	99.4	0.019	0.178	1.89	17.98	19.9
	33.9	100.3	0.019	0.180	1.92	18.14	20.1
	35.2	99.8	0.019	0.179	1.88	18.07	20.0
	34.9	99.4	0.019	0.178	1.89	17.99	19.9
	34.7						
51.5	**19.5**	99.5	0.023	0.175	2.33	17.57	19.9
	20.4	99.5	0.023	0.175	2.31	17.59	19.9
	20.0						

EXPERIMENT 2 - Commercial LTS (Initial Performance, $WHSV_{dry}$ = 2.0 hr^{-1})

Time-on-stream (hours)	X_{CO} (%)	C balance (%)	x_{CO}	x_{CO2}	F'_{CO} (mol/s)	F'_{CO2} (mol/s)	F'_{CO+CO2} (mol/s)
9	**92.6**	*100.0*		0.193	*0.21*	19.79	*20.0*
	93.8	*100.0*		0.193	*0.18*	19.82	*20.0*
	91.8	*100.0*		0.193	*0.24*	19.76	*20.0*
	90.7	*100.0*		0.192	*0.27*	19.73	*20.0*
	92.2						
19.5	**73.6**	*100.0*		0.188	*0.77*	19.23	*20.0*
	74.7	*100.0*		0.189	*0.73*	19.27	*20.0*
	76.8	*100.0*		0.189	*0.67*	19.33	*20.0*
	77.0	*100.0*		0.189	*0.67*	19.33	*20.0*
	77.9	*100.0*		0.189	*0.64*	19.36	*20.0*
	76.1						
27.5	**62.4**	99.8	0.011	0.185	1.09	18.87	20.0
	64.1	98.4	0.010	0.183	1.04	18.65	19.7
	63.8	98.7	0.010	0.184	1.05	18.69	19.7
	63.7	99.4	0.010	0.185	1.05	18.83	19.9
	63.5						
49.5	**46.8**	98.9	0.015	0.180	1.54	18.24	19.8
	45.9	100.3	0.015	0.182	1.57	18.49	20.1
	45.8	99.8	0.016	0.182	1.57	18.39	20.0
	46.7	99.8	0.015	0.182	1.55	18.41	20.0
	46.3						
68	**32.2**	99.3	0.019	0.177	1.97	17.90	19.9
	32.3	99.7	0.019	0.178	1.96	17.97	19.9
	33.4	99.2	0.019	0.177	1.93	17.91	19.8
	33.1	99.4	0.019	0.178	1.94	17.94	19.9
	32.8						
79	**23.0**	99.9	0.022	0.176	2.23	17.74	20.0
	22.8	100.3	0.022	0.177	2.24	17.83	20.1
	23.7	100.5	0.022	0.178	2.21	17.89	20.1
	23.2						

EXPERIMENT 3 - Commercial LTS (Initial Performance, std conditions)

Time-on-stream (hours)	X_{CO} (%)	C balance (%)	x_{CO}	x_{CO2}	F'_{CO} (mol/s)	F'_{CO2} (mol/s)	F'_{CO+CO2} (mol/s)
0.5	**95.9**	*100.0*		0.193	*0.12*	19.88	*20.0*
	90.6	*100.0*		0.192	*0.27*	19.73	*20.0*
	92.9	*100.0*		0.193	*0.21*	19.79	*20.0*
	93.1						
4.5	**90.9**	*100.0*		0.192	*0.26*	19.74	*20.0*
	91.8	*100.0*		0.193	*0.24*	19.76	*20.0*
	94.0	*100.0*		0.193	*0.17*	19.83	*20.0*
	92.2						
11.5	**83.0**	*100.0*		0.190	*0.49*	19.51	*20.0*
	88.7	*100.0*		0.192	*0.33*	19.67	*20.0*
	88.7	*100.0*		0.192	*0.33*	19.67	*20.0*
	86.8						
20.5	**75.8**	*100.0*		0.189	*0.70*	19.30	*20.0*
	78.7	*100.0*		0.189	*0.62*	19.38	*20.0*
	79.7	*100.0*		0.190	*0.59*	19.41	*20.0*
	75.6	*100.0*		0.189	*0.71*	19.29	*20.0*
	79.3	*100.0*		0.190	*0.60*	19.40	*20.0*
	74.2	*100.0*		0.188	*0.75*	19.25	*20.0*
	74.9	*100.0*		0.189	*0.73*	19.27	*20.0*
	76.9						
26	**73.3**	98.6	0.008	0.186	0.78	18.95	19.7
	72.5	98.8	0.008	0.186	0.80	18.96	19.8
	74.9	98.3	0.007	0.185	0.73	18.92	19.7
	74.7	99.3	0.007	0.187	0.73	19.12	19.9
	72.4	99.4	0.008	0.187	0.80	19.08	19.9
	74.2	98.5	0.007	0.186	0.75	18.95	19.7
	75.3	97.9	0.007	0.185	0.72	18.86	19.6
	73.4						
31	**70.0**	99.8	0.009	0.187	0.87	19.09	20.0
	69.4	98.6	0.009	0.185	0.89	18.84	19.7
	69.7	99.5	0.009	0.186	0.88	19.02	19.9
	70.1	99.7	0.009	0.187	0.87	19.07	19.9
	72.4	99.7	0.008	0.187	0.80	19.13	19.9
	70.3						
36	**66.6**	99.2	0.009	0.185	0.97	18.87	19.8
	68.7	98.3	0.009	0.184	0.91	18.76	19.7
	68.0	99.4	0.009	0.186	0.93	18.95	19.9
	67.8						
45	**66.0**	98.1	0.010	0.183	0.99	18.63	19.6
	64.1	98.6	0.010	0.183	1.04	18.68	19.7
	66.5	98.6	0.010	0.184	0.97	18.75	19.7
	65.7	98.0	0.010	0.182	1.00	18.60	19.6
	65.6	98.2	0.010	0.183	1.00	18.65	19.6
	65.6						

Time-on-stream (hours)	X_{CO} (%)	C balance (%)	x_{CO}	x_{CO2}	F'_{CO} (mol/s)	F'_{CO2} (mol/s)	F'_{CO+CO2} (mol/s)
52	**62.5**	98.5	0.011	0.183	1.09	18.62	19.7
	65.0	99.2	0.010	0.185	1.01	18.83	19.8
	62.3	99.3	0.011	0.184	1.09	18.76	19.9
	64.3	99.7	0.010	0.186	1.04	18.91	19.9
	63.4	100.3	0.010	0.187	1.06	19.00	20.1
	63.5						
60.5	**62.1**	99.6	0.011	0.185	1.10	18.81	19.9
	62.4	99.5	0.011	0.185	1.09	18.82	19.9
	63.1	100.1	0.011	0.186	1.07	18.95	20.0
	63.0	99.4	0.011	0.185	1.07	18.80	19.9
	63.0	98.0	0.011	0.182	1.07	18.53	19.6
	62.7						
69	**62.7**	99.9	0.011	0.186	1.08	18.90	20.0
	61.4	98.9	0.011	0.183	1.12	18.67	19.8
	62.6	100.7	0.011	0.187	1.08	19.06	20.1
	61.9	99.9	0.011	0.185	1.11	18.88	20.0
	63.0	98.8	0.011	0.183	1.07	18.68	19.8
	62.3	99.7	0.011	0.185	1.09	18.86	19.9
	61.9	99.6	0.011	0.185	1.10	18.82	19.9
	61.7	100.1	0.011	0.186	1.11	18.91	20.0
	62.2						
75.5	**62.4**	99.7	0.011	0.185	1.09	18.85	19.9
	62.3	100.8	0.011	0.187	1.09	19.06	20.2
	62.5	99.7	0.011	0.185	1.09	18.85	19.9
	61.8	98.8	0.011	0.183	1.11	18.65	19.8
	62.3						

EXPERIMENT 4 - Commercial LTS (Initial Performance, std conditions)

Time-on-stream (hours)	X_{CO} (%)	C balance (%)	x_{CO}	x_{CO2}	F'_{CO} (mol/s)	F'_{CO2} (mol/s)	F'_{CO+CO2} (mol/s)
0.75	**94.2**	*100.0*		0.193	*0.17*	19.83	*20.0*
	94.5	*100.0*		0.193	*0.16*	19.84	*20.0*
	94.9	*100.0*		0.193	*0.15*	19.85	*20.0*
	94.5						
6.25	**92.6**	*100.0*		0.193	*0.22*	19.78	*20.0*
	91.3	*100.0*		0.192	*0.25*	19.75	*20.0*
	91.9						
12.25	**86.8**	*100.0*		0.191	*0.38*	19.62	*20.0*
	85.2	*100.0*		0.191	*0.43*	19.57	*20.0*
	86.3	*100.0*		0.191	*0.40*	19.60	*20.0*
	85.4	*100.0*		0.191	*0.42*	19.58	*20.0*
	83.8	*100.0*		0.191	*0.47*	19.53	*20.0*
	85.5						
21.5	**77.0**	*100.0*		0.189	0.67	19.33	*20.0*
	72.3	*100.0*		0.188	0.80	19.20	*20.0*
	82.1	*100.0*		0.190	0.52	19.48	*20.0*
	82.0	*100.0*		0.190	0.52	19.48	*20.0*
	73.2	*100.0*		0.188	0.78	19.22	*20.0*
	78.2	*100.0*		0.189	0.63	19.37	*20.0*
	82.4	*100.0*		0.190	0.51	19.49	*20.0*
	74.9	*100.0*		0.189	0.73	19.27	*20.0*
	74.7	*100.0*		0.189	0.73	19.27	*20.0*
	77.8						
27.75	**70.2**	100.1	0.008	0.188	0.86	19.15	20.0
	69.8	99.4	0.009	0.186	0.88	19.00	19.9
	71.6	100.5	0.008	0.189	0.82	19.28	20.1
	70.4	100.0	0.008	0.188	0.86	19.14	20.0
	69.2	100.3	0.009	0.188	0.89	19.17	20.1
	70.6	99.4	0.008	0.187	0.85	19.03	19.9
	69.5	99.4	0.009	0.186	0.88	18.99	19.9
	70.2						
36.25	**68.7**	99.9	0.009	0.187	0.90	19.08	20.0
	68.8	100.7	0.009	0.189	0.90	19.23	20.1
	68.2	100.9	0.009	0.189	0.92	19.26	20.2
	68.1	101.5	0.009	0.190	0.92	19.38	20.3
	68.2	101.1	0.009	0.189	0.92	19.29	20.2
	68.0	100.5	0.009	0.188	0.92	19.17	20.1
	68.9	100.8	0.009	0.189	0.90	19.26	20.2
	68.4						

Time-on-stream (hours)	X_{CO} (%)	C balance (%)	x_{CO}	x_{CO2}	F'_{CO} (mol/s)	F'_{CO2} (mol/s)	F'_{CO+CO2} (mol/s)
45.75	**64.7**	101.1	0.010	0.188	1.02	19.19	20.2
	65.1	98.7	0.010	0.184	1.01	18.72	19.7
	64.9	102.0	0.010	0.190	1.02	19.38	20.4
	64.5	100.8	0.010	0.188	1.03	19.14	20.2
	64.2	100.1	0.010	0.186	1.04	18.98	20.0
	64.9	102.5	0.010	0.191	1.02	19.48	20.5
	64.6	101.9	0.010	0.190	1.03	19.36	20.4
	64.7						
51.75	**61.4**	101.4	0.011	0.188	1.12	19.17	20.3
	61.5	101.6	0.011	0.189	1.12	19.19	20.3
	60.7	101.5	0.011	0.188	1.14	19.16	20.3
	62.4	99.6	0.011	0.185	1.09	18.82	19.9
	61.2	100.0	0.011	0.185	1.13	18.88	20.0
	62.2	100.6	0.011	0.187	1.10	19.02	20.1
	61.1	99.8	0.011	0.185	1.13	18.84	20.0
	61.5	100.7	0.011	0.187	1.12	19.02	20.1
	62.1	100.1	0.011	0.186	1.10	18.93	20.0
	61.6						
60.25	**60.6**	100.3	0.011	0.186	1.14	18.91	20.1
	61.7	101.2	0.011	0.188	1.11	19.13	20.2
	62.0	99.4	0.011	0.184	1.10	18.78	19.9
	61.9	98.2	0.011	0.182	1.10	18.53	19.6
	61.3	100.4	0.011	0.186	1.12	18.96	20.1
	61.7	100.0	0.011	0.186	1.11	18.89	20.0
	61.0	100.8	0.011	0.187	1.13	19.04	20.2
	61.5						
89.5	**61.9**	99.8	0.011	0.185	1.11	18.85	20.0
	61.9	99.5	0.011	0.185	1.10	18.79	19.9
	62.0	98.7	0.011	0.183	1.10	18.65	19.7
	61.9						
104	**62.3**	98.4	0.011	0.183	1.09	18.58	19.7
	62.2	99.2	0.011	0.184	1.10	18.74	19.8
	61.9	99.4	0.011	0.184	1.10	18.78	19.9
	62.1						
142.75	**61.5**	99.7	0.011	0.185	1.12	18.81	19.9
	60.8	99.8	0.011	0.185	1.14	18.83	20.0
	61.9	100.1	0.011	0.186	1.11	18.92	20.0
	61.4						
178	**61.6**	99.1	0.011	0.184	1.11	18.70	19.8
	60.8	99.5	0.011	0.184	1.14	18.76	19.9
	61.2	98.8	0.011	0.183	1.13	18.63	19.8
	61.2						

EXPERIMENT 4 - Commercial LTS ($WHSV_{dry}$ = 2.0 hr^{-1})

Time-on-stream (hours)	Temperature (°C)	X_{CO} (%)	C balance (%)	x_{CO}	x_{CO2}	F'_{CO} (mol/s)	F'_{CO2} (mol/s)	F'_{CO+CO2} (mol/s)
147.75	**188**	**75.7**	99.6	0.007	0.188	0.71	19.22	19.9
		73.9	99.4	0.007	0.187	0.76	19.12	19.9
		77.0	100.0	0.007	0.189	0.67	19.33	20.0
		74.0	98.7	0.007	0.186	0.75	18.98	19.7
		74.1	99.4	0.007	0.187	0.75	19.13	19.9
		74.2	99.6	0.007	0.188	0.75	19.17	19.9
		74.5						
152.5	**192**	**86.9**	*100.0*		0.191	*0.38*	19.62	*20.0*
		82.6	*100.0*		0.190	*0.50*	19.50	*20.0*
		84.1	*100.0*		0.191	*0.46*	19.54	*20.0*
		80.9	*100.0*		0.190	*0.55*	19.45	*20.0*
		86.3	*100.0*		0.191	*0.40*	19.60	*20.0*
		86.6	*100.0*		0.191	*0.39*	19.61	*20.0*
		88.1	*100.0*		0.192	*0.35*	19.65	*20.0*
		86.3	*100.0*		0.191	*0.40*	19.60	*20.0*
		85.1	*100.0*		0.191	*0.43*	19.57	*20.0*
		85.2						
165.5	**196**	**92.5**	*100.0*		0.193	*0.22*	19.78	*20.0*
		89.7	*100.0*		0.192	*0.30*	19.70	*20.0*
		93.7	*100.0*		0.193	*0.18*	19.82	*20.0*
		91.1	*100.0*		0.192	*0.26*	19.74	*20.0*
		89.8	*100.0*		0.192	*0.30*	19.70	*20.0*
		89.7	*100.0*		0.192	*0.30*	19.70	*20.0*
		98.5	*100.0*		0.194	*0.04*	19.96	*20.0*
		92.1						
170.5	**200**	**96.7**	*100.0*		0.194	*0.09*	19.91	*20.0*
		92.0	*100.0*		0.193	*0.23*	19.77	*20.0*
		93.1	*100.0*		0.193	*0.20*	19.80	*20.0*
		93.9						
172.75	**204**	**95.3**	*100.0*		0.193	*0.14*	19.86	*20.0*
		93.6	*100.0*		0.193	*0.19*	19.81	*20.0*
		94.1	*100.0*		0.193	*0.17*	19.83	*20.0*
		94.3						

EXPERIMENT 4 - Commercial LTS ($WHSV_{dry}$ = 4.0 hr^{-1})

Time-on-stream (hours)	Temperature (°C)	X_{CO} (%)	C balance (%)	x_{CO}	x_{CO2}	F'_{CO} (mol/s)	F'_{CO2} (mol/s)	F'_{CO+CO2} (mol/s)
111	188	54.3	99.5	0.013	0.183	1.32	18.57	19.9
		54.2	99.7	0.013	0.183	1.33	18.61	19.9
		54.5	99.5	0.013	0.183	1.32	18.59	19.9
		54.1	99.6	0.013	0.183	1.33	18.59	19.9
		54.5	100.4	0.013	0.185	1.32	18.75	20.1
		54.0	100.8	0.013	0.185	1.33	18.83	20.2
		54.3						
118.25	188	53.6	100.8	0.013	0.185	1.35	18.82	20.2
		54.7	99.6	0.013	0.183	1.31	18.61	19.9
		54.4	100.6	0.013	0.185	1.32	18.79	20.1
		54.1	101.0	0.013	0.186	1.33	18.87	20.2
		54.2						
51.75	192	62.0	99.4	0.011	0.185	1.10	18.79	19.9
		61.6	101.4	0.011	0.188	1.11	19.16	20.3
		60.6	99.6	0.011	0.185	1.14	18.78	19.9
		62.3	95.7	0.011	0.177	1.09	18.05	19.1
		61.1	100.0	0.011	0.185	1.13	18.88	20.0
		60.7	100.8	0.011	0.187	1.14	19.02	20.2
		62.5	99.7	0.011	0.185	1.09	18.84	19.9
		61.5	100.7	0.011	0.187	1.12	19.02	20.1
		62.0	100.1	0.011	0.186	1.10	18.93	20.0
		61.6						
60.25	192	61.9	100.1	0.011	0.186	1.10	18.92	20.0
		61.7	101.2	0.011	0.188	1.11	19.13	20.2
		61.9	99.4	0.011	0.184	1.10	18.78	19.9
		61.9	100.1	0.011	0.186	1.11	18.92	20.0
		61.2	100.4	0.011	0.186	1.12	18.96	20.1
		61.6	100.0	0.011	0.186	1.11	18.89	20.0
		62.3	100.7	0.011	0.187	1.09	19.04	20.1
		61.8						
71.75	196	71.2	99.1	0.008	0.186	0.83	18.98	19.8
		70.5	95.6	0.008	0.179	0.85	18.26	19.1
		69.7	98.3	0.009	0.184	0.88	18.78	19.7
		70.2	99.9	0.008	0.187	0.86	19.11	20.0
		70.4	99.2	0.008	0.186	0.86	18.98	19.8
		70.4						
76.5	196	69.0	99.4	0.009	0.186	0.90	18.99	19.9
		70.3	99.5	0.008	0.187	0.86	19.04	19.9
		69.3	97.9	0.009	0.183	0.89	18.68	19.6
		70.6	97.0	0.008	0.182	0.85	18.56	19.4
		69.4	98.8	0.009	0.185	0.89	18.86	19.8
		69.3	98.6	0.009	0.185	0.89	18.83	19.7
		67.9	98.7	0.009	0.184	0.93	18.80	19.7
		70.5	98.1	0.008	0.184	0.86	18.76	19.6
		69.5	100.1	0.009	0.188	0.88	19.13	20.0
		68.8	97.3	0.009	0.182	0.91	18.55	19.5
		69.5						

Time-on-stream (hours)	Temperature (°C)	X_{CO} (%)	C balance (%)	x_{CO}	x_{CO2}	F'_{CO} (mol/s)	F'_{CO2} (mol/s)	F'_{CO+CO2} (mol/s)
83.5	**196**	**70.5**	99.5	0.008	0.187	0.86	19.04	19.9
		70.8	100.5	0.008	0.189	0.85	19.25	20.1
		69.9	102.1	0.009	0.192	0.87	19.55	20.4
		70.4	99.7	0.008	0.187	0.86	19.08	19.9
		69.2	99.2	0.009	0.186	0.89	18.95	19.8
		69.2	99.0	0.009	0.185	0.89	18.91	19.8
		70.2	98.8	0.008	0.185	0.86	18.90	19.8
		70.0						
84.75	**200**	**74.9**	99.2	0.007	0.187	0.73	19.11	19.8
		74.8	101.4	0.007	0.191	0.73	19.55	20.3
		74.7	101.0	0.007	0.191	0.73	19.47	20.2
		74.6	100.2	0.007	0.189	0.74	19.30	20.0
		74.8	99.8	0.007	0.188	0.73	19.23	20.0
		74.6	99.4	0.007	0.187	0.74	19.14	19.9
		74.8	99.4	0.007	0.187	0.73	19.15	19.9
		73.9	100.1	0.007	0.189	0.76	19.27	20.0
		75.2	101.0	0.007	0.191	0.72	19.47	20.2
		74.7						
93.5	**200**	**74.4**	99.4	0.007	0.187	0.74	19.14	19.9
		75.6	98.9	0.007	0.187	0.71	19.07	19.8
		75.3	100.1	0.007	0.189	0.72	19.30	20.0
		75.4	98.9	0.007	0.187	0.71	19.06	19.8
		75.2	98.8	0.007	0.186	0.72	19.05	19.8
		74.9	99.8	0.007	0.188	0.73	19.23	20.0
		75.1	100.7	0.007	0.190	0.72	19.42	20.1
		75.8	99.7	0.007	0.188	0.70	19.24	19.9
		75.0	99.3	0.007	0.187	0.73	19.12	19.9
		75.2						
101	**200**	**74.7**	101.3	0.007	0.191	0.73	19.52	20.3
		76.4	99.7	0.007	0.188	0.68	19.25	19.9
		75.6	101.3	0.007	0.191	0.71	19.54	20.3
		72.6	99.8	0.008	0.188	0.80	19.16	20.0
		74.7	99.5	0.007	0.188	0.73	19.16	19.9
		74.8	99.7	0.007	0.188	0.73	19.21	19.9
		73.9	101.0	0.007	0.190	0.76	19.44	20.2
		74.7						
108	**204**	**81.8**	*100.0*		0.190	*0.53*	19.47	*20.0*
		75.2	*100.0*		0.189	*0.72*	19.28	*20.0*
		77.9	*100.0*		0.189	*0.64*	19.36	*20.0*
		81.0	*100.0*		0.190	*0.55*	19.45	*20.0*
		79.0						

EXPERIMENT 4 - Commercial LTS ($WHSV_{dry}$ = 6.0 hr^{-1})

Time-on-stream (hours)	Temperature (°C)	X_{CO} (%)	C balance (%)	x_{CO}	x_{CO2}	F'_{CO} (mol/s)	F'_{CO2} (mol/s)	F'_{CO+CO2} (mol/s)
120.25	**188**	**37.6**	100.9	0.018	0.182	1.81	18.38	20.2
		38.7	99.0	0.018	0.178	1.78	18.03	19.8
		38.2	99.4	0.018	0.179	1.79	18.10	19.9
		37.8	99.9	0.018	0.180	1.80	18.18	20.0
		38.0	99.2	0.018	0.179	1.80	18.05	19.8
		38.9	99.9	0.018	0.180	1.77	18.22	20.0
		38.2	99.1	0.018	0.178	1.79	18.03	19.8
		38.9	99.7	0.018	0.180	1.77	18.17	19.9
		38.4						
122.25	**192**	**46.4**	98.2	0.015	0.179	1.55	18.09	19.6
		48.4	99.9	0.015	0.182	1.49	18.48	20.0
		45.4	99.7	0.016	0.181	1.58	18.37	19.9
		46.8	100.2	0.015	0.182	1.54	18.49	20.0
		44.5	100.8	0.016	0.183	1.61	18.54	20.2
		44.3	99.0	0.016	0.180	1.62	18.18	19.8
		45.7	99.7	0.016	0.181	1.58	18.37	19.9
		45.2	98.4	0.016	0.179	1.59	18.09	19.7
		46.1						
125.25	**192**	**45.2**	99.9	0.016	0.182	1.59	18.39	20.0
		48.1	98.4	0.015	0.179	1.51	18.17	19.7
		44.5	97.1	0.016	0.176	1.61	17.81	19.4
		45.7	99.3	0.016	0.180	1.58	18.28	19.9
		46.0	101.3	0.015	0.184	1.57	18.69	20.3
		47.4	98.2	0.015	0.179	1.53	18.12	19.6
		45.8						
131.25	**196**	**54.6**	99.2	0.013	0.182	1.32	18.53	19.8
		52.9	101.2	0.013	0.186	1.36	18.88	20.2
		52.4	99.2	0.014	0.182	1.38	18.46	19.8
		53.9	100.2	0.013	0.184	1.34	18.71	20.0
		54.3	102.0	0.013	0.188	1.33	19.07	20.4
		54.3	99.6	0.013	0.183	1.33	18.59	19.9
		53.7						
134.25	**200**	**56.7**	99.0	0.012	0.182	1.26	18.54	19.8
		56.9	100.6	0.012	0.186	1.25	18.87	20.1
		56.9	100.0	0.012	0.185	1.25	18.76	20.0
		57.1	99.6	0.012	0.184	1.24	18.67	19.9
		58.6	101.6	0.012	0.188	1.20	19.12	20.3
		57.0	99.0	0.012	0.183	1.25	18.55	19.8
		56.7	99.0	0.012	0.182	1.26	18.55	19.8
		58.0	101.3	0.012	0.187	1.22	19.04	20.3
		57.3						
137.75	**204**	**61.8**	99.1	0.011	0.184	1.11	18.72	19.8
		61.1	100.1	0.011	0.186	1.13	18.89	20.0
		61.1	98.6	0.011	0.183	1.13	18.60	19.7
		61.3						

EXPERIMENT 5 - Au/LTS-38 (Initial Performance, std conditions)

Time-on-stream (hours)	X_{CO} (%)	C balance (%)	x_{CO}	x_{CO2}	F'_{CO} (mol/s)	F'_{CO2} (mol/s)	F'_{CO+CO2} (mol/s)
0.75	**94.5**	*100.0*		0.193	*0.16*	19.84	*20.0*
	94.1	*100.0*		0.193	*0.17*	19.83	*20.0*
	92.8	*100.0*		0.193	*0.21*	19.79	*20.0*
	95.7	*100.0*		0.193	*0.13*	19.87	*20.0*
	94.3						
6.75	**93.6**	*100.0*		0.193	*0.18*	19.82	*20.0*
	93.0	*100.0*		0.193	*0.20*	19.80	*20.0*
	94.5	*100.0*		0.193	*0.16*	19.84	*20.0*
	89.7	*100.0*		0.192	*0.30*	19.70	*20.0*
	92.7						
13.5	**89.4**	*100.0*		0.192	*0.31*	19.69	*20.0*
	86.9	*100.0*		0.191	*0.38*	19.62	*20.0*
	90.6	*100.0*		0.192	*0.27*	19.73	*20.0*
	87.1	*100.0*		0.191	*0.38*	19.62	*20.0*
	89.8	*100.0*		0.192	*0.30*	19.70	*20.0*
	88.3						
22.5	**77.2**	*100.0*		0.189	*0.66*	19.34	*20.0*
	79.3	*100.0*		0.190	*0.60*	19.40	*20.0*
	78.7	*100.0*		0.189	*0.62*	19.38	*20.0*
	75.4	*100.0*		0.189	*0.71*	19.29	*20.0*
	76.8	*100.0*		0.189	*0.67*	19.33	*20.0*
	78.4	*100.0*		0.189	*0.63*	19.37	*20.0*
	77.5						
29.5	**71.0**	99.0	0.008	0.186	0.84	18.97	19.8
	73.2	99.0	0.008	0.186	0.78	19.01	19.8
	72.2	98.9	0.008	0.186	0.81	18.97	19.8
	72.0	98.7	0.008	0.185	0.81	18.93	19.7
	71.3	99.9	0.008	0.188	0.83	19.14	20.0
	71.9						
37.25	**68.8**	99.2	0.009	0.186	0.90	18.93	19.8
	71.5	98.6	0.008	0.185	0.83	18.88	19.7
	69.2	99.3	0.009	0.186	0.89	18.96	19.9
	69.2	98.6	0.009	0.185	0.89	18.84	19.7
	68.0	100.0	0.009	0.187	0.93	19.07	20.0
	69.4						
47.25	**68.8**	99.6	0.009	0.186	0.91	19.01	19.9
	69.9	99.9	0.009	0.187	0.88	19.10	20.0
	68.4	99.5	0.009	0.186	0.92	18.98	19.9
	68.2	99.1	0.009	0.185	0.92	18.89	19.8
	68.2	98.0	0.009	0.183	0.92	18.67	19.6
	69.8	98.7	0.009	0.185	0.88	18.87	19.7
	68.9						

	X_{CO} (%)	C balance (%)	x_{CO}	x_{CO2}	F'_{CO} (mol/s)	F'_{CO2} (mol/s)	F'_{CO+CO2} (mol/s)
50.75	**68.9**	98.1	0.009	0.183	0.91	18.71	19.6
	67.8	98.5	0.009	0.184	0.94	18.76	19.7
	68.6	100.4	0.009	0.188	0.92	19.17	20.1
	68.0	98.3	0.009	0.184	0.93	18.74	19.7
	69.6	99.3	0.009	0.186	0.89	18.97	19.9
	68.6						
54.5	**68.7**	99.6	0.009	0.186	0.91	19.01	19.9
	67.9	98.5	0.009	0.184	0.93	18.77	19.7
	68.0	101.2	0.009	0.189	0.93	19.32	20.2
	66.8	98.4	0.009	0.184	0.97	18.72	19.7
	69.0	99.3	0.009	0.186	0.90	18.95	19.9
	68.1						
60.75	**68.8**	100.2	0.009	0.188	0.91	19.13	20.0
	68.0	99.1	0.009	0.185	0.93	18.90	19.8
	68.5	99.7	0.009	0.187	0.92	19.03	19.9
	67.6	99.8	0.009	0.187	0.94	19.03	20.0
	68.0	100.0	0.009	0.187	0.93	19.08	20.0
	67.0	99.3	0.009	0.185	0.96	18.90	19.9
	68.0						
71.25	**67.4**	99.2	0.009	0.185	0.95	18.90	19.8
	68.1	97.4	0.009	0.182	0.93	18.55	19.5
	67.9	100.9	0.009	0.189	0.93	19.24	20.2
	68.1	100.1	0.009	0.187	0.93	19.09	20.0
	68.2	98.3	0.009	0.184	0.92	18.74	19.7
	67.9						
115.5	**67.2**	99.9	0.009	0.187	0.95	19.02	20.0
	67.3	99.8	0.009	0.187	0.95	19.02	20.0
	67.9	99.3	0.009	0.186	0.94	18.93	19.9
	67.4						

EXPERIMENT 5 - Au/LTS-38 ($WHSV_{dry}$ = 2.0 hr^{-1})

Time-on-stream (hours)	Temperature (°C)	X_{CO} (%)	C balance (%)	x_{CO}	x_{CO2}	F'_{CO} (mol/s)	F'_{CO2} (mol/s)	F'_{CO+CO2} (mol/s)
98.75	**192**	**89.5**	*100.0*		0.192	*0.31*	19.69	*20.0*
		86.9	*100.0*		0.191	*0.38*	19.62	*20.0*
		88.1	*100.0*		0.192	*0.35*	19.65	*20.0*
		86.7	*100.0*		0.191	*0.39*	19.61	*20.0*
		88.0	*100.0*		0.192	*0.35*	19.65	*20.0*
		87.8						
102.25	**196**	**91.3**	*100.0*		0.192	*0.25*	19.75	*20.0*
		93.6	*100.0*		0.193	*0.18*	19.82	*20.0*
		94.1	*100.0*		0.193	*0.17*	19.83	*20.0*
		92.7	*100.0*		0.193	*0.21*	19.79	*20.0*
		92.9						
110.75	**200**	**94.2**	*100.0*		0.193	*0.17*	19.83	*20.0*
		94.1	*100.0*		0.193	*0.17*	19.83	*20.0*
		95.9	*100.0*		0.193	*0.12*	19.88	*20.0*
		93.9	*100.0*		0.193	*0.18*	19.82	*20.0*
		94.5						

EXPERIMENT 5 - Au/LTS-38 ($WHSV_{dry}$ = 4.0 hr^{-1})

Time-on-stream (hours)	Temperature (°C)	X_{CO} (%)	C balance (%)	x_{CO}	x_{CO2}	F'_{CO} (mol/s)	F'_{CO2} (mol/s)	F'_{CO+CO2} (mol/s)
75	**188**	**59.10**	99.2	0.012	0.183	1.19	18.65	19.8
		59.02	100.9	0.012	0.187	1.19	18.99	20.2
		58.09	100.2	0.012	0.185	1.22	18.82	20.0
		58.99	99.2	0.012	0.183	1.19	18.65	19.8
		58.80						
71.25	**192**	**67.27**	99.2	0.009	0.185	0.95	18.90	19.8
		68.09	99.3	0.009	0.186	0.93	18.94	19.9
		67.92	98.2	0.009	0.183	0.93	18.70	19.6
		68.09	100.1	0.009	0.187	0.93	19.09	20.0
		68.24	99.7	0.009	0.186	0.92	19.01	19.9
		67.92						
80	**196**	**72.22**	97.8	0.008	0.184	0.81	18.76	19.6
		71.61	98.7	0.008	0.185	0.82	18.92	19.7
		72.54	99.3	0.008	0.187	0.80	19.07	19.9
		72.44	100.5	0.008	0.189	0.80	19.31	20.1
		71.01	100.5	0.008	0.189	0.84	19.25	20.1
		71.96						
86	**200**	**73.40**	99.0	0.008	0.186	0.77	19.04	19.8
		73.98	97.8	0.007	0.184	0.75	18.82	19.6
		73.42	98.5	0.008	0.185	0.77	18.92	19.7
		74.15	100.1	0.007	0.189	0.75	19.27	20.0
		73.74						

EXPERIMENT 6 - Au/HTS-42 (Initial Performance, std conditions)

Time-on-stream (hours)	X_{CO} (%)	C balance (%)	x_{CO}	x_{CO2}	F'_{CO} (mol/s)	F'_{CO2} (mol/s)	F'_{CO+CO2} (mol/s)
1	**33.7**	100.0	0.019	0.179	1.92	18.08	20.0
	33.6	99.1	0.019	0.177	1.93	17.90	19.8
	33.7	98.6	0.019	0.176	1.92	17.80	19.7
	33.7	100.5	0.019	0.180	1.92	18.18	20.1
	33.0	100.3	0.019	0.179	1.94	18.12	20.1
	33.5						
6	**20.3**	100.6	0.023	0.177	2.31	17.80	20.1
	20.5	101.4	0.023	0.179	2.31	17.98	20.3
	19.5	100.8	0.023	0.177	2.33	17.83	20.2
	20.5	98.5	0.023	0.173	2.31	17.39	19.7
	20.2						
13	**15.5**	98.0	0.024	0.171	2.45	17.15	19.6
	17.0	98.8	0.024	0.173	2.41	17.35	19.8
	17.0	99.7	0.024	0.174	2.41	17.53	19.9
	17.6	98.0	0.024	0.171	2.39	17.21	19.6
	16.4	101.4	0.024	0.178	2.43	17.85	20.3
	16.7						
22.5	**13.7**	100.8	0.025	0.176	2.50	17.65	20.2
	13.6	100.5	0.025	0.175	2.51	17.59	20.1
	13.7	99.3	0.025	0.173	2.50	17.36	19.9
	13.2	99.2	0.025	0.173	2.52	17.33	19.8
	11.8	98.2	0.025	0.170	2.56	17.09	19.6
	13.2						
25	**13.3**	100.0	0.025	0.174	2.51	17.49	20.0
	13.1	100.0	0.025	0.174	2.52	17.48	20.0
	12.0	98.0	0.025	0.170	2.55	17.05	19.6
	12.5	100.5	0.025	0.175	2.54	17.55	20.1
	12.7						
30	**10.9**	100.1	0.026	0.174	2.58	17.44	20.0
	12.5	98.5	0.025	0.171	2.54	17.17	19.7
	9.9	98.7	0.026	0.171	2.61	17.13	19.7
	11.6	98.1	0.026	0.170	2.56	17.07	19.6
	10.8	98.3	0.026	0.170	2.59	17.08	19.7
	11.0	100.1	0.026	0.174	2.58	17.43	20.0
	11.1						
38	**9.2**	98.5	0.026	0.170	2.63	17.07	19.7
	7.7	100.5	0.027	0.174	2.68	17.43	20.1
	8.6	98.1	0.026	0.169	2.65	16.96	19.6
	8.3	99.9	0.027	0.173	2.66	17.32	20.0
	8.4						

EXPERIMENT 6 - Au/HTS-42 ($WHSV_{dry}$ = 2.0 hr^{-1})

Time-on-stream (hours)	Temperature (°C)	X_{CO} (%)	C balance (%)	x_{CO}	x_{CO2}	F'_{CO} (mol/s)	F'_{CO2} (mol/s)	F'_{CO+CO2} (mol/s)
60.75	**220**	**12.4**	99.6	0.025	0.173	2.54	17.38	19.9
		12.4	98.3	0.025	0.171	2.54	17.12	19.7
		12.1	98.9	0.025	0.172	2.55	17.22	19.8
		12.3						
74	**220**	**12.2**	99.9	0.025	0.174	2.55	17.43	20.0
		12.2	98.8	0.025	0.171	2.55	17.21	19.8
		12.8	98.7	0.025	0.171	2.53	17.21	19.7
		12.4						
82	**240**	**13.9**	99.8	0.025	0.174	2.50	17.45	20.0
		14.0	98.6	0.025	0.172	2.49	17.23	19.7
		13.9						

EXPERIMENT 6 - Au/HTS-42 ($WHSV_{dry}$ = 4.0 hr^{-1})

Time-on-stream (hours)	Temperature (°C)	X_{CO} (%)	C balance (%)	x_{CO}	x_{CO2}	F'_{CO} (mol/s)	F'_{CO2} (mol/s)	F'_{CO+CO2} (mol/s)
37.5	**192**	**9.2**	101.4	0.026	0.176	2.63	17.64	20.3
		7.7	100.5	0.027	0.174	2.68	17.43	20.1
		8.6	98.1	0.026	0.169	2.65	16.96	19.6
		8.3	99.9	0.027	0.173	2.66	17.32	20.0
		8.4						
48	**196**	**7.5**	98.7	0.027	0.170	2.68	17.06	19.7
		6.5	98.5	0.027	0.170	2.70	16.99	19.7
		7.0	100.9	0.027	0.175	2.69	17.49	20.2
		6.9	100.0	0.027	0.173	2.69	17.32	20.0
		7.0						
52.5	**200**	**8.9**	98.7	0.026	0.170	2.64	17.09	19.7
		7.4	100.2	0.027	0.173	2.69	17.36	20.0
		7.6	99.2	0.027	0.171	2.68	17.17	19.8
		8.9	98.0	0.026	0.169	2.64	16.97	19.6
		9.1	100.0	0.026	0.173	2.63	17.36	20.0
		8.4						
56	**210**	**8.0**	100.5	0.027	0.174	2.67	17.44	20.1
		9.0	100.1	0.026	0.173	2.64	17.39	20.0
		9.7	99.3	0.026	0.172	2.62	17.24	19.9
		8.9						
59	**220**	**8.7**	99.6	0.026	0.172	2.65	17.28	19.9
		9.8	99.2	0.026	0.172	2.61	17.23	19.8
		9.3						

EXPERIMENT 7 - Au/ZnO-27 (Initial Performance, std conditions)

Time-on-stream (hours)	X_{CO} (%)	C balance (%)	x_{CO}	x_{CO2}	F'_{CO} (mol/s)	F'_{CO2} (mol/s)	F'_{CO+CO2} (mol/s)
1	**24.8**	100.5	0.022	0.180	2.22	18.09	20.3
	25.0	100.5	0.022	0.180	2.21	18.10	20.3
	26.0	100.3	0.022	0.180	2.18	18.09	20.3
	24.5	100.0	0.022	0.178	2.22	17.97	20.2
	24.8	99.7	0.022	0.178	2.22	17.92	20.1
	25.0						
6.75	**20.2**	100.3	0.023	0.178	2.35	17.90	20.3
	20.9	100.1	0.023	0.178	2.33	17.88	20.2
	21.1	99.7	0.023	0.177	2.32	17.81	20.1
	20.7						
12.5	**17.8**	99.1	0.024	0.175	2.42	17.60	20.0
	17.2	99.9	0.024	0.177	2.44	17.74	20.2
	17.4	99.0	0.024	0.175	2.43	17.57	20.0
	16.8	99.2	0.024	0.175	2.45	17.59	20.0
	17.3						
25.5	**15.2**	99.2	0.025	0.175	2.50	17.54	20.0
	14.2	99.9	0.025	0.176	2.53	17.64	20.2
	14.5	100.0	0.025	0.176	2.52	17.68	20.2
	14.7	99.1	0.025	0.174	2.51	17.51	20.0
	14.6						
30.5	**13.5**	100.5	0.025	0.177	2.55	17.75	20.3
	13.8	99.5	0.025	0.175	2.54	17.56	20.1
	14.1	100.1	0.025	0.176	2.53	17.69	20.2
	13.7	99.2	0.025	0.174	2.54	17.49	20.0
	13.8						
38	**12.2**	100.5	0.026	0.177	2.58	17.72	20.3
	12.9	99.0	0.026	0.174	2.57	17.44	20.0
	12.4	100.2	0.026	0.176	2.58	17.66	20.2
	12.4	99.9	0.026	0.175	2.58	17.59	20.2
	13.2	100.3	0.025	0.176	2.56	17.71	20.3
	12.6						
48.5	**11.2**	100.2	0.026	0.176	2.62	17.63	20.2
	10.5	99.6	0.026	0.174	2.64	17.48	20.1
	10.7	99.4	0.026	0.174	2.63	17.45	20.1
	10.1	100.4	0.026	0.176	2.65	17.63	20.3
	10.7	99.4	0.026	0.174	2.63	17.46	20.1
	10.6						

Time-on-stream (hours)	X_{CO} (%)	C balance (%)	x_{CO}	x_{CO2}	F'_{CO} (mol/s)	F'_{CO2} (mol/s)	F'_{CO+CO2} (mol/s)
54	**10.3**	100.0	0.026	0.175	2.64	17.56	20.2
	10.8	99.5	0.026	0.174	2.63	17.48	20.1
	10.6	100.5	0.026	0.176	2.63	17.67	20.3
	10.2	99.8	0.026	0.175	2.64	17.52	20.2
	10.5						
60.5	**9.8**	100.2	0.026	0.175	2.66	17.59	20.2
	8.7	100.3	0.027	0.175	2.69	17.58	20.3
	8.6	100.6	0.027	0.176	2.69	17.63	20.3
	9.1	100.6	0.027	0.176	2.68	17.65	20.3
	9.7	100.1	0.027	0.175	2.66	17.57	20.2
	9.2						
72.25	**8.7**	100.6	0.027	0.176	2.69	17.64	20.3
	8.4	100.3	0.027	0.175	2.70	17.57	20.3
	8.0	99.9	0.027	0.174	2.71	17.48	20.2
	8.4	100.6	0.027	0.176	2.70	17.61	20.3
	8.4						
78.5	**8.8**	100.4	0.027	0.175	2.69	17.59	20.3
	8.1	99.8	0.027	0.174	2.71	17.45	20.2
	9.4	100.3	0.027	0.175	2.67	17.58	20.3
	7.6	99.9	0.027	0.174	2.72	17.46	20.2
	8.5						
110	**8.4**	100.4	0.027	0.175	2.70	17.58	20.3
	8.2	99.7	0.027	0.174	2.70	17.44	20.1
	8.2	100.4	0.027	0.175	2.70	17.58	20.3
	7.3	100.4	0.027	0.175	2.73	17.56	20.3
	8.0						

EXPERIMENT 7 - Au/ZnO-27 ($WHSV_{dry}$ = 2.0 hr^{-1})

Time-on-stream (hours)	Temperature (°C)	X_{CO} (%)	C balance (%)	x_{CO}	x_{CO2}	F'_{CO} (mol/s)	F'_{CO2} (mol/s)	F'_{CO+CO2} (mol/s)
97.25	**188**	**15.3**	99.0	0.025	0.174	2.50	17.51	20.0
		15.2	99.0	0.025	0.174	2.50	17.50	20.0
		14.1	100.3	0.025	0.176	2.53	17.72	20.3
		14.5	99.6	0.025	0.175	2.52	17.60	20.1
		14.8						
100	**192**	**18.0**	99.7	0.024	0.176	2.41	17.73	20.1
		17.3	99.3	0.024	0.175	2.44	17.63	20.1
		17.9	98.9	0.024	0.175	2.42	17.56	20.0
		17.6	99.7	0.024	0.176	2.43	17.72	20.1
		17.7						
103.75	**196**	**20.6**	99.5	0.023	0.176	2.34	17.75	20.1
		20.1	98.9	0.023	0.175	2.35	17.63	20.0
		21.1	99.5	0.023	0.177	2.32	17.78	20.1
		20.7	100.2	0.023	0.178	2.34	17.90	20.2
		20.6						
106	**200**	**24.2**	100.0	0.022	0.178	2.23	17.96	20.2
		24.0	99.3	0.022	0.177	2.24	17.83	20.1
		24.4	99.2	0.022	0.177	2.23	17.81	20.0
		23.9	98.6	0.022	0.176	2.24	17.68	19.9
		24.1						
110.5	**204**	**33.7**	99.0	0.019	0.179	1.95	18.04	20.0
		34.4	100.4	0.019	0.182	1.93	18.35	20.3
		33.9	99.7	0.019	0.180	1.95	18.19	20.1
		34.8	99.3	0.019	0.180	1.92	18.13	20.1
		34.2						

EXPERIMENT 7 - Au/ZnO-27 ($WHSV_{dry}$ = 4.0 hr^{-1})

Time-on-stream (hours)	Temperature (°C)	X_{CO} (%)	C balance (%)	x_{CO}	x_{CO2}	F'_{CO} (mol/s)	F'_{CO2} (mol/s)	F'_{CO+CO2} (mol/s)
90	**188**	**6.4**	100.1	0.028	0.174	2.76	17.46	20.2
		6.1	98.7	0.028	0.171	2.76	17.18	19.9
		6.0	99.4	0.028	0.173	2.77	17.31	20.1
		5.8	98.9	0.028	0.172	2.77	17.20	20.0
		6.1						
78.5	**192**	**8.8**	98.5	0.027	0.172	2.69	17.21	19.9
		8.6	99.7	0.027	0.174	2.69	17.46	20.1
		8.9	99.0	0.027	0.173	2.68	17.32	20.0
		7.6	99.9	0.027	0.174	2.72	17.46	20.2
		8.5						
80.5	**196**	**10.8**	99.5	0.026	0.174	2.63	17.48	20.1
		11.3	99.3	0.026	0.174	2.61	17.44	20.1
		11.8	99.7	0.026	0.175	2.60	17.55	20.1
		11.9	99.7	0.026	0.175	2.59	17.55	20.1
		11.6	99.7	0.026	0.175	2.60	17.53	20.1
		11.5						
86	**200**	**14.7**	98.6	0.025	0.173	2.51	17.40	19.9
		14.1	99.1	0.025	0.174	2.53	17.49	20.0
		13.3	100.0	0.025	0.176	2.55	17.64	20.2
		14.2	99.4	0.025	0.175	2.53	17.55	20.1
		14.1						
86	**204**	**16.7**	98.6	0.024	0.174	2.45	17.47	19.9
		16.1	99.5	0.025	0.175	2.47	17.63	20.1
		17.0	98.8	0.024	0.174	2.44	17.51	20.0
		16.6						

EXPERIMENT 8 - Au/ZnO-71 (Initial Performance, std conditions)

Time-on-stream (hours)	X_{CO} (%)	C balance (%)	x_{CO}	x_{CO2}	F'_{CO} (mol/s)	F'_{CO2} (mol/s)	F'_{CO+CO2} (mol/s)
1	**14.4**	99.3	0.025	0.175	2.52	17.53	20.1
	14.4	98.5	0.025	0.173	2.52	17.38	19.9
	14.4	98.1	0.025	0.172	2.52	17.29	19.8
	15.3	99.1	0.025	0.175	2.50	17.53	20.0
	15.3	99.0	0.025	0.174	2.49	17.51	20.0
	14.8						
5.25	**13.3**	98.9	0.025	0.174	2.55	17.42	20.0
	12.2	98.7	0.026	0.173	2.59	17.34	19.9
	14.1	98.7	0.025	0.173	2.53	17.42	19.9
	11.7	99.6	0.026	0.175	2.60	17.51	20.1
	12.8						
13.5	**11.0**	99.2	0.026	0.174	2.62	17.43	20.0
	9.1	99.6	0.027	0.174	2.68	17.44	20.1
	9.6	99.4	0.027	0.174	2.66	17.42	20.1
	11.5	98.2	0.026	0.172	2.61	17.23	19.8
	10.2	99.2	0.026	0.173	2.64	17.40	20.0
	10.3						
22	**7.0**	100.1	0.027	0.175	2.74	17.49	20.2
	7.8	98.7	0.027	0.172	2.72	17.21	19.9
	7.7	99.4	0.027	0.173	2.72	17.36	20.1
	8.2	99.3	0.027	0.173	2.70	17.35	20.1
	7.7						
29.5	**3.8**	99.0	0.028	0.172	2.83	17.17	20.0
	4.8	99.2	0.028	0.172	2.80	17.23	20.0
	6.1	99.8	0.028	0.174	2.77	17.39	20.2
	5.1	99.6	0.028	0.173	2.79	17.33	20.1
	5.0						
36.75	**3.5**	100.4	0.028	0.174	2.84	17.44	20.3
	4.4	99.5	0.028	0.173	2.82	17.28	20.1
	4.7	98.9	0.028	0.171	2.81	17.17	20.0
	3.9	99.3	0.028	0.172	2.83	17.22	20.1
	4.3	99.6	0.028	0.173	2.82	17.31	20.1
	3.7	99.0	0.028	0.171	2.84	17.16	20.0
	4.2						
46.5	**3.5**	98.9	0.028	0.171	2.84	17.14	20.0
	4.3	99.6	0.028	0.173	2.82	17.30	20.1
	3.0	99.1	0.029	0.171	2.86	17.16	20.0
	2.3	100.1	0.029	0.173	2.88	17.34	20.2
	4.7	99.1	0.028	0.172	2.81	17.21	20.0
	3.6						

Time-on-stream (hours)	X_{CO} (%)	C balance (%)	x_{CO}	x_{CO2}	F'_{CO} (mol/s)	F'_{CO2} (mol/s)	F'_{CO+CO2} (mol/s)
53.5	**3.5**	100.3	0.028	0.174	2.84	17.42	20.3
	3.0	99.5	0.029	0.172	2.86	17.24	20.1
	3.8	99.7	0.028	0.173	2.83	17.32	20.1
	2.7	98.9	0.029	0.171	2.87	17.12	20.0
	3.2						
78	**1.6**	100.4	0.029	0.174	2.90	17.39	20.3
	2.4	100.2	0.029	0.173	2.88	17.36	20.2
	3.0	99.1	0.029	0.171	2.86	17.15	20.0
	2.2	100.4	0.029	0.174	2.88	17.40	20.3
	2.3						

EXPERIMENT 8 - Au/ZnO-71 ($WHSV_{dry}$ = 2.0 hr^{-1})

Time-on-stream (hours)	Temperature (°C)	X_{CO} (%)	C balance (%)	x_{CO}	x_{CO2}	F'_{CO} (mol/s)	F'_{CO2} (mol/s)	F'_{CO+CO2} (mol/s)
67.5	**188**	**4.8**	99.7	0.028	0.173	2.80	17.34	20.1
		6.0	99.6	0.028	0.173	2.77	17.35	20.1
		6.0	100.4	0.028	0.175	2.77	17.51	20.3
		5.2	100.1	0.028	0.174	2.79	17.42	20.2
		5.5						
70	**192**	**8.6**	99.0	0.027	0.173	2.69	17.31	20.0
		7.7	100.0	0.027	0.174	2.72	17.49	20.2
		8.7	99.1	0.027	0.173	2.69	17.33	20.0
		7.8	98.6	0.027	0.172	2.72	17.20	19.9
		8.2						
73.25	**196**	**9.8**	99.4	0.026	0.174	2.66	17.42	20.1
		8.6	99.6	0.027	0.174	2.69	17.42	20.1
		8.6	99.3	0.027	0.173	2.69	17.37	20.1
		8.7	98.8	0.027	0.172	2.69	17.26	20.0
		8.9						
76	**200**	**8.3**	100.0	0.027	0.175	2.70	17.50	20.2
		9.0	99.2	0.027	0.173	2.68	17.36	20.0
		9.3	98.7	0.027	0.172	2.67	17.27	19.9
		9.8	99.6	0.026	0.174	2.66	17.46	20.1
		9.1						

EXPERIMENT 8 - Au/ZnO-71 ($WHSV_{dry}$ = 4.0 hr^{-1})

Time-on-stream (hours)	Temperature (°C)	X_{CO} (%)	C balance (%)	x_{CO}	x_{CO2}	F'_{CO} (mol/s)	F'_{CO2} (mol/s)	F'_{CO+CO2} (mol/s)
65	**188**	**1.8**	100.1	0.028	0.174	2.85	17.38	20.2
		1.7	99.7	0.029	0.173	2.85	17.28	20.1
		1.2	99.6	0.029	0.172	2.87	17.25	20.1
		1.7	100.2	0.028	0.174	2.85	17.38	20.2
		1.6						
53.5	**192**	**3.4**	100.1	0.028	0.174	2.80	17.42	20.2
		2.6	99.3	0.028	0.172	2.82	17.24	20.1
		2.1	99.7	0.028	0.173	2.83	17.31	20.1
		2.2	98.7	0.028	0.171	2.83	17.11	19.9
		2.6						
59	**196**	**4.1**	100.3	0.028	0.175	2.78	17.48	20.3
		3.2	100.0	0.028	0.174	2.81	17.40	20.2
		3.4	100.1	0.028	0.174	2.80	17.41	20.2
		3.6	99.9	0.028	0.174	2.80	17.38	20.2
		3.6						
62.5	**200**	**4.9**	98.5	0.028	0.171	2.76	17.15	19.9
		5.0	99.2	0.028	0.173	2.76	17.28	20.0
		4.6	99.1	0.028	0.172	2.77	17.26	20.0
		4.6	98.9	0.028	0.172	2.77	17.21	20.0
		4.8						

EXPERIMENT 9 - Au/ZnO-06 (Initial Performance, std conditions)

Time-on-stream (hours)	X_{CO} (%)	C balance (%)	x_{CO}	x_{CO2}	F'_{CO} (mol/s)	F'_{CO2} (mol/s)	F'_{CO+CO2} (mol/s)
1	**6.9**	101.2	0.027	0.175	2.74	17.51	20.2
	6.3	99.5	0.028	0.171	2.76	17.15	19.9
	7.0	99.8	0.027	0.172	2.74	17.22	20.0
	6.9	101.0	0.027	0.174	2.74	17.46	20.2
	6.8						
10.5	**3.8**	100.5	0.028	0.173	2.83	17.27	20.1
	4.2	100.1	0.028	0.172	2.82	17.20	20.0
	4.1	100.5	0.028	0.173	2.83	17.27	20.1
	5.0	100.1	0.028	0.172	2.80	17.23	20.0
	4.3						
21.5	**4.2**	101.3	0.028	0.174	2.82	17.43	20.3
	3.0	100.6	0.029	0.172	2.86	17.26	20.1
	3.1	100.6	0.029	0.173	2.85	17.27	20.1
	3.6	101.6	0.028	0.175	2.84	17.48	20.3
	3.5						
27.5	**2.9**	99.4	0.029	0.170	2.86	17.02	19.9
	3.2	101.0	0.028	0.173	2.85	17.35	20.2
	3.6	98.9	0.028	0.169	2.84	16.95	19.8
	3.2	99.4	0.028	0.170	2.85	17.02	19.9
	3.2						
34.5	**2.2**	99.9	0.029	0.171	2.88	17.09	20.0
	3.8	100.2	0.028	0.172	2.83	17.20	20.0
	2.0	100.4	0.029	0.172	2.89	17.19	20.1
	3.4	99.4	0.028	0.170	2.84	17.04	19.9
	2.9						
73.75	**3.0**	100.3	0.029	0.172	2.86	17.20	20.1
	2.8	99.5	0.029	0.170	2.86	17.04	19.9
	2.9						

EXPERIMENT 9 - Au/ZnO-06 ($WHSV_{dry}$ = 2.0 hr^{-1})

Time-on-stream (hours)	Temperature (°C)	X_{CO} (%)	C balance (%)	x_{CO}	x_{CO2}	F'_{CO} (mol/s)	F'_{CO2} (mol/s)	F'_{CO+CO2} (mol/s)
63	**188**	**4.8**	98.7	0.028	0.171	2.80	17.12	19.9
		5.4	99.6	0.028	0.173	2.79	17.34	20.1
		4.7	99.5	0.028	0.173	2.81	17.29	20.1
		5.7	98.9	0.028	0.172	2.78	17.20	20.0
		5.1						
69.5	**192**	**6.7**	99.2	0.027	0.172	2.75	17.28	20.0
		6.9	98.6	0.027	0.171	2.74	17.18	19.9
		7.7	99.9	0.027	0.174	2.72	17.46	20.2
		7.3						
58.5	**196**	**8.0**	99.8	0.027	0.174	2.71	17.44	20.2
		8.2	99.1	0.027	0.173	2.70	17.31	20.0
		8.6	98.9	0.027	0.172	2.69	17.29	20.0
		8.7	98.8	0.027	0.172	2.69	17.26	20.0
		8.4						
53.5	**200**	**9.9**	98.9	0.026	0.173	2.65	17.32	20.0
		9.6	98.6	0.027	0.172	2.66	17.26	19.9
		8.9	98.7	0.027	0.172	2.68	17.26	19.9
		9.3	99.7	0.027	0.174	2.67	17.47	20.1
		9.4						

EXPERIMENT 9 - Au/ZnO-06 ($WHSV_{dry}$ = 4.0 hr^{-1})

Time-on-stream (hours)	Temperature (°C)	X_{CO} (%)	C balance (%)	x_{CO}	x_{CO2}	F'_{CO} (mol/s)	F'_{CO2} (mol/s)	F'_{CO+CO2} (mol/s)
40.5	**188**	**0.7**	98.9	0.029	0.171	2.88	17.10	20.0
		1.1	100.0	0.029	0.173	2.87	17.33	20.2
		0.7	99.6	0.029	0.172	2.88	17.23	20.1
		0.7	98.4	0.029	0.170	2.88	17.00	19.9
		0.8						
34.5	**192**	**2.4**	98.4	0.028	0.170	2.83	17.06	19.9
		2.1	99.1	0.028	0.172	2.83	17.19	20.0
		2.9	99.8	0.028	0.173	2.81	17.35	20.2
		3.0	100.1	0.028	0.174	2.80	17.42	20.2
		2.6						
44	**196**	**3.4**	99.5	0.028	0.173	2.80	17.30	20.1
		3.5	99.4	0.028	0.173	2.80	17.29	20.1
		4.2	99.2	0.028	0.172	2.78	17.25	20.0
		3.0	99.1	0.028	0.172	2.81	17.21	20.0
		3.7						
48.5	**200**	**4.3**	100.0	0.028	0.174	2.78	17.43	20.2
		3.5	99.8	0.028	0.173	2.80	17.35	20.2
		4.2	100.0	0.028	0.174	2.78	17.42	20.2
		4.0	99.9	0.028	0.174	2.79	17.40	20.2
		4.0						

EXPERIMENT 10 - Commercial ZnO ($WHSV_{dry}$ = 4.0 hr^{-1})

Time-on-stream (hours)	Temperature (°C)	X_{CO} (%)	C balance (%)	x_{CO}	x_{CO2}	F'_{CO} (mol/s)	F'_{CO2} (mol/s)	F'_{CO+CO2} (mol/s)
1.25	**192**	**0.0**	99.5	0.029	0.172	2.90	17.19	20.1
		-0.4	99.1	0.029	0.171	2.91	17.11	20.0
		-0.8	99.0	0.029	0.171	2.92	17.07	20.0
		0.0	99.0	0.029	0.171	2.90	17.10	20.0
		0.2	99.3	0.029	0.172	2.89	17.16	20.1
		-0.3						
5.25	**196**	**-0.1**	100.3	0.029	0.174	2.90	17.35	20.3
		-0.3	100.0	0.029	0.173	2.92	17.28	20.2
		-0.1	100.3	0.029	0.173	2.91	17.34	20.3
		0.3	98.9	0.029	0.171	2.89	17.08	20.0
		0.0						
9.25	**200**	**-0.1**	100.4	0.029	0.174	2.90	17.37	20.3
		0.0	99.0	0.029	0.171	2.90	17.09	20.0
		-0.7	98.9	0.029	0.171	2.92	17.07	20.0
		-0.5	100.3	0.029	0.173	2.91	17.35	20.3
		-0.3						
14.5	**210**	**-0.2**	100.4	0.029	0.174	2.91	17.37	20.3
		0.1	99.3	0.029	0.172	2.90	17.17	20.1
		0.0	100.2	0.029	0.173	2.90	17.35	20.2
		0.0						
18.75	**220**	**-1.3**	99.6	0.029	0.172	2.94	17.19	20.1
		-0.6	98.8	0.029	0.170	2.92	17.04	20.0
		-0.1	99.8	0.029	0.173	2.90	17.26	20.2
		-0.7						

EXPERIMENT 11 - AUS (Initial Performance, std conditions)

Time-on-stream (hours)	X_{CO} (%)	C balance (%)	x_{CO}	x_{CO2}	F'_{CO} (mol/s)	F'_{CO2} (mol/s)	F'_{CO+CO2} (mol/s)
0.75	**4.1**	99.3	0.028	0.172	2.82	17.23	20.0
	4.5	98.6	0.028	0.171	2.81	17.11	19.9
	3.8	99.5	0.028	0.172	2.83	17.26	20.1
	3.7	99.0	0.028	0.171	2.84	17.17	20.0
	4.0						
7.5	**4.0**	99.0	0.028	0.172	2.83	17.18	20.0
	4.5	100.1	0.028	0.174	2.81	17.41	20.2
	3.5	100.3	0.028	0.174	2.84	17.42	20.3
	4.0						
14.5	**3.7**	98.6	0.028	0.171	2.84	17.09	19.9
	3.5	99.5	0.028	0.172	2.84	17.25	20.1
	4.2	99.0	0.028	0.171	2.82	17.17	20.0
	3.8						
29.75	**4.5**	98.7	0.028	0.171	2.81	17.13	19.9
	3.2	99.6	0.028	0.172	2.85	17.26	20.1
	4.2	98.9	0.028	0.171	2.82	17.15	20.0
	3.8	100.4	0.028	0.174	2.83	17.44	20.3
	3.9						

EXPERIMENT 11 - AUS ($WHSV_{dry}$ = 2.0 hr^{-1})

Time-on-stream (hours)	Temperature (°C)	X_{CO} (%)	C balance (%)	x_{CO}	x_{CO2}	F'_{CO} (mol/s)	F'_{CO2} (mol/s)	F'_{CO+CO2} (mol/s)
57.50	**200**	**5.6**	99.4	0.028	0.173	2.78	17.31	20.1
		5.7	98.9	0.028	0.172	2.78	17.20	20.0
		5.5	98.4	0.028	0.171	2.78	17.10	19.9
		5.6						
61	**220**	**5.2**	98.6	0.028	0.171	2.79	17.14	19.9
		4.6	100.0	0.028	0.174	2.81	17.39	20.2
		6.1	99.4	0.028	0.173	2.77	17.31	20.1
		5.3						
68.5	**240**	**5.0**	98.8	0.028	0.171	2.80	17.16	20.0
		4.7	99.7	0.028	0.173	2.81	17.33	20.1
		4.9	99.5	0.028	0.173	2.80	17.31	20.1
		4.8						
72	**280**	**5.8**	98.9	0.028	0.172	2.77	17.20	20.0
		5.0	99.5	0.028	0.173	2.80	17.30	20.1
		4.9	99.7	0.028	0.173	2.80	17.34	20.1
		5.2						
76	**320**	**4.8**	100.2	0.028	0.174	2.80	17.43	20.2
		5.3	99.2	0.028	0.172	2.79	17.24	20.0
		5.2	100.2	0.028	0.174	2.79	17.45	20.2
		4.6	99.6	0.028	0.173	2.81	17.30	20.1
		5.0						

EXPERIMENT 11 - AUS ($WHSV_{dry}$ = 4.0 hr^{-1})

Time-on-stream (hours)	Temperature (°C)	X_{CO} (%)	C balance (%)	x_{CO}	x_{CO2}	F'_{CO} (mol/s)	F'_{CO2} (mol/s)	F'_{CO+CO2} (mol/s)
48	**192**	**2.3**	100.4	0.028	0.174	2.83	17.46	20.3
		2.0	99.4	0.028	0.172	2.84	17.25	20.1
		2.7	98.9	0.028	0.171	2.82	17.16	20.0
		2.3						
52.5	**200**	**3.2**	98.5	0.028	0.171	2.81	17.08	19.9
		2.3	99.1	0.028	0.172	2.82	17.20	20.0
		2.4	99.7	0.028	0.173	2.82	17.31	20.1
		2.7						

EXPERIMENT 12 - LTS ($WHSV_{dry}$ = 4.0 hr^{-1})

Temperature (°C)	Pressure (barg)	X_{CO} (%)	C balance (%)	x_{CO}	x_{CO2}	F'_{CO} (mol/s)	F'_{CO2} (mol/s)	F'_{CO+CO2} (mol/s)
204	**10**	**77.4**	99.3	0.006	0.190	0.66	19.40	20.1
		78.2	98.3	0.006	0.188	0.63	19.23	19.9
		78.0	100.2	0.006	0.192	0.64	19.60	20.2
		77.6	97.8	0.006	0.187	0.65	19.10	19.8
		77.8						
204	**15**	**78.6**	98.7	0.006	0.189	0.62	19.32	19.9
		77.9	99.1	0.006	0.190	0.64	19.38	20.0
		78.1	98.2	0.006	0.188	0.64	19.21	19.8
		78.2						
204	**20**	**78.4**	98.6	0.006	0.189	0.63	19.30	19.9
		79.3	100.1	0.006	0.192	0.60	19.61	20.2
		78.9	99.3	0.006	0.190	0.61	19.45	20.1
		79.4	98.9	0.006	0.190	0.60	19.39	20.0
		79.0						
204	**25**	**80.4**	98.2	0.006	0.188	0.57	19.27	19.8
		79.4	99.5	0.006	0.191	0.60	19.49	20.1
		79.6	100.1	0.006	0.192	0.59	19.63	20.2
		80.2	99.0	0.006	0.190	0.57	19.43	20.0
		79.9						

EXPERIMENT 13 - Au/ZnO-27 ($WHSV_{dry}$ = 2.0 hr^{-1})

Temperature (°C)	Pressure (barg)	X_{CO} (%)	C balance (%)	x_{CO}	x_{CO2}	F'_{CO} (mol/s)	F'_{CO2} (mol/s)	F'_{CO+CO2} (mol/s)
204	**10**	**31.1**	97.8	0.020	0.176	2.03	17.74	19.8
		30.2	99.1	0.020	0.178	2.05	17.96	20.0
		30.3	98.3	0.020	0.177	2.05	17.81	19.9
		30.6	98.8	0.020	0.177	2.04	17.91	19.9
		30.6						
204	**15**	**32.5**	99.2	0.020	0.179	1.99	18.06	20.0
		32.3	99.6	0.020	0.180	1.99	18.12	20.1
		32.3	98.7	0.020	0.178	1.99	17.95	19.9
		32.3						
204	**20**	**33.7**	99.0	0.019	0.179	1.95	18.04	20.0
		34.4	100.4	0.019	0.182	1.93	18.35	20.3
		33.9	99.7	0.019	0.180	1.95	18.19	20.1
		34.8	99.3	0.019	0.180	1.92	18.13	20.1
		34.2						
204	**25**	**35.3**	98.6	0.019	0.178	1.91	18.01	19.9
		36.0	99.6	0.019	0.181	1.88	18.24	20.1
		36.0	100.3	0.019	0.182	1.88	18.38	20.3
		34.8	99.5	0.019	0.180	1.92	18.17	20.1
		35.5						

APPENDIX III

Determination of Equilibrium CO Conversion

Table AIII-1 : The Molar Heat Capacities of Gases in the Ideal Gas State

Compound	a	$b \times 10^2$	$c \times 10^5$	$d \times 10^9$	Temperature Range, K
Hydrogen	6.952	- 0.04576	0.09563	- 0.2079	273 - 1800
Carbon monoxide	6.726	0.04001	0.1283	- 0.5307	273 - 1800
Carbon dioxide	5.316	1.4285	- 0.8362	1.7840	273 - 1800
Water vapour	7.700	0.04594	0.2521	- 0.8587	273 - 1800

Source : S. Sandler, Chemical and Engineering Thermodynamics (2nd edition), John Wiley & Sons, 1989

Constants are for the equation $C_p = a + b.T + c.T^2 + d.T^3$, where T is in degrees Kelvin and C_p is in cal.(mol.K)$^{-1}$.

Table AIII-2 : Heats and Gibbs Free Energies of Formation of Gases

Compound	State	$\Delta H^f_{25°C}$ kcal/mol	$\Delta G^f_{25°C}$ kcal/mol
Hydrogen	g	0	0
Carbon monoxide	g	- 26.416	- 32.808
Carbon dioxide	g	- 94.052	- 94.260
Water vapour	g	- 57.7979	-54.6351

Source : S. Sandler, Chemical and Engineering Thermodynamics (2nd edition), John Wiley & Sons, 1989

Table A1II-3 : Mass Balance Compound Conversion Table for Water Gas Shift

$$CO + H_2O \rightleftharpoons CO_2 + H_2$$

Compound	Gases In	Gases Out	LTS Gas In
Carbon monoxide	$CO_{(i)}$	$CO_i - CO_i.X$	2.9
Water vapour	$H_2O_{(i)}$	$H_2O_{(i)} - CO_i.X$	(variable)
Carbon dioxide	$CO_{2(i)}$	$CO_{2(i)} + CO_i.X$	17.1
Hydrogen	$H_{2(i)}$	$H_{2(i)} + CO_i.X$	78.3
Nitrogen	N_2	N_2	1.7

where : X = fractional CO conversion

For Low Temperature Shift Conditions :

$$K_p = \frac{P_{CO_2}.P_{H_2}}{P_{CO}.P_{H_2O}} = \frac{(17.1+2.9X).(78.3+2.9X)}{(2.9-2.9X).(Y-2.9X)} \qquad \text{where : Y = 50 to 150}$$

The equilibrium constant for the reaction is also defined by the relationship below :

$$K = K_p = e^{(-\Delta G_{rxn}/RT)} \qquad \textbf{eqn AIII-1}$$

The Gibbs free energy of reaction at the particular reaction condition is a function of temperature only.

The Gibbs free energy of reaction and the standard heat of reaction can be determined from the standard Gibbs free energies of formation and standard heats of formation respectively, via the expression below :

$$\Delta G^{rxn}_{298K} = \Delta G^f_{CO_2} + \Delta G^f_{H_2} - \Delta G^f_{CO} - \Delta G^f_{H_2O} \qquad \textbf{eqn AIII-2}$$

$$\Delta H^{rxn}_{298K} = \Delta H^f_{CO_2} + \Delta H^f_{H_2} - \Delta H^f_{CO} - \Delta H^f_{H_2O} \qquad \textbf{eqn AIII-3}$$

In order to calculate the equilibrium constant K_p using the Gibbs free energies of formation, it can be seen that :

$$\frac{\partial}{\partial T}\left(\frac{\overline{G}_i}{T}\right)_P = \frac{1}{T}\left(\frac{\partial \overline{G}_i}{\partial T}\right)_P - \frac{\overline{G}_i}{T^2} = -\frac{\overline{S}_i}{T} - \frac{\overline{H}_i}{T^2} + \frac{\overline{S}_i}{T} = -\frac{\overline{H}_i}{T^2} \qquad \textbf{eqn AIII-4}$$

Using the fact that $\ln K_p = -\dfrac{\sum \nu_i \Delta \underline{G}^\circ_{f,i}}{RT}$, we obtain the van't Hoff equation:

$$\left(\frac{\partial \ln K_p}{\partial T}\right)_P = -\frac{1}{R}\frac{\partial}{\partial T}\left[\frac{\sum_i \nu_i \Delta \underline{G}^\circ_{f,i}}{T}\right] = \frac{1}{RT^2}\sum_i \nu_i \Delta \underline{H}^\circ_{f,i} = \frac{\Delta H^\circ_{rxn}(T)}{RT^2} \qquad \textbf{eqn AIII-5}$$

Therefore, $$\ln(K_p)_T - \ln(K_p)_{298K} = \int_{298K}^{T} \frac{\Delta H^{rxn}}{R.T^2} dT \qquad \textbf{eqn AIII-6}$$

But since $$\Delta H^{rxn}(T) = \Delta H^{rxn}_{298K} + \int_{298K}^{T} \Delta C_p dT \qquad \textbf{eqn AIII-7}$$

And knowing that

$$\begin{aligned}\Delta H^{rxn}_{298K} &= \Delta H^f_{CO_2} + \Delta H^f_{H_2} - \Delta H^f_{CO} - \Delta H^f_{H_2O} \\ &= (-393.5) + (0) - (-110.5) - (-241.8) \\ &= -41.16 \text{ kJ/mol at 298 K}\end{aligned}$$

$$\Delta G^{rxn}_{298K} = \Delta G^{f}_{CO_2} + \Delta G^{f}_{H_2} - \Delta G^{f}_{CO} - \Delta G^{f}_{H_2O}$$
$$= (-394.4) + (0) - (-137.3) - (-228.6)$$
$$= -28.52 \text{ kJ/mol at 298 K}$$

$$\Delta C_p = C_{p,CO_2} + C_{p,H_2} - C_{p,CO} - C_{p,H_2O}$$
$$= (22.242 + 5.977\times10^{-2}.T - 3.499\times10^{-5}.T^2 - 7.464\times10^{-9}.T^3)$$
$$+ (29.087 - 1.915\times10^{-3}.T - 3.990\times10^{-6}.T^2 - 8.699\times10^{-10}.T^3)$$
$$- (28.142 + 1.674\times10^{-3}.T - 5.368\times10^{-6}.T^2 - 2.220\times10^{-9}.T^3)$$
$$- (32.217 + 1.922\times10^{-3}.T + 1.055\times10^{-5}.T^2 - 3.593\times10^{-9}.T^3)$$
$$= -9.029 + 5.426\times10^{-2}.T - 4.691\times10^{-5}.T^2 - 1.241\times10^{-8}.T^3$$

and

$$K_{p,\,298K} = e^{-\Delta G^{rxn}_{298}/R.T}$$
$$= e^{-(-28495)/8.314\times298}$$
$$= 98832.26$$

Equation AIII-7 can then be expanded to

$$\Delta H^{rxn}(T) = \Delta H^{rxn}_{298K} + \int_{298K}^{T} 9.03 + 5.43\times10^{-2}T - 4.69\times10^{-5}T^2 - 1.24\times10^{-8}T^3 dT$$

Therefore,

$$\Delta H^{rxn}(T) = \Delta H^{rxn}_{298K} + 9.03(T-298) + \frac{5.43\times10^{-2}}{2}(T^2 - 298^2)$$
$$- \frac{4.69\times10^{-5}}{3}(T^3 - 298^3) - \frac{1.24\times10^{-8}}{4}(T^4 - 298^4)$$

K_p can be algebraically determined at various temperatures from Equation AIII-6 by means of a spreadsheet package, and thus the conversion of CO can be calculated from the compound table expression for K_p in terms of conversion at different steam to dry gas ratios. Figure AIII-1 represents the equilibrium curves of CO conversion at the industrially applicable steam to gas quantities. As expected, the equilibrium conversion decreases as the temperature increases

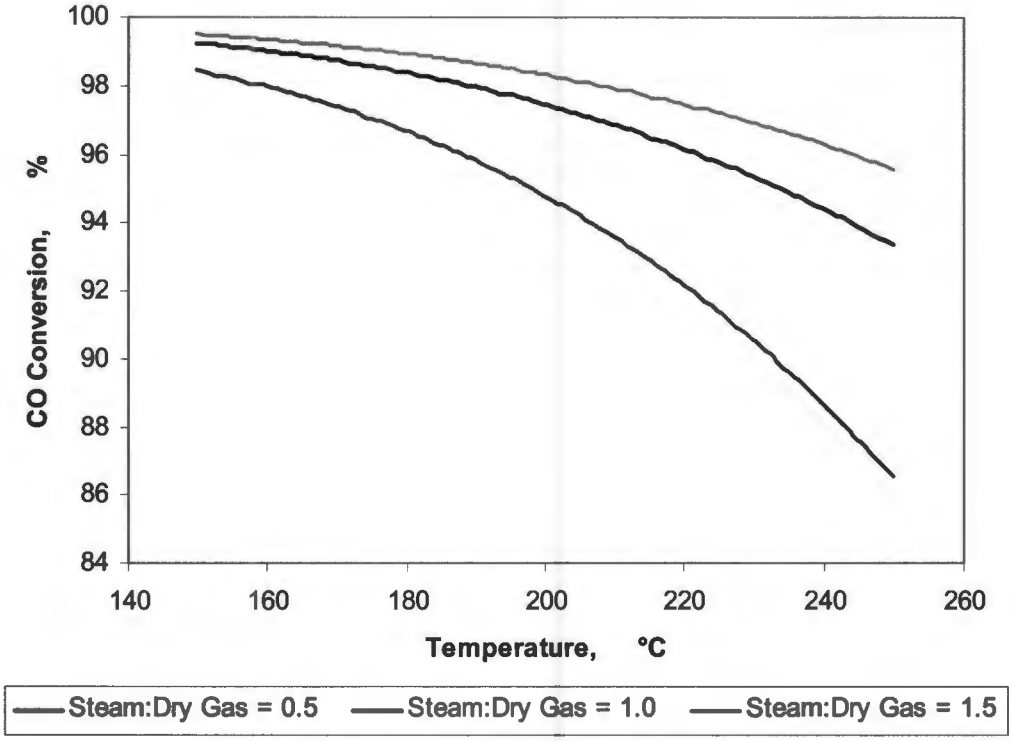

Figure AIII-1 : Equilibrium curves for CO conversion under LTS conditions using the experimentally applied feed conditions

APPENDIX IV

Diagrammatic Representation of the Reactor

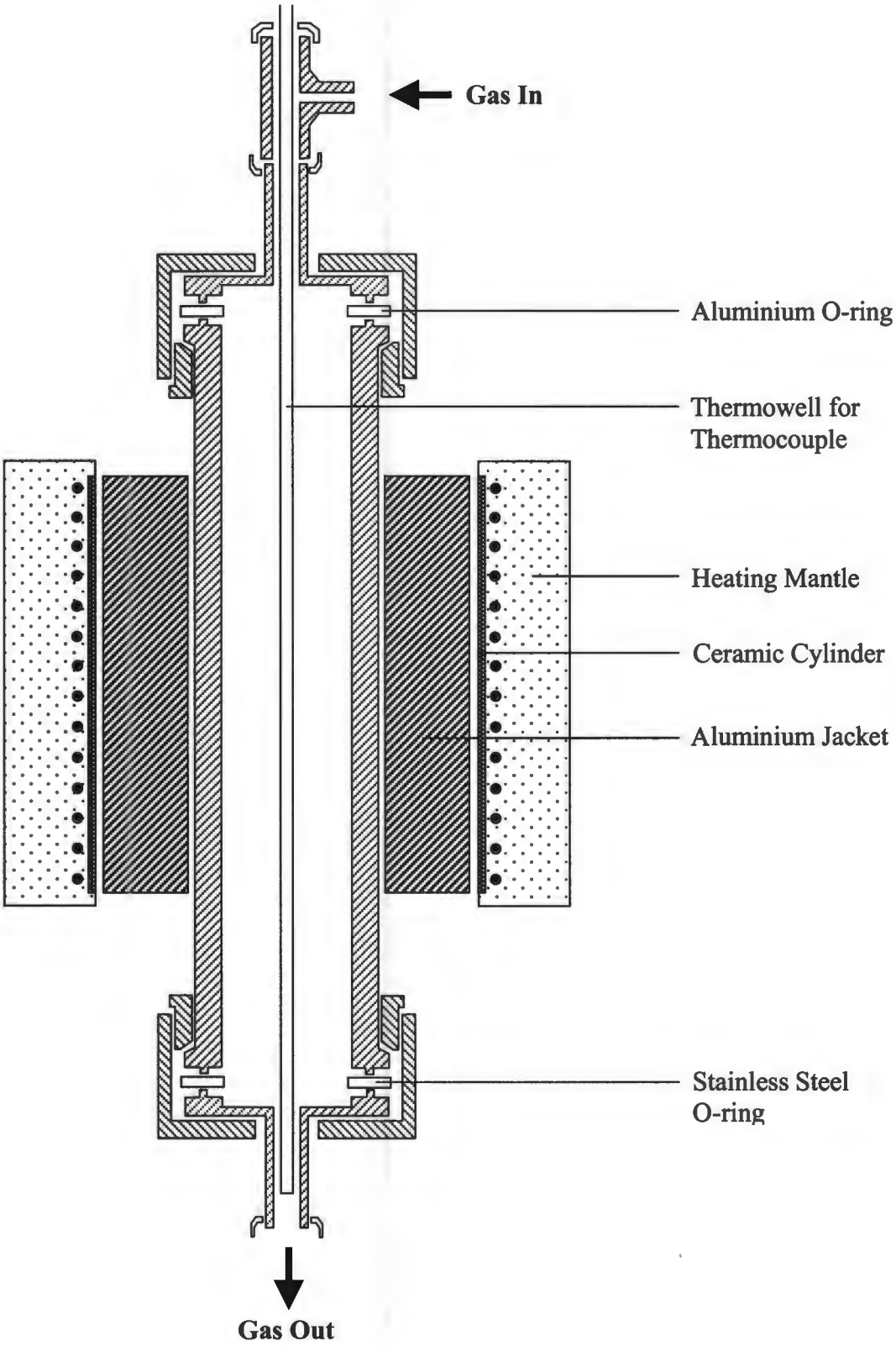

APPENDIX V

CO_2 Solubility in Condensed Water

Due to the nature of the detecting device, the water had to be removed to a sufficiently low level before analysis. A dual condensation and knock-out vessel configuration operating at 1°C was used to achieve as low a water partial pressure as possible; however, due to the *relatively* high solubility of CO_2 in water (refer to Table AV-1) it was necessary to ascertain whether the loss of CO_2 from the product gas is significant.

Table AV-1 : The solubility of gases (present in the dry gas mixture) in water

Compound	Solubility ($g / 100\ cm^3$ at 0°C)
Carbon Dioxide	0.348
Carbon Monoxide	2.914×10^{-3}
Hydrogen	1.926×10^{-4}
Nitrogen	4.377×10^{-3}

At a dry gas weight hourly space velocity of 4.0 hr^{-1} and a steam : dry gas ratio of 1, the reactor set-up conditions yielded a gas flow rate of 108.7 ml/min (at standard conditions) and a water flow rate of 0.08 ml/min. The CO_2 made up 17.1 mol % of the reaction gas mixture.

Under these conditions, 45.5 g CO_2 enter the condenser per 100 ml of water; and since the solubility is a mere 0.348 g / 100 ml, it is calculated that 99.4 % of the entering CO_2 exits the condenser to be analysed. This difference is smaller than the usual fluctuation in peak area integration.

This was indeed confirmed by experiment — the reaction gas mixture was firstly analysed after bypassing the reactor and passing it though the condenser and secondly by passing it directly to the TCD detector from the gas cylinder. No distinguishable differences (i.e. differences within the usual integral peak area fluctuations) were observed. The other gases in the reaction gas mixture, namely hydrogen, nitrogen and carbon monoxide have lower solubilities in water than carbon dioxide and therefore these gases were not considered for loss calculations.